T.C.
REPUBLIC OF TURKEY
HACETTEPE UNIVERSITY
GRADUATE SCHOOL OF HEALTH SCIENCES

Investigation of Possible Protective Effects of Certain Xenobiotics on Aluminum Toxicity in SH-SY5Y Cell Line

Sonia SANAJOU, Pharm D., DVM

Program of Pharmaceutical Toxicology
DOCTOR OF PHILOSOPHY THESIS

ANKARA
2023

T.C.
REPUBLIC OF TURKEY
HACETTEPE UNIVERSITY
GRADUATE SCHOOL OF HEALTH SCIENCES

Investigation of Possible Protective Effects of Certain Xenobiotics on Aluminum Toxicity in SH-SY5Y Cell Line

Sonia SANAJOU, Pharm D., DVM

Program of Pharmaceutical Toxicology
DOCTOR OF PHILOSOPHY THESIS

Thesis Supervisor
Prof. Terken Baydar, Ph.D.

ANKARA

2023

Investigation of Possible Protective Effects of Certain Xenobiotics on Aluminum Toxicity in SH-SY5Y Cell Line

Sonia SANAJOU

Supervisor: Prof. Dr. Terken BAYDAR

This thesis study has been approved and accepted as a PhD dissertation in "Pharmaceutical Toxicology Program" by the assessment committee, whose members are listed below, on 25/10/2023

Chairman of the Committee: Prof. Dr. Gönül ŞAHİN
(Adakent University)

Member: Prof. Dr. Aylin ÜSTÜNDAĞ
(Ankara University)

Member: Prof. Dr. Ü. Pınar Erkekoğlu
(Hacettepe University)

Member: Prof. Dr. Sevtap AYDIN
(Hacettepe University)

Member: Assoc. Prof. Dr. Gözde GİRGİN
(Hacettepe University)

This dissertation has been approved by the above committee in conformity to the related issues of Hacettepe University Graduate Education and Examination Regulation.

Prof. Müge YEMİŞCİ ÖZKAN, MD, PhD

Director

16 Kasım 2023

YAYINLAMA VE FİKRİ MÜLKİYET HAKLARI BEYANI

Enstitü tarafından onaylanan lisansüstü tezimin/raporumun tamamını veya herhangi bir kısmını, basılı (kağıt) ve elektronik formatta arşivleme ve aşağıda verilen koşullarla kullanıma açma iznini Hacettepe Üniversitesine verdiğimi bildiririm. Bu izinle Üniversiteye verilen kullanım hakları dışındaki tüm fikri mülkiyet haklarım bende kalacak, tezimin tamamının ya da bir bölümünün gelecekteki çalışmalarda (makale, kitap, lisans ve patent vb.) kullanım hakları bana ait olacaktır.

Tezin kendi orijinal çalışmam olduğunu, başkalarının haklarını ihlal etmediğimi ve tezimin tek yetkili sahibi olduğumu beyan ve taahhüt ederim. Tezimde yer alan telif hakkı bulunan ve sahiplerinden yazılı izin alınarak kullanılması zorunlu metinlerin yazılı izin alınarak kullandığımı ve istenildiğinde suretlerini Üniversiteye teslim etmeyi taahhüt ederim.

Yükseköğretim Kurulu tarafından yayınlanan "**Lisansüstü Tezlerin Elektronik Ortamda Toplanması, Düzenlenmesi ve Erişime Açılmasına İlişkin Yönerge**" kapsamında tezim aşağıda belirtilen koşullar haricince YÖK Ulusal Tez Merkezi / H.Ü. Kütüphaneleri Açık Erişim Sisteminde erişime açılır

- o Enstitü / Fakülte yönetim kurulu kararı ile tezimin erişime açılması mezuniyet tarihimden itibaren 2 yıl ertelenmiştir. (1)

- o Enstitü / Fakülte yönetim kurulunun gerekçeli kararı ile tezimin erişime açılması mezuniyet tarihimden itibaren ... ay ertelenmiştir. (2)

- o Tezimle ilgili gizlilik kararı verilmiştir. (3)

15/11/2023

Sonia SANAJOU

[1] "Lisansüstü Tezlerin Elektronik Ortamda Toplanması, Düzenlenmesi ve Erişime Açılmasına İlişkin Yönerge"

(1) Madde 6. 1. Lisansüstü tezle ilgili patent başvurusu yapılması veya patent alma sürecinin devam etmesi durumunda, tez danışmanının önerisi ve enstitü anabilim dalının uygun görüşü üzerine enstitü veya fakülte yönetim kurulu iki yıl süre ile tezin erişime açılmasının ertelenmesine karar verebilir.

(2) Madde 6. 2. Yeni teknik, materyal ve metotların kullanıldığı, henüz makaleye dönüşmemiş veya patent gibi yöntemlerle korunmamış ve internetten paylaşılması durumunda 3. şahıslara veya kurumlara haksız kazanç imkanı oluşturabilecek bilgi ve bulguları içeren tezler hakkında tez danışmanının önerisi ve enstitü anabilim dalının uygun görüşü üzerine enstitü veya fakülte yönetim kurulunun gerekçeli kararı ile altı ayı aşmamak üzere tezin erişime açılması engellenebilir.

(3) Madde 7. 1. Ulusal çıkarları veya güvenliği ilgilendiren, emniyet, istihbarat, savunma ve güvenlik, sağlık vb. konulara ilişkin lisansüstü tezlerle ilgili gizlilik kararı, tezin yapıldığı kurum tarafından verilir *. Kurum ve kuruluşlarla yapılan işbirliği protokolü çerçevesinde hazırlanan lisansüstü tezlere ilişkin gizlilik kararı ise, ilgili kurum ve kuruluşun önerisi ile enstitü veya fakültenin uygun görüşü üzerine üniversite yönetim kurulu tarafından verilir. Gizlilik kararı verilen tezler Yükseköğretim Kuruluna bildirilir. Madde 7.2. Gizlilik kararı verilen tezler gizlilik süresince enstitü veya fakülte tarafından gizlilik kuralları çerçevesinde muhafaza edilir, gizlilik kararının kaldırılması halinde Tez Otomasyon Sistemine yüklenir.

*Tez danışmanının önerisi ve enstitü anabilim dalının uygun görüşü üzerine enstitü veya fakülte yönetim kurulu tarafından karar verilir.

ETHICAL DECLARATION

In this thesis study, I declare that all the information and documents have been obtained in the base of the academic rules and all audio-visual and written information and results have been presented according to the rules of scientific ethics. I did not do any distortion in data set. In case of using other works, related studies have been fully cited in accordance with the scientific standards. I also declare that my thesis study is original except cited references. It was produced by myself in consultation with supervisor Prof. Terken BAYDAR, Ph.D. and written according to the rules of thesis writing of Hacettepe University Institute of Health Sciences.

Sonia SANAJOU DVM, Pharm.D

ACKNOWLEDGEMENT

My transformative four-year PhD journey, fulfilling a long-held dream, involved a transition from professional practice to academia. It was marked by profound experiences and unwavering support from exceptional individuals, to whom I owe immense gratitude.

Foremost, Prof. Dr. Gönül Şahin's mentorship and encouragement shaped my path. Her esteemed reputation and wisdom inspired me to excel.

Equally deserving of appreciation is my esteemed advisor, Prof. Dr. Terken Baydar, whose belief in my potential paved the way for academic growth. Her dedication nurtured my curiosity and led to significant contributions to publications.

I extend my gratitude to Prof. Dr. Pinar Erkekoğlu for her unwavering support and invaluable insights, which shaped the precision and validity of my results.

Saeed Kamali, my pillar of unwavering belief and emotional support, gave me the strength to persevere through doubt.

My loving family provided invaluable mental and monetary support, allowing me to focus on my academic pursuits. My parents' unconditional love and encouragement were a source of strength. Their financial assistance eased my financial worries.

I am profoundly thankful to my family for caring for my beloved dog, allowing me to concentrate on my research.

My family's emotional and practical support sustained me through moments of triumph and adversity. Their love, understanding, and sacrifices have profoundly shaped the person I've become.

In the company of extraordinary friends, lab mates, colleagues, and the research team – Anil Yirun, Deniz Çakir, and Assist. Prof. Dr. Göksun Demirel – I cherish the camaraderie, support, and collaborative spirit that enriched my academic experience.

ABSTRACT

Sanajou, S., Investigation of Possible Protective Effects of Certain Xenobiotics on Aluminum Toxicity in SH-SY5Y Cell Line, Hacettepe University Graduate School of Health Sciences, Department of Pharmaceutical Toxicology Doctor of Philosophy Thesis, Ankara, 2023. Aluminum, a neurotoxic metal, is widely present in our daily lives, exposing us extensively. Aluminum exposure is a potential Alzheimer's risk factor, with no cure yet. Researchers are actively seeking new treatments or repurposing existing drugs to fight this challenging condition. This thesis explores metformin, naltrexone, and dihydrolipoic acid's neuroprotective potential on an Alzheimer's disease model (differentiated SH-SY5Y cells exposed to chronic aluminum). It delves into their impact on GSK-3β and Wnt signaling pathways. Results reveal that chronic aluminum exposure triggers oxidative stress, elevates tau protein levels, increases GSK-3β activity, and diminishes Wnt signaling pathway activity. Encouragingly, the studied xenobiotics promise to mitigate these detrimental effects. They effectively reduce tau protein levels, modulate GSK-3β and Akt activity, and restore Wnt signaling pathway functionality. Additionally, these compounds significantly alleviate oxidative stress, highlighting their potential as neuroprotective agents against chronic aluminum exposure in AD. In conclusion, further clinical investigations are essential to establish optimal dosages and treatment strategies. Dihydrolipoic acid may be a dietary supplement, potentially slowing AD progression when added to patient diets. Lower-dose naltrexone shows promise in mitigating neuroinflammation in Alzheimer's, warranting exploration as a novel therapy. Considering Alzheimer's as a metabolic disorder akin to diabetes, metformin emerges as a potential treatment. These findings highlight the need for urgent clinical trials and translational research, offering the potential to reshape AD treatment and provide renewed hope for patients and families.

Keywords: Aluminum, Alzheimer's disease, Dihydrolipoic acid, GSK, Metformin, Naltrexone, Wnt

ÖZET

Sanajou, S., SH-SY5Y Hücre Hattında Bazı Ksenobiyotiklerin Alüminyum Toksisitesi Üzerine Olası Koruyucu Etkilerinin Araştırılması, Hacettepe Üniversitesi Sağlık Bilimleri Enstitüsü Farmasötik Toksikoloji Programı Doktora Tezi, Ankara, 2023. Alüminyumun Alzheimer hastalığı için potansiyel bir risk faktörü olduğu bilinmektedir, ancak bu hastalığın tedavisi henüz bilinmemektedir. Bu nedenle, araştırmacılar yeni tedaviler araştırmak veya mevcut ilaçları yeniden tasarlamak için çaba sarf etmektedir. Bu çalışmada, metformin, naltrekson ve dihidrolipoik asidin Alzheimer hastalığı modeli üzerindeki etkileri incelenmektedir. Sonuçlar, alüminyum maruziyetinin oksidatif stresi artırdığını, tau protein seviyelerini yükselttiğini ve GSK-3β ve Wnt sinyal yolaklarını etkilediğini göstermektedir. Ancak, incelenen ksenobiyotiklerin bu negatif etkileri azaltabilme potansiyeline sahip olduğu belirlenmiştir. Ayrıca, bu bileşiklerin Alzheimer hastalığına karşı nöroprotektif etkileri olduğu ve oksidatif stresi azalttığı görülmüştür. Daha fazla çalışma yapılması gerekmektedir, ancak dihidrolipoik asit ve naltreksonun Alzheimer hastalığının ilerlemesini yavaşlatabileceği, metformin ise potansiyel bir tedavi olarak kullanılabileceği öne sürülmektedir. Bu bulgular, Alzheimer tedavisinde umut verici yeni yaklaşımların araştırılması gerektiğini vurgulamaktadır.

Anahtar kelimeler: Alüminyum, Metformin, Naltrexone, Alzheimer, GSK, Wnt, Diydrolipoic acid

TABLE OF CONTENTS

ABBREVIATIONS

AD	Alzheimer's Disease
AGEs	Advanced Glycation End Substance
AKT	Serine/Threonine-Protein Kinase
AKT1	Human Rac-Alpha Serine/Threonine-Protein Kinase Elisa Kit
Al	Aluminum
AlCl₃	Aluminum chloride
α-LA	Alpha Lipoic Acid
AlOH₃	Aluminum hydroxide
ALP	Alkaline Phosphatase
ALS	Amyotrophic Lateral Sclerosis
ALT	Alanine Aminotransferase
AMPK	AMP-activated protein kinase
ANDRO	Andrographolide
APP	Amyloid Precursor Protein
AST	Aspartate Aminotransferase
ATP	Adenosine Triphosphate
Aβ	Amyloid-Beta
BACE	Beta-secretase
BBB	Blood Brain Barrier
BCA	Bicinchoninic Acid
BCL	B-cell lymphoma?
BMP	Bone Morphogenetic Protein
BDNF	Brain-Derived Neurotrophic Factor
cAMP	Cyclic Adenosine Monophosphate
CAT	Catalase
CD	Cluster of Differentiation
CDK5	Cyclin-Dependent Kinase-5
CNS	Central Nervous System
CRP	C-Reactive Protein
DHLA	Dihydrolipoic Acid
DIFFM1	Differentiation Medium 1
DIFFM2	Differentiation Medium 2
DMEM-F12	Dulbecco's Modified Eagle's Medium - F12 W/L-Glutamine W/15 mM Hepes
DMSO	Dimethyl Sulfoxide
DNPH	2,4-Dinitrophenylhydrazine
DPBS	Dulbecco's Phosphate Buffered Saline
DRG	Dorsal root ganglia
Dvl	Disheveled protein
Dvl2	Disheveled Segment Polarity Protein 2
EDTA	Ethylenediaminetetraacetic acid
F	Fluoride

FBS	Fetal Bovine Serum
FDA	The Us Food and Drug Administration
GPCR	G-Protein-Coupled Receptor
GPx	Glutathione Peroxidase
GSH	Glutathione
GSK-3	Glycogen Synthase Kinase-3
GSK-3β	Glycogen Synthase Kinase -3 Beta
HbA1C	Glycosylated Hemoglobin, Type A1C
HCL	Hydrochloric Acid
HRP	Horseradish Peroxidase
IC20	Inhibitory Concentration 20
IC30	Inhibitory Concentration 30
IC50	Inhibitory Concentration 50
IL	Interleukin
JNK	C-Jun N-Terminal Kinase
Lef1	Lymphoid Enhancer-Binding Factor 1
LPS	Lipopolysaccharide
LRP5	low-density lipoprotein receptor-related protein 5
LTP	Long-Term Potentiation
MDA	Malondialdehyde
mDA	Midbrain Dopaminergic
MIF	Macrophage Migration Inhibitory Factor
MIP-1α	Macrophage Inflammatory Protein-1Alpha
MOR	Mu Opioid Receptor
MTT	3-(4,5-Dimethylthiazol-2-Yl)-2,5-Diphenyltetrazolium Bromide
NA	Norepinephrine
NADPH	Nicotinamide Adenine Dinucleotide Phosphate
NFTs	Neurofibrillary Tangles
NF-κB	Nuclear Factor Kappa B
NGF	Nerve Growth Factor
NIDDM	Not Insulin-Dependent
NLRP3	PYD Domains-Containing Protein 3
NSAIDs	Non-steroidal Anti-inflammatory Drugs
NGF	Nerve Growth Factor
NSC	Neural Stem Cells
OD	Optical Density
OECD	Organization for Economic Cooperation and Development
OTCs	Organic Cation Transporters
PBS	Phosphate Buffered Serum Physiological
PCO	Protein Carbonyl
PD	Parkinson's Disease
PHF	Paired Helical Filaments
PI3K	Phosphoinositide 3-Kinase
PICOs	Polycystic Ovary Syndrome

PP2A	Human Protein Phosphatase 2A
PPP1CA	Human Serine/Threonine-Protein Phosphatase Pp1-Alpha Catalytic Subunit
PS1	mutant Presenilin 1
RA	Retinoic Acid
ROS	Reactive Oxygen Species
SD	Standard Deviation
SOD	Superoxide Dismutase
TAOC	Total Antioxidant Capacity
TBA	Thiobarbituric Acid
TBARS	Thiobarbituric Acid Reactive Substances
TCA	Trichloroacetic Acid
Tcf3	Transcription Factor 3
TCF-4	Transcription factor 4
TCF/LEF	T-cell factor/lymphoid enhancer factor
T2D	Type 2 Diabetes
TGFβ1	Transforming Growth Factor Beta 1
TNF-α	Tumor Necrosis Factor-Alpha
WNT	Wingless-INT

LIST OF FIGURES

LIST OF TABLES

1. INTRODUCTION

The lightweight and silvery look of aluminum (Al), the third most prevalent metal in the Earth's crust, distinguishes it. It occurs naturally in the environment due to processes such as rock weathering and volcanic activity, and it is also released into the environment due to human activities such as mining. Al levels in various environmental media can vary greatly depending on location and sample site. Al baseline levels in the atmosphere are generally low, ranging from around 0.005 to 0.18 g/m^3. At the same time, concentrations in urban and industrial regions are sometimes higher. Al levels in surface water usually are relatively low (0.1 mg/L). In contrast, acidic or humic-rich waters may have higher soluble Al levels due to the enhanced solubility of Al oxide and salts. Al concentrations in soil vary greatly, ranging from roughly 7 to more than 100 g/kg (1,2).

For the general population, the predominant route of exposure is through food intake, with modest exposures happening through drinking water ingestion and ambient air inhalation. Al is also included in over-the-counter drugs such as antacids, buffered aspirin, and food additives. Al is also found in various consumer items like antiperspirants, first aid antibiotics, antiseptics, and cosmetic products. Al concentrations in meals and drinks vary based on food type, processing techniques, and agricultural zones (3–5).

Given that humans are exposed to Al from various sources, including anthropogenic sources, there is rising worry about possible human health risks. Al intoxication can cause oxidative stress in the brain, liver, and kidneys, affecting the balance between free radicals and enzyme antioxidant ability. Al can disrupt or impede more than 200 important biological functions and harm the central nervous system (CNS) by interfering with or suppressing enzymes, protein synthesis, nucleic acid activity, and cell membrane permeability (6).

Al neurotoxicity has been linked to various brain development mechanisms, including axonal transport, neurotransmitter synthesis, synaptic transmission, protein phosphorylation or de-phosphorylation, protein degradation, gene expression, peroxidation, and inflammatory responses. Al levels are elevated in the brain tissue of people suffering from neurodegenerative disorders such as Alzheimer's disease (AD).

AD is a progressive neurological ailment that causes cognitive decline and dementia, typically in the elderly. The disorder is characterized by slow cognitive ability reduction, memory loss, visual-spatial problems, confusion, and disorientation. The buildup of extracellular A and the development of neurofibrillary tangles (NFTs) are the major pathogenic characteristics of AD, leading to synaptic dysfunction and neuronal abnormalities (7).

Currently, AD therapy focuses mainly on providing supportive and symptomatic care with little influence on the overall prognosis. The predominant therapeutic choices are cholinesterase inhibitors and memantine, which provide relief by increasing memory and cognitive function or alertness and cognitive ability, respectively. These drugs, however, have little effect on the overall course of AD dementia or life expectancy (8).

In addition to researching known treatments, researchers are increasingly looking into the possibility of repurposing therapies that have demonstrated efficacy in treating other medical diseases. The emphasis is on addressing the pathogenic aspects of AD, notably amyloid-β (Aβ) and p-tau, as major targets for future therapeutics. However, early successes seen in comparative studies and smaller clinical trials have not yet been consistently replicated in larger-scale administrations, highlighting the complexity of AD and the need for more comprehensive research to develop truly effective treatments (8).

Investigating pharmaceutical treatments with promising outcomes in treating other diseases may increase therapeutic possibilities for AD. Researchers are working feverishly to develop fresh techniques for managing this difficult and deadly disorder, and using established drugs from other medical sectors might be a significant step forward in the ongoing struggle against AD.

This thesis explores the neuroprotective impacts of entrained xenobiotics in mitigating the neurotoxic repercussions induced by Al exposure, specifically within differentiated SH-SY5Y cell lines. The primary focus is on modulating the GSK-3β and Wnt signaling pathways as pivotal mechanisms through which these entrained xenobiotics could potentially exert their protective effects.

2. LITERATURE REVIEW

2.1 Toxicokinetic of Aluminum

2.1.1. Absorption

The absorption rate of Al depends on its chemical properties, pH of the environment, ionic strength, presence of competing elements such as silicon, and chelating agents like citrate. Generally, Al's absorption rate from the gastrointestinal tract is low, approximately 1-2% (9). In vivo studies reported that citrate-containing compounds increase Al absorption and accumulation in brain and bone tissues (10). Besides, elements such as silicon, phosphate and polyphenols decrease Al absorption due to the formation of insoluble complexes that cannot be absorbed (9).

Oral Absorption

Following ingestion, the primary pathway for Al to be systemically deposited in animals and humans is through gastrointestinal absorption, predominantly occurring in the duodenum (11). Al uptake through the gastrointestinal system is complex and influenced by various factors, including individual variations, age, pH levels, stomach contents, and the specific form of Al. Notably, water intake (approximately 0.3%) contributes more to Al absorption than food intake (approximately 0.1%). Organic substances contained in food, such as phytates and polyphenols, were traditionally thought to form complexes with Al ions, limiting their absorption. In contrast, the presence of citrate, maltol, lactate, or fluoride in water or food and chronic renal problems might increase Al absorption through the gastrointestinal system (12).

On the other hand, the intake of Al with phosphate, silicon, polyphenols, and sialic acid, or in individuals with iron overload, can reduce its absorption. It is important to note that Al is completely absorbed from parenteral fluids and vaccines, distributed throughout various body areas (11). Oral ingestion is the primary means for this metal to enter the bloodstream.

Dermal Absorption

With a total area of 1.5 square meters, the skin is the largest organ in the human body. It has a complex structure with diverse functions (13). The skin has three layers: the first outermost layer is the epidermis provides a waterproof barrier. The second layer dermis contains connective tissue, hair follicles and sweat glands, and the third layer is subcutaneous or hypodermis. The stratum corneum, the outer part of the epidermis, consists of keratin-rich cells within the lipid intercellular matrix (14).

Exposure to metals through the skin occurs through direct contact with metals or objects containing metals. Metals in contact with skin can be absorbed into the epidermis; even in some cases, absorption to the dermis and penetration to the systemic circulation was reported. Allergic reaction is the primary local effect of contact with metals such as chromium, nickel or cobalt. However, the metals' skin permeation rates have been underestimated (15).
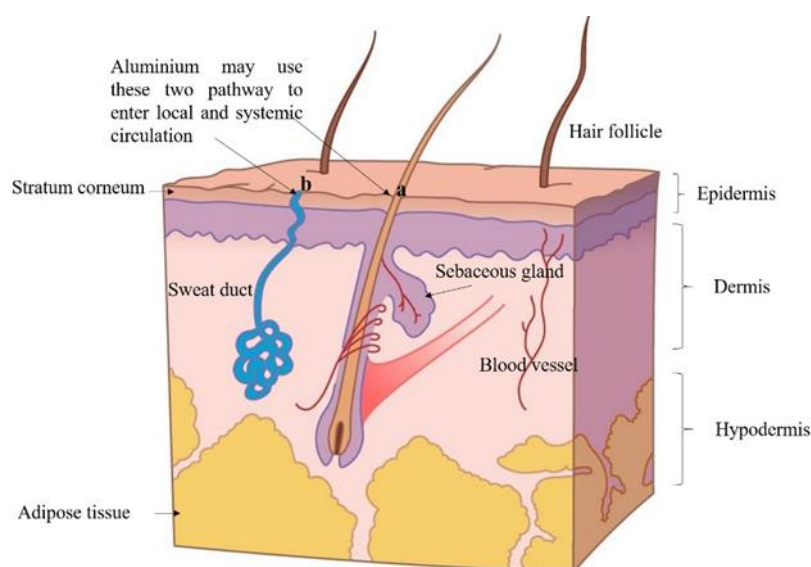
Figure 2.1. The major layers of normal skin.

Hair follicles and sweat ducts are the possible vessels by which Al accesses the epidermis, dermis and lymphatic system (Figure 2.1.). However, there is no considerable evidence that Al applied on the skin enters the bloodstream and is excreted from the kidney. Nevertheless, it does not mean that Al cannot enter the circulatory system from the skin. Considering the Al formulation in cosmetics, the frequency of applying these products on the skin and the regulations about these

products' safety indicate that Al in cosmetic and personal care products is an important source of local and systemic Al (16).

There is limited information on Al absorption and distribution following dermal exposure. Anane et al. (17) exposed Swiss mice to 0.4 µg /day its chloride salt (AlCl$_3$) for 20 days during gestation. They reported that the Al level in mice's liver, brain, lung and kidney and their offspring increased significantly and concluded that transdermal absorption of Al should be considered. Flarend et al. (18) measured the amount of Al absorbed from two volunteers' skin (one male and one female) who exposed the skin to radiolabeled AlCl$_3$ on a bandage. The absorption rate was measured by measuring the amount of Al excreted by the urine. Only a small amount of Al was absorbed (0.012% of the applied concentration), which may not harm antiperspirant users. Another study was conducted in 2012, according to the Organization for Economic Cooperation and Development (OECD). Pineau et al. (19) measured the amount of Al absorbed through the skin utilizing FranzTM diffusion cell. Aerosol, roll-on, and stick-type antiperspirants were tested on five skin samples. They reposted that the amount of Al absorbed through the skin was insignificant. The sample (strip skin) exposed to the stick-type antiperspirant showed higher absorption rates.

Inhalation Absorption

Dust from soil and rocks is the most prevalent contributor of Al-containing particles in the atmosphere. Human activities, such as mining and agriculture, generate wind-borne dust (20). Anthropogenic emissions account for approximately 13% of the Al in the atmosphere. The primary anthropogenic sources of Al-containing particulate matter are industrial activities such as burning coal, Al output, iron and steel manufacturing facilities, brass and bronze refineries, transportation emissions, and processes involving Al metals such as melting, submission, slicing, and welding (21). Cigarette smoke has the potential to increase airborne Al levels. Airborne Al particles or droplets are the sources of inhaled Al aerosols. Al compounds become embedded in the lungs after breathing (22). The lungs are constantly exposed to Al, mostly Al silicates and other insoluble substances. The amount of Al in the lungs typically rises with age, which might contribute to respiratory problems in locations where Al

accumulates. There is no evidence that particulate or soluble Al penetrates the circulation from the lungs and then travels to other organs in the body (11).

Occupational exposure studies and animal research suggest that the lungs and nervous system are particularly susceptible to toxicity following inhalation exposure. Workers exposed to Al dust or fumes have reported respiratory symptoms, such as reduced lung function and fibrosis; however, these effects have not been consistently observed across all studies (23). Co-exposure to other substances may have contributed to the reported results. Respiratory consequences, such as granulomatous lesions, have also been observed in rats, hamsters, and guinea pigs. However, there is concern that these effects may be caused by dust overload rather than the presence of Al in lung tissue. Occupational studies involving workers exposed to McIntyre powder, Al dust and fumes in pot rooms, and Al fumes during welding suggest a potential association between chronic Al exposure and subclinical neurological effects. These effects include impairments on neurobehavioral tests assessing psychomotor and cognitive performance and an increased incidence of subjective neurological symptoms. However, apart from a few isolated cases, inhalation exposure has not been conclusively linked to overt neurotoxic effects. Comprehensive descriptions of Al exposure are lacking, a common limitation in occupational exposure research. Neurological endpoints studied thus far have focused solely on brain weight and brain histology, with no functional tests conducted. The current body of animal inhalation studies is inadequate for fully evaluating the possibility of Al-induced neurotoxicity (2).

2.1.2. Distribution

Transferrin distributes Al due to the oxidative state of Al (Al^{3+}), which is the same as blood iron (Fe^{3+}) (24). Approximately 0.005% of Al-protein complexes enter the brain through this route (25). Al accounts for half of the body's burden; it can travel from the placenta to the fetus and from the mother's milk to the newborn. Al accumulates in the brain, and the buildup rate rises with age (9). In healthy human beings, total Al levels range between 30 and 50 mg/kg body weight. The typical serum Al concentration is 1-3 g/L. Approximately one-half of the Al in the human body accumulates in the skeleton, while approximately one-fourth is in the lungs (from the

accumulation of inhaled insoluble Al compounds). Al levels in the human skeleton range from 5 to 10 mg/kg. Al can also be found in the human skin, lower gastrointestinal system, lymph nodes, adrenals, parathyroid glands, and most soft tissue organs. Higher levels of Al were identified in rats' spleen, liver, bone, and kidney than in the brain, muscle, heart, or lung (25).

Approximately ninety percent of the circulating Al in the bloodstream is transported by transferrin, a protein responsible for transporting iron. At the same time, the remaining portion binds to albumin and citrate. The uptake of Al by cells in tissues is believed to occur through endocytosis, with intracellular transfer of Al bound to transferrin. However, it is uncertain whether the Al-transferrin complex interacts with the transferrin receptor, suggesting the possibility of an alternative mechanism for Al absorption within cells (26).

Among individuals not exposed to Al or antacids, the mean serum Al level was 1.6 µg/L in a study of 44 subjects (27). In contrast, hemodialysis patients exhibited serum Al levels ten times higher than those of unexposed individuals, as Chen et al. (28) reported. In experimental animals, Al levels in tissues and organs such as bone, muscle, lung, liver, and kidney tend to rise with age. Furthermore, Al has been discovered to swiftly penetrate the brain, extracellular fluid, and cerebrospinal fluid, albeit in less amounts than in circulation. Iron status is inversely related to Al deposition in organs, and animal studies have shown that calcium and magnesium shortages might lead to Al accumulation in the brain and bone (29).

As an element, Al is constantly present in combination with other compounds, and these affinities can change throughout the body. Al is assumed to exist in living organisms in four states: free ions, low-molecular-weight complexes, physically bound macromolecular complexes, and covalently bonded macromolecular complexes (2,30). Because Al^{3+} is easily linked to a wide range of molecules and structures, its destiny is determined by its affinity for each of the ligands, as well as their relative amounts and metabolism. Al may also form low-molecular-weight compounds by combining with organic acids, amino acids, nucleotides, phosphates, and carbohydrates. These low-molecular-weight compounds chelate often and have the potential to be highly stable. Complexes, especially nonpolar ones, are biologically active. Because Al has a high affinity for proteins, polynucleotides, and

glycosaminoglycans, much of the Al in the body may exist as physically bonded macromolecular complexes with these substances. These macromolecular complexes should be metabolically much less active than the smaller, low-molecular-weight complexes. Al may also form irreversible stable compounds with macromolecules. Evidence shows that Al binding occurs often in the nucleus and chromatin of cells (31).

2.1.3. Excretion/Elimination

Al clearance rates vary per compartment; for example, removal from the lungs may take 100 days. Its removal from the brain, however, takes more than 100 days. This prolonged clearance interval produces Al buildup in the brain, which causes neurotoxic consequences (32). The excretion half-life grows to more than 50 years as Al consumption increases. The extended excretion half-life could explain why Al accumulates so extensively in many body regions (33). Unabsorbed Al is substantially eliminated by feces (34).

Most Al ions in the bloodstream (approximately 95%) are eliminated by the kidneys through urine, likely in the form of Al citrate. When the binding capacity of transferrin for Al is exceeded, the presence of citrates and fluorides helps limit the accumulation of Al in tissues by facilitating renal excretion. Al is also detected in various bodily fluids and substances, including milk, bile, feces, perspiration, hair, nails, sebum, and sperm. Chemical chelators such as deferoxamine, as well as acids like malic, malonic, citric, oxalic, and succinic acids, have been shown to enhance the excretion of Al through urine (11).

2.2. Toxicity

The toxic effects of Al are diverse and can lead to complex systemic toxicosis. Its molecular action targets exert cellular effects and disrupt cellular homeostasis, resulting in cellular lesions that contribute to structural and functional abnormalities in organs. The pro-oxidant activity of Al is primarily responsible for its toxic effects, leading to oxidative stress, free radical attacks, and the oxidation of cellular proteins and lipids (16). When Al ions interact with protein polypeptides with oxygen-

containing amino acids side chains or protein backbones, they undergo denaturation, conformational changes, or structural modifications, as observed in Aβ (22,35)

Exposure to Al promotes the aggregation and precipitation of Aβ, which has been linked to AD (22,36). This phenomenon may contribute to neuritic plaque accumulation, neuron death, and dysregulation in neuronal regeneration. Al exposure induces fibrillation and clumping of amylin, resulting in the formation of β-pleated sheet structures, which may predispose pancreatic β-cells to damage (37,38). Additionally, Al hinders the proteolytic breakdown of amyloid peptides, leading to increased amyloid formation (39). Interaction between Al and cell components may cause inhibition or stimulation effects (40). Enzymes can be either inhibited or activated when they interact with Al. Al can also interact with the phosphate groups of nucleotides like ATP, influencing energy metabolism. Al exposure in liver cells inhibits ATP synthesis. It disrupts glycolysis and the tricarboxylic acid (Krebs) cycle, which enhances macromolecule oxidation, resulting in a switch in metabolism towards lipogenesis (41). These alterations in metabolism may explain weight loss and reduced eggs produced in Al-exposed animals (42).

Exposure to Al can disrupt iron homeostasis, resulting in iron excess. Al has been shown to enhance oxidative stress and iron-mediated damage. Increased cellular iron levels can exacerbate oxidative damage and have been implicated in the development of neurodegenerative diseases (43,44). Al-induced iron overload has been associated with elevated lipid peroxidation, genetic material damage, and reactive oxygen species (ROS)-related apoptosis. Al ions promote apoptosis in erythrocytes, lymphocytes, and osteoblasts (45,46). In osteoblasts, oxidative damage has been shown to trigger the apoptotic pathway C-jun N-terminal kinase (JNK). The anti-apoptotic B-cell lymphoma (Bcl)-2 protein is inhibited to promote osteoblast mortality in culture. In contrast, the pro-apoptotic Bax (Bcl-2 associated X, apoptosis regulator), Bak (Bcl-2 antagonist/killer), and Bim (Bcl-2 interacting mediator of cell death) proteins are increased. Al exposure may reduce ferritin production while increasing transferrin receptor expression, disrupting the normal balance between transferrin and ferritin synthesis receptors. This results in elevated free iron levels within cells and increased oxidative damage through the Fenton reaction (47). Al exposure also affects the activities of antioxidant enzymes, including superoxide dismutase (SOD), catalase

(CAT), glutathione peroxidase (GPx), and glutathione (GSH), due to oxidative stress (Campbell et al., 1999; Oteiza et al., 1993). Abnormal increases in malondialdehyde (MDA) and thiobarbituric acid reactive substances (TBARS), along with decreased levels of antioxidants such as GSH, GPx, SOD, and CAT, have been observed in tissue homogenates of rats exposed to Al (48,49).

Al's harmful effects can also lead to mutagenesis, gene function changes, and transcriptional expression alterations (16). Al exposure in mice has been linked to somatic and germinal genotoxicity, characterized by chromosomal abnormalities and mitotic depression (50). Al-DNA binding can affect neuronal gene expression (51), potentially predisposing cells to genotoxicity. Additionally, Al exposure may impair cell growth, differentiation, and neurogenesis (52,53). Suppression and blockade of the Wingless-INT (Wnt)/β-catenin signaling pathway by Al have been shown to reduce osteoblastic proliferation and differentiation. Al can also hinder osteoblast development by inhibiting the bone morphogenetic protein (BMP)-2 signaling pathway (54).

Al has demonstrated pro-inflammatory properties in various tissues, resulting from oxidative stress and the generation of free radicals (16,55,56). Exposure to Al has been shown to increase levels of pro-inflammatory cytokines, such as interleukin (IL) -1 and tumor necrosis factor-alpha (TNF-α), in a dose-dependent way (57,58). Al exposure significantly upregulates the expression of genes involved in pro-inflammatory signaling. These Al-induced cytokines can attract leukocytes, emitting pro-inflammatory cytokines and chemokines, aggravating inflammation (59). Long-term contact of mice with Al sulfate in drinking water caused time-varying systemic inflammation, as measured by increased levels of IL-6, TNF-α, C reactive protein (CRP), and a trio of pro-inflammatory microRNAs, as well as inflammation markers, indicating progressive chronic inflammation in the exposed animals (60). Toxic exposure to Al causes immunotoxicity, affecting the functioning of lymphocytes and macrophages. Immunosuppression is caused by oxidative stress, which is linked to lymphocyte apoptosis and thymocyte and lymphocyte destruction. In vitro, Al inhibits the immunological activities of splenic B- and T-lymphocytes by decreasing lymphocyte division, cytokine production, and the proportions of cluster of differentiation (CD)-3(+) and CD-4(+) lymphocytes (61). Al inhibits

lipopolysaccharide (LPS)-induced nucleotide-binding oligomerization domain-like receptor family pyrin domain containing 3 (NLRP3) inflammasome activation and the expression and release of IL-1, IL-6, and TNF-α in peritoneal macrophages. In vivo, Al enhances norepinephrine release and activates the β-adrenoceptors/cyclic adenosine monophosphate (cAMP) pathway, inhibiting macrophage migration inhibitory factor (MIF) and TNF-α macrophage expressions (62). Contact allergy to Al has been identified as an abnormal immune response in individuals with atopic dermatitis (63). Al accumulation in endocrine glands induces oxidative stress, leading to decreased hormone levels in the bloodstream and organ hypofunction. For instance, testicular and ovarian failures have been reported due to inadequate levels of androgenic hormones (64,65). In conditions of low calcium levels, Al ions can interact more efficiently with calcium-sensing receptors than calcium, reducing receptor expression in the gland. The metabolic effect of declining certain thyroxine (T3 and T4) levels without a change in free T4 levels remains unknown (66).

Following exposure to Al, the activity of ATPase in the cell membrane may be compromised, leading to disturbances in transmembrane ion transport regulation. Al has been demonstrated to inhibit the activities of Na^+K^+-ATPase, Mg^{2+}-ATPase, and Ca^{2+}-ATPase in various cell types (67), including rat erythrocytes, vascular endothelial cells, testes, and ovaries (68). Changes in erythrocyte size and shape, such as the production of echinocytes, acanthocytes, and stomatocytes, have been observed due to altered membrane morphology because of Al exposure (69,70). Rat peripheral blood samples stained after prolonged oral consumption of Al revealed the presence of schistocytes and target cells (71). In lymphocytes, morphological changes in the lipid bilayer of plasma and mitochondrial membranes have been observed (72). During Al exposure, membrane protein components may undergo degradation or inadequate expression, resulting in the loss of some proteins and their inactivation of the cell membrane. Al exposure can also impact the cell membrane surface through phosphatidylserine externalization after apoptosis and dysregulation of erythroid progenitors (73,74).

2.3. Ageing and Alzheimer's Disease

Recent health science and technology achievements have made disease diagnosis and treatment more attainable, and the average human lifespan has increased in the last decades. However, the risk of neurodegenerative diseases also increases with the ageing population (75). Among the neurodegenerative diseases, AD has the highest incidence in the elderly. AD is suggested to affect >55 million people worldwide; each year, the number of people diagnosed with AD increases (76). According to a report published in 2020 by the Turkish Alzheimer Association, over 600,000 people in Turkey are struggling with AD (77). American Alzheimer's Association reported that by 2050, >88 million people in the USA will be diagnosed with AD (78). On the other hand, 8% of people aged over 60 years are estimated to be diagnosed with AD by 2040 in Europe (79). Moreover, it is estimated that 6.19 million people have AD in the Middle East and North Africa (80).

Alois Alzheimer was the first scientist who reported that amyloid plaques and loss of neurons in patients suffering from memory loss were observed in patients with dementia in 1906-1907. Although the disease was not named Alzheimer's then, in the 8th edition of his Handbook of Psychiatry in Chapter' Presenile and Senile Dementia', Kraepelin named Alzheimer's disease (81). AD usually starts more than 20 years before noticing its signs or symptoms. Patients diagnosed with AD after 65 years of age are considered late-onset AD. After years, memory loss and speaking problems are noticed as the neurons responsible for cognitive function are damaged. As the disease progresses, neurons in other brain parts also get involved. The patient loses his or her ability to do basic daily tasks (79). Therefore, the patient needs a 7/24 caregiver (78).

Preclinical stage	Very mild stage	Mild stage	Moderate stage	Severe stage
Earliest signs of AD like abnormal level of Aβ in cerebrospinal fluid and decline in glucose metabolism can be measured by positron emission tomography.	-Patient will experience low degrees of memory loss like forgetting about family members. -In some cases, the disease does not progress to further stages.	-The patient experiences dementia by noticeably cognitive impairments. -However, most of the patients in this stage still can continue their life without everyday assistance. -Patients also experience difficulty in expressing thoughts. -Misplacing belongings	-Patient needs daily assistance; acts suspicious or agitated. -Increased poor judgment and confusion.	-Patient needs fulltime caregiver. -Patient may become bed-bounded. -As consequence of bed bounding, other problems like inflammation, organ failure can be observed.

Figure 2.2. Alzheimer disease stages.

On the other hand, some patients are diagnosed with early-onset AD at earlier ages (45-65 years). These patients show more significant neocortical pathology, particularly in the parietal cortex, greater tau levels than an amyloid burden (82), and less hippocampal damage. They have non-amnestic, phenotypic variants which show more aggressive clinical signs, and these AD patients have worse attention, executive functions, ideomotor praxis, and visuospatial skills (83). The stages of AD are summarized in figure 2.2.

2.3.1. Pathophysiology of Alzheimer's disease

Primary pathophysiological changes in AD are cholinergic lesions, neurofibrillary tangles (which accumulate in the neuron), extracellular accumulation of Aβ and loss of neurons. Other lesions, such as neuropil threads, dystrophic neurites and synaptic loss, have also been reported (84).

The deposition of Aβ plaques is believed to cause loss of basal forebrain cholinergic neurons, damage to axons dendrites, and loss of synapses, which in turn cause cognitive impairment. However, the exact mechanism behind most AD cases is still unknown. Aβ is a normal amyloid precursor protein (APP) cleavage in the human CNS. Aβ, with a half-life of approximately nine hours, usually turns over rapidly in the human CNS. However, Aβ turnover kinetics are altered in AD (85). The plaque can be neurotic, dense-cored or compact. Proteolytic cleavage enzymes, β-secretase and γ-secretase, cleave APP into fragments with specific amino acids. The formation of $A\beta_{40}$ and $A\beta_{42}$ fragments has mainly reported AD. The insoluble forms of Aβ

monomers are from the amyloid fibrils, and the soluble form is distributed in the brain. As humans age, the rate of Aβ turnover and clearance decreases. The chance of Aβ aggregation and conformation change increases, though the exact mechanism behind this phenomenon is still under investigation (86).

Tau phosphoproteins are important in the integrity of the structure of microtubules. Tau regulates axonal transport and stabilizes the microtubules in neurons. In AD, tau is hyperphosphorylated; after hyperphosphorylation, tau protein has a reduced ability to bind to microtubules, thus dysregulating the microtubule network and causing cell death. NFTs accumulate in neural pericardial cytoplasm, axons, and dendrites, which causes a loss of cytoskeletal microtubules and tubulin-associated proteins (87). Tau phosphorylation at the proline-rich region and C-terminal tail decreases its activity. The pathological features of AD-like NFTs and senile plaques can be observed as the normal ageing process. Thus, these features are present in some people without cognitive or memory functions (88).

Additionally, some cases of AD disease can be diagnosed without Aβ plaques (89). There are still unknown cofactors that may contribute to AD progression, and Al may be one of these factors (90). In the brains of some AD patients, hyperphosphorylated tau is observed as intraneuronal neurofibrillary tangles of paired helical filaments (PHF). Several kinases regulate the phosphorylation of tau, and glycogen synthase kinase-3beta (GSK-3β) and cyclin-dependent kinase-5 (CDK5) are the most important enzymes for this regulatory process (91).

The cholinergic theory shifted AD research from descriptive neuropathology to the contemporary idea of synaptic neurotransmission, revolutionizing the discipline (92). Because acetylcholine is crucial in cognitive processes, the cholinergic system has been implicated in various dementias, including AD. Cholinergic transmission deficits can affect many aspects of cognition and behavior, including cortical and hippocampal information processing (93). This theory is based on three turning points (94): (i) the discovery of shrinking presynaptic cholinergic markers in the cerebral cortex. (ii) the discovery that neurofibrillary degeneration of the cholinergic nucleus basalis of Meynert neurons, known as Ch4, was already present in the early stages of AD. (iii) the cholinergic antagonists impair memory while agonists improve.

The severity of dementia in AD was shown to be linked to the extent of cholinergic depletion, and animals with cholinergic lesions and resulting cognitive impairment were identified as AD models. Choline absorption, decreased acetylcholine release, impairments in the expression of nicotinic and muscarinic receptors, defective neurotrophin support, and axonal transport deficits are the key modifications in cholinergic neurons evaluated in this concept. In addition, amyloid interacts with cholinergic receptors and changes their activity (95). According to molecular modelling research, acetylcholine interacts with the Aβ peptide and stimulates the development of amyloid fibrils. Kinetic analysis revealed that a structural motif in acetylcholine could stimulate amyloid production and integration into developing A-fibrils (93). Even though abnormalities in other cortical neurotransmitters such as dopamine, norepinephrine, and histamine have been identified in AD, the cholinergic lesion is significantly earlier, more extensive, and more persistent than other neurotransmitter system pathologies (96).

2.4. Glycogen synthase kinase

GSK-3 enzyme regulates glycogen synthesis, glucose transport, metabolism, pro-apoptotic factors, and insulin signaling pathway. This kinase consists of two isomers, GSK-3α and GSK-3β. GSK-3β isoform dominates the brain, controlling various signaling pathways (97). It is shown that GSK-3 participates in cellular activities, such as the formation of cell structure, cell cycle regulation, gene expression and transcription, cell apoptosis, protein transcription and protein synthesis, mRNA stability, lipid deposition and lipid accumulation (98). In addition, GSK-3 plays a role in tumor suppression and neuronal function (99). The dysfunction of GSK-3 has been reported in pathological conditions like sporadic and familial types of AD, diabetes, bipolar disorder, schizophrenia, inflammation (100), and cancers (101). As shown in figure 2.3, three main signaling pathways inactivate GSK3: (i) The insulin signaling pathway activates phosphoinositide 3-kinase (PI3K), thus activating Akt, which results in the deactivation of GSK-3 by phosphorylating it at the N-terminal serine residue; deactivating the GSK-3 prevents cell death. (ii) In the presence of nutrients like amino acids, the mammalian target of the rapamycin (mTOR) signaling pathway inactivates GSK-3 by phosphorylating it at the N-terminal. (iii) In the absence of the Wnt

signaling pathway, GSK-3 degrades β-catenin, driving cell proliferation and tissue renewal.

In the Wnt signaling pathway, GSK-3 is inactivated by releasing GSK-3 from a multi-protein complex (β-catenin, axon and adenomatous polyposis coli). This phenomenon leads to the induction of β-catenin dependent gene transcription (102).
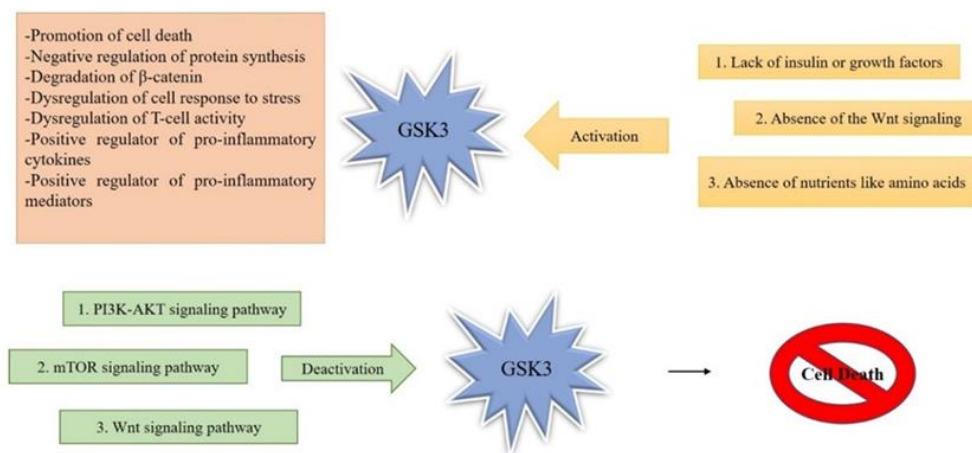

Figure 2.3. Inactivation of GSK-3 by signaling pathways.

GSK-3β has been proposed to link between Aβ and tau in AD. Aβ activates GSK-3β, then GSK-3β cause tau phosphorylation. APP is regulated by GSK-3β, which in turn causes amyloid formation. In vivo, studies in mice have concluded that GSK-3β inhibitors reduce senile plaque and tau hyperphosphorylation and enhance cognitive skills. Additionally, mice with GSK-3β overexpression show AD signs, such as NFTs and Aβ. However, in the absence of the tau gene, the mice show milder AD signs (103). The tau protein contains a large number of amino-acid residues that GSK-3 phosphorylates. Tau overexpression in the presence of over-activated GSK-3β interrupts the regular axonal transport—consequently, synaptic failure, neuronal dysfunction, and neurodegeneration (86). In a splenectomized rat model, inhibiting GSK-3 protects cells from neurodegeneration. It significantly reduces phospho-tau levels, spatial learning, and memory deficits (104).

GSK-3α regulates the production of Aβ. Exposure to Aβ causes inhibition of the PI3K pathway, which increases the GSK-3β activity. Insulin signaling pathways that decrease the activity of GSK-3 have been shown to increase the expression of insulin-degrading enzymes. The increase in the cleavage rate of APP with the non-

amyloidogenic β-secretase enzyme decreases the rate of production of Aβ. Moreover, GSK-3 inhibitors like lithium chloride and valproic acid have been shown to decrease Aβ production in vitro studies. In addition, specific GSK-3 inhibitors decreased transcription and expression of the beta-secretase 1 (BACE1) gene, resulting in a decrease in the production of Aβ. It is important as the BACE1 levels in AD patients were reported to be elevated (105). Figure 2.4. illustrates the role of GSK-3 in Aβ aggregation. GSK-3 also regulates synaptic plasticity by managing long-term potentiation (LTP) and long-term depression (LTD) (106). Upon LTP induction, GSK-3β is inhibited by an increase in Ser 9 phosphorylation. Overexpression of GSK-3β in neurons decreases postsynaptic density and volume in hippocampal granule neurons. These decreases induce cognitive impairment and alter LTP production (104).
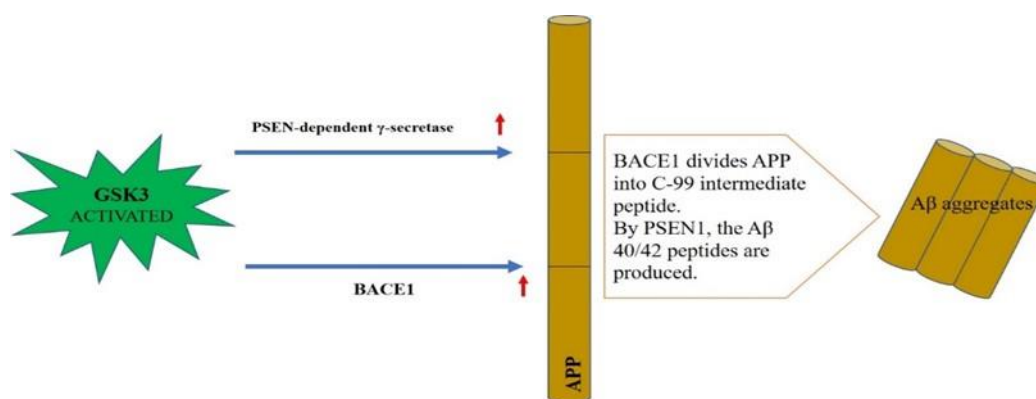
Figure 2.4. Activation of GSK3 and Aβ aggregates.

Aβ: amyloid-beta; APP: amyloid-beta precursor protein; BACE1: beta-secretase 1; GSK3: glycogen synthase kinase-3; PSEN1: presenilin-1.

According to one study, lowering the expression of β-catenin, a hippocampus transcription factor, hinders memory consolidation. GSK-3 activation decreases β-catenin stability and leads to its ubiquitination, whereas GSK-3 inhibition stabilizes β-catenin and boosts its ability to modulate synaptic plasticity. According to another study, the β-catenin signaling pathway and brain-derived neurotrophic factor (BDNF) govern neural stem cell growth in mice, and the BDNF pathway may interact with the β-catenin path. Moreover, researchers confirmed that BDNF is a direct target of the β-catenin transduction pathway and that β-catenin regulates BDNF expression. Specific properties of Al, such as its small molecular size, near-maximal charge, and strong affinity for metal-binding sites in enzymes, may contribute to its effects on LTP and

lead to the involvement of the GSK-3 and β-catenin signaling–mediated BDNF pathway (107).

2.5. Wnt signaling Pathway

The Wnt pathway is an evolutionarily conserved signal transduction pathway that regulates a wide range of cellular functions during development and adulthood. It controls cell proliferation, fate determination, apoptosis, migration, and cell polarity. Wnt genes, including int-1, are highly conserved across multiple species and are involved in wing development, segmentation, and body axis formation. Wnt proteins are secreted, lipid-modified glycoproteins and act as ligands interacting with Frizzled (FZD) receptors on the cell surface. Co-receptors, such as the low-density lipoprotein receptor-related protein (LRP), may mediate Wnt signaling (108,109).

Upon activation, a signal is transduced by the pathway-activating protein Disheveled, which can be branched off into multiple downstream pathways. The Wnt pathway can be categorized into the canonical Wnt pathway (β-catenin dependent pathway) and non-canonical Wnt pathways (β-catenin independent pathways), including polarity and the Wnt/Ca^{2+} pathway (108).

The Wnt pathway plays a crucial role in various aspects of CNS functioning, including neuronal differentiation, neurogenesis, synapse formation, and neuroprotection (110,111). It also participates in synaptic plasticity, which is required for higher brain activities like learning and memory, and its impairment has been related to mental decline in neurodegenerative illnesses like AD. These proteins help establish synapses and influence neural communication both pre- and post-synaptically (112). Moreover, the Wnt/β-catenin signaling pathway is essential for preserving, integrity, and operating the blood-brain barrier (BBB), which is disturbed in AD and other neurodegenerative illnesses (113). Over the past decade, the importance of Wnt/β-catenin signaling in midbrain dopaminergic neuron formation and adult hippocampal neurogenesis has been recognized. Wnt ligands and components of the pathway have been identified in normal midbrains and animal models of Parkinson's disease (PD), AD, amyotrophic lateral sclerosis (ALS), and other neurodegenerative diseases, suggesting that dysregulation of this pathway may contribute to their pathogenesis (114–116).

Wnt/β-catenin signaling works as a sensor of the milieu in the intact CNS, balancing cell survival and cell death. By blocking GSK-3-induced phosphorylation and degradation of β-catenin, Wnt ligands and agonists promote the Wnt-ON state. This β-catenin stabilization causes it to accumulate in the cytosol and translocate to the nucleus, where it acts as a co-activator for TCF/LEF-mediated transcription and supports the expression of Wnt target genes related to neuron survival and elasticity, maintaining neuron integrity. Antioxidants, anti-inflammatory compounds, and neuroprotective drugs can directly or indirectly activate this signaling pathway (117,118).

Wnt antagonists, inflammation, oxidative stress, neurotoxic medications, growth factor deprivation, and ageing, on the other hand, can suppress Wnt/ β-catenin signaling (Wnt-OFF state) in neurons. Excess β-catenin is quickly phosphorylated and destroyed in the Wnt-OFF state, inhibiting Wnt target gene transcription crucial in neuron survival. The microglial and astrocytic components of the CNS govern the balance of Wnt-ON and Wnt-OFF states in neurons. Dysregulation of neuron-glia interaction can lead to cell death and decreased neuroprotection, eventually leading to neurodegeneration. Emerging data show that Wnt signaling may potentially influence neuroinflammation in neurodegenerative illnesses such as PD via bidirectional contact between glial cells and neurons (118–120). Astrocytes and microglial cells in the brain release Wnts and Wnt-like molecules. Wnt receptors are expressed, regulating the neuroimmune response in an autocrine/paracrine way. Wnt/-catenin signaling activation mediated by glial-derived Wnts and Wnt-like molecules can provide neuroprotective benefits in neurons that express Wnt receptors. However, oxidative stress, neurotoxic drugs, growth factor deficiency, or ageing can decrease astrocyte anti-inflammatory and neuroprotective capabilities, exacerbating the pro-inflammatory phenotype in microglia. This, in turn, suppresses Wnt/β-catenin signaling and downregulates Wnt1 expression, potentially leading to neuron degeneration (121).

2.6. Naltrexone

Naltrexone was initially produced in 1963 as an orally active, competitive, non-selective opioid receptor antagonist. It is structurally and functionally comparable to

another opioid antagonist, naloxone, but has a longer biological half-life and better oral bioavailability. In 1984, the US Food and Drug Administration (FDA) authorized naltrexone hydrochloride for the treatment of opiate addiction (122), the reduction of withdrawal symptoms (123), and the relief of physical dependency (123,124). A 50 mg/day dosage of naltrexone is indicated for drug withdrawal and relapse prevention. In contrast, a 5 mg/day dose treats autoimmune illnesses and chronic pain syndrome. Low-dose naltrexone has been studied in illnesses such as fibromyalgia, inflammatory bowel disease, diabetic neuropathy, cancer, and inflammatory dermatologic disorders (125).

The endogenous opioid system comprises opioid peptides, endorphins, enkephalins, and dynorphins with variable affinities for opioid receptors. The main opioid receptors are mu, delta, and kappa. However, additional receptors, such as G-protein coupled receptors, also play a role. The opioid system's downstream effects are determined by several parameters, including opioid peptide level, receptor makeup, and signaling effectors. As an exogenous modulator, naltrexone operates as an antagonist at mu and delta receptors while less affecting kappa receptors. The action of naltrexone can be influenced by its many stereoisomers (126,127). Furthermore, naltrexone inhibits non-opioid receptors on macrophages such as microglia (128).

Recent studies have demonstrated that naloxone exhibits neuroprotective benefits in neuroglia cultures against degeneration caused by inflammatory stimuli and A by decreasing TNF-α production by microglia (129,130). Furthermore, naloxone (82.5 nmol) has been shown in rats to have neuroprotective properties against brain ischemia damage via an unknown mechanism (129).

The opioid system is critical for learning and memory, and its dysregulation can result in cognitive impairment (131). The dysregulation in the endogenous opioid system has been reported in AD. Radioligand studies have revealed a decrease in overall opioid receptor avidity. Patients with AD may have altered reactions to pain, opioids, and opioid antagonists (132). Interestingly, injection of naloxone into rats has been demonstrated to boost their reactivity to environmental cues, indicating that opioid antagonists may improve attention. Furthermore, naltrexone has been shown to boost human attentiveness and performance (125,133).

Overall, naltrexone and opioid receptors play critical roles in various physiological processes, and their dysregulation may have consequences for illnesses such as dementia, AD, and pain management. More study is required to completely comprehend these substances' complicated relationships and possible medicinal applications.

2.7. Metformin

Metformin, also known as dimethylbiguanide, is a synthetic derivative of biguanide that received FDA approval in 1994. Over the course of more than six decades, extensive research has consistently demonstrated that metformin is the most effective initial treatment option for individuals diagnosed with type 2 diabetes (T2D). The product exhibits a cost that is within a reasonable range and has shown to have a positive safety record when used for an extended period of time (134). The biodistribution and pharmacodynamics of the drug depend on transporters that facilitate the transportation of cationic compounds. The transporters encompassed in this category are organic cation transporters (OCTs), plasma membrane monoamine transporter, and multidrug and toxin extrusion proteins. Metformin demonstrates a relatively short duration of action in the bloodstream, with a plasma half-life ranging from 2 to 6 hours (135). These results in the maintenance of a consistent concentration range of about 4 to 15 μM (equivalent to about 0.5 to 2.0 μg/ml) among those diagnosed with T2D. Preliminary investigations have suggested that the liver serves as the primary site for metformin's mechanism of action in the regulation of hepatic glucose production. The observed effects result from a confluence of mechanisms, encompassing both pathways dependent on AMP-activated protein kinase (AMPK) and pathways dependent on AMPK (136).

Nevertheless, recent research indicates that various other factors, such as the gastrointestinal tract, gut microbiota, and tissue-resident immune cells, may also exert significant influences (135). Metformin improves insulin sensitivity, decreases gastrointestinal glucose absorption, and increases glucose uptake in peripheral tissues, lowering blood glucose levels and the need for insulin production (137). Moreover, metformin can reduce glycated hemoglobin (HbA1c) by 1%–2% without causing weight gain (138).

The potential therapeutic applications of guanidines and biguanides across various diseases have attracted considerable attention in the field of medical research. The investigation into the molecular targets of metformin has yet to yield a comprehensive understanding of its mechanism of action within a specific organ. However, existing evidence indicates that metformin exerts its beneficial effects through various mechanisms in multiple organs (139). Nonetheless, there is a potential for achieving a degree of agreement among the proposed mechanisms. The intracellular compartment contains all of the suggested cellular targets of metformin, while no known interactions with cell surface receptors have been documented. It is widely acknowledged in the scientific community that metformin undergoes negligible metabolic alterations in humans, resulting in the absence of any active drug metabolites. Hence, the identification of metformin's target tissues can be achieved by examining the cellular uptake of the drug. Consequently, investigating the biodistribution of metformin in patients emerges as a compelling approach to support inquiries into the mechanisms underlying its mode of action (134).

Metformin has been extensively studied for its potential therapeutic applications in a range of medical conditions, including polycystic ovary syndrome (140), cancer (141), rheumatoid arthritis, neurodegenerative diseases associated with cognitive dysfunction and dementia (142,143), anti-ageing interventions, parasitic infections such as malaria, antibiotic applications, and even the treatment of COVID-19 (135).

Diabetes has been linked to various neurological conditions, including stroke, dementia (specifically Alzheimer's disease and vascular dementia), and PD. Due to its association with impaired insulin signaling and glucose metabolism, AD has been likened to a neurologically specific form of diabetes. It is noteworthy that there exists a positive correlation between elevated glucose levels and a heightened susceptibility to dementia among individuals without diabetes, thereby suggesting the potential utility of metformin.

Metformin has been found to potentially possess additional advantages, including the reduction of adverse consequences associated with protein glycation and advanced glycation end substances (AGEs), both of which are implicated in the development of degenerative diseases and the ageing process. It is worth mentioning

that metformin possesses the capability to traverse the BBB, rendering it a potential insulin sensitizer with central activity. The potential neuroprotective properties of metformin can be attributed to its vascular protection, anti-ageing effects, and anti-inflammatory properties (144).

Although a body of pre-clinical and clinical research supports the hypothesis regarding the neuroprotective benefits of metformin, the available data present a mixed picture, as not all studies demonstrate its direct protective effects. Multiple meta-analyses have presented divergent findings regarding the association between metformin usage and dementia. Some studies have reported a reduced occurrence of dementia with metformin usage, while others have found no significant advantage. Conversely, certain analyses have suggested a potential increase in the risk of PD (136).

In summary, the existing literature regarding the neuroprotective effects of metformin remains inconclusive. Although metformin's anti-hyperglycemic and vascular properties appear intriguing, it is important to consider other drawbacks, such as the potential reduction in mitochondrial function, which may outweigh its potential advantages. Further investigation is warranted to fully comprehend the extent of metformin's impact on neurodegenerative diseases, particularly in individuals without diabetes. Moreover, before expanding the utilization of metformin to more diverse populations, examining potential negative consequences and thoroughly ensuring patient adherence is imperative. It is noteworthy that several other medications for diabetes have exhibited advantageous effects, thereby indicating that the neuroprotective properties of metformin are not exclusive.

2.8. Dihydrolipoic acid

The reduced form of alpha-lipoic acid (α-LA), dihydrolipoic acid (DHLA), is both hydrophilic and hydrophobic, making it easier to distribute throughout the body (145). α-LA is transformed into DHLA by enzymes such as glutathione reductase, thioredoxin, and lipoamide hydrogenase. Due to their capacity to postpone or stop the oxidation of suberate even at low concentrations, α-LA and DHLA are both recognized as universal antioxidants (146). In particular, against environmental contaminants like

heavy metals, their responsibilities include scavenging free radicals, chelating metals, and replenishing intracellular glutathione levels (145,147).

By regenerating vitamins C and E without consuming them, dietary supplements with α-LA and DHLA greatly lower oxidative stress. Unlike vitamins C and E, which are largely lipophilic, they may exercise their antioxidant action in the cytosol and plasma thanks to this special characteristic. Other antioxidants, such as glutathione, can also be restored by DHLA (148,149). Additionally, in vivo and in vitro investigations have shown that DHLA functions as a metal chelator, producing stable complexes with metals, including iron and copper (150). Additionally, it improves glucose absorption in muscle regions that are both insulin-sensitive and insulin-resistant (146).

Increased oxidative damage has been identified as an early stage in the development of AD, according to studies employing mice models of the disease. Antioxidants may be able to reduce this damage. Although non-steroidal anti-inflammatory drugs (NSAIDs) have been investigated for AD treatment, long-term use of these medications can be harmful to the digestive system. As a result, developing treatment options for AD has shifted its attention to investigating methods to prevent or minimize oxidative damage, with antioxidants playing a significant role (151).

Studies conducted in vitro have shown that α-LA has neuroprotective properties against cytotoxicity brought on by adenosine, activating the PKB/Akt signaling pathway and protecting cortical and hippocampal neurons from toxicity brought on by adenosine and oxidative stress. Additionally, via activating choline acetyltransferase, α-LA has demonstrated promise in enhancing acetylcholine synthesis, which is essential for cognitive function. The anti-inflammatory effects of α-LA are further influenced by its antioxidant characteristics, which lower free radicals, pro-inflammatory cytokines, and indicators like TNF-α. Additionally, α-LA may affect signal transduction pathways and epigenetic processes important for managing and preventing AD. In the search for neuroprotective treatments for AD, α-LA and DHLA are excellent options due to their diverse effects (152).

2.9. Thesis Objectives:

The major goal of this research is to explore the potential neuroprotective effects of naltrexone, metformin, and dihydrolipoic acid on aluminum-induced neurotoxicity in the differentiated SH-SY5Y cell line. These xenobiotics have been investigated for their impact on the GSK-3β and Wnt signaling pathways, both of which play critical roles in Alzheimer's disease pathogenesis. Specifically, the thesis aims to achieve the following objectives:

Objective 1: Establish a robust differentiation protocol for the SH-SY5Y cell line, enhancing its resemblance to neuronal cells and increasing tau expression. This cellular model will enable the investigation of toxic effects induced by aluminum on neuronal-like cells.

Objective 2: Evaluate the potential of naltrexone, known as an opioid antagonist, at lower doses than typically used for addiction treatment, as a promising candidate for therapeutic intervention in Alzheimer's disease. By studying its effects on the GSK-3β and Wnt signaling pathways, the research seeks to elucidate its neuroprotective mechanisms.

Objective 3: Investigate the efficacy of metformin, a widely used antidiabetic medication, as a potential therapeutic agent for Alzheimer's disease and related conditions. The focus has been on how metformin regulates the GSK-3β and Wnt pathways to confer neuroprotection.

Objective 4: Explore the potential of dihydrolipoic acid, the reduced form of α-lipoic acid, as a dietary supplement for Alzheimer's disease patients and individuals with metal intoxication. The research aims to assess its antioxidant properties and its ability to counteract neurotoxicity induced by aluminum.

Through comprehensive investigations into these objectives, this research seeks to contribute valuable insights into the neuroprotective properties of the studied xenobiotics, potentially opening up new avenues for the development of therapeutic strategies to combat neurotoxicity in Alzheimer's disease and related conditions.

3. METHOD AND MATERIAL

3.1. List of Instruments

Instruments	Brand/Trademark
CO_2 Incubator	HERAEUS
Cell Culture Flasks (25, 75 cm^2)	Isolab
Cryovials	Grenier Bio-One
Analytical Balance	Mettler Toledo XS105
Horizontal Laminar Flow Cabinet	Holten
Barnstead Water Purification System	Barnstead
Distilled water system	MES Minipure/Thermo Scientific
Refrigerator	Arçelik
96-wellplate	Greiner Bio-One
Neubauer Chamber	Marienfeld
Microscope Slide and Cover Glass	Isolab
Centrifuge	Heraeus, Hettich, Rotofix 32A
Laboratory Water Bath	Memmert
Vortex	LMS, Mixer Uzusio VTX-3000L
Sterile Serologic Pipets (5, 10, 25 ml)	Greiner Bio-One
Sterile Centrifuge Tubes (15 and 50 ml)	Greiner Bio-One
Autoclave	Nüve NC40M
Laboratory Cube Ice Maker	Scotsman AF100
Laboratory water bath	Memmert, Edelstaht Rostfrei
Spectrophotometer	Molecular Devices, SpektraMax, M2
-20°C Freezer	Arçelik
-80°C Freezer	Revco, Legaci
Light Microscope	Leica DM 6000, Leica TP1020
Parafilm	Bemis
Micropipettes (1-10 µl, 10-100 µl, 20-200 µl, 100-1000 µl, 1-5 ml)	Eppendorf, Finn pipette, Lab systems
Micropipette tips (1-10 µl, 10-200 µl, 100-1000 µl, 1-5 ml)	Eppendorf, Top-Line

3.2. List of chemicals

Chemicals and Kits	Brand
GSH(Glutathione) ELISA Kit	Elabscience
Protein Determination kit	Cayman Chemical
Fetal Bovine Serum (FBS)	Biowest
Fluorometric Intracellular Ros Kit	Sigma Aldrich
Ethanol, absolute	Merck
DMEM F12 (Dulbecco's Modified Eagle's Medium - F12 W/ L-Glutamine W/15 mM Hepes)	Biowest
Dimethyl sulfoxide (DMSO)	Merck
3-(4,5-Dimethylthiazol-2-yl)-2,5-Diphenyltetrazolium Bromide (MTT)	Sigma-Aldrich
Trypsin-EDTA (0.25%), phenol red	Gibco
Total Antioxidant Capacity (TAOC) Assay Kit	Cayman Chemical
TBARS Assay Kit	Cayman Chemical
SH-SY5Y cell line	ATCC
Protein Carbonyl Colorimetric Assay Kit	Cayman Chemical
Penicillin-Streptomycin Solution 100x	Biowest
Metformin Hydrochloride	Sigma-Aldrich
Dihydrolipoic acid	Sigma-Aldrich
Naltrexone Hydrochloride	Sigma-Aldrich
Aluminum Hydroxide	InvivoGen
Retinoic acid	Cayman Chemical
Brain-derived neurotrophic factor (BDNF)	Sigma-Aldrich
Dulbecco's Phosphate Buffered Saline (DPBS)	Biowest
Human GSK3β (Glycogen Synthase Kinase 3 Beta) ELISA Kit	Elabscience
Human RAC-alpha serine/threonine-protein kinase ELISA Kit (AKT1)	MyBioSource
Human MAP τ (Microtubule Associated Protein Tau/Tau Protein) ELISA Kit	Elabscience

Human Protein Wnt-5a ELISA Kit	MyBioSource
Human Serine/threonine-protein phosphatase PP1-alpha catalytic subunit ELISA Kit	MyBioSource
Human Protein Phosphatase 2A ELISA Kit	BT LAB
Human CTNNβ1(Catenin, Beta 1) ELISA Kit	Elabscience

3.3. SH-SY5Y cell line

General

The human neuroblastoma cell line (SH-SY5Y, ATCC CRL-2266TM) was used in the studies conducted within the scope of the thesis. The SH-SY5Y cell line is a subline of SK-N-SH (ATCC HTB-11), an epithelial morphology neuroblastoma cell line derived from a metastatic bone marrow tumor tissue from 4-year-old cancer patient in 1970. It consists of both adherent and suspended cells. SH-SY5Y cells were purchased from the American Type Cell Collection (ATCC). Cells were incubated in Dulbecco's Modified Eagle's Medium-Ham's F12 (DMEM F12) medium with 15% FBS, 1% penicillin/streptomycin, added L-glutamine and 15 mM HEPES at 37°C and in an incubator with 5% CO_2 and humidity.

Sterilization protocols were meticulously followed in cell culture to prevent contamination and protect the integrity of cells and samples. All equipment and materials utilized were sterile obtained by autoclaving, filtration, or chemical treatment with chemicals such as ethanol or bleach. The biosafety cabinet and laboratory bench surfaces were disinfected with ethanol before the cell culture procedure began. To guarantee maximum cell viability and development, all components, including the medium, serum, trypsin-ethylenediaminetetraacetic acid (EDTA), and other additives, were pre-warmed to 37°C and kept there to minimize rapid temperature fluctuations that may stress the cells.

3.4. Preparation of solutions related to cell culture

<u>Growth medium:</u> DMEM-F12 containing glutamine and 15 mM HEPES was purchased from Biowest company. 15% (v/v) FBS and 1% penicillin/streptomycin were added to this medium.

2X Trypsin-EDTA Solution: The 10X trypsin-EDTA solution was diluted to 2X using DPBS.

Freezing medium: Mix 20% FBS and 1% DMSO in DMEM-F12. The freezing medium can be prepared fresh or aliquoted to be kept at -20°C for long-term usage.

Differentiation Medium 1 (DIFFM1): 1% penicillin/streptomycin, 1% (v/v) FBS, and 10µM retinoic acid were added to 500ml of DMEM-F12.

Differentiation Medium 2 (DIFFM2): 1% penicillin/streptomycin, 1% (v/v) FBS and BDNF (2.5 ng/ml) were added to 500ml of DMEM-F12.

Thawing

Cells previously frozen in cryovials were carefully retrieved from a -80°C freezer. The cryovial was then carefully heated in a water bath until the contents were entirely thawed to aid in dissolving. The entire cryovial cell solution was transferred to a falcon tube, and 4 ml of medium was added. The cells were evenly distributed inside the medium using diligent pipetting. The falcon tube was then exposed to 5 minutes of centrifugation at 1500 rpm.

After centrifugation, the supernatant was carefully sucked off using a pipette. 1 mL of new media was added to the pellet to create ideal circumstances for the cells, and the cells were pipetted homogeneously once more. 9 mL of media was added to a cell culture flask to encourage cell development, followed by the previously scattered cells. The flask was thoroughly checked under a microscope before proceeding to ensure the existence of live and healthy cells. Following the microscopic examination, the flasks were incubated at 37°C, with a controlled environment of 5% CO_2 and sufficient humidity.

Subculturing

Under a microscope, the cellular morphology of the flask was carefully examined. It was established that the cells were ready for passage when they achieved a 70-80% density. A serological pipette was used to remove the old media from the flask. 3 mL of 2X trypsin-EDTA was added to detach and separate the cells from the flask surface.

Washing the flask surface gently collected the cells, which were then transferred to 15 mL Falcon tubes. The tubes were centrifuged at 1500 rpm for 5 minutes before carefully removing the supernatant. To resuspend the cell pellet, 2 mL of media was added, and the cells were pipetted homogeneously.

Each flask was filled with 9 mL of media to create new cell culture flasks. The cells were now uniformly dispersed throughout the media and split among the flasks. A final check under the microscope was performed to confirm the number and condition of cells in each flask. The flasks were then incubated at 37°C with a 5% CO_2-controlled environment and sufficient humidity. The 14th passage was used in developing the AD model.

Freezing

The 75 cm^3 flask, which had attained 70-80% confluency, was chosen, and the medium aspirated. The cells were rinsed with phosphate-buffered saline (PBS). The flask was then filled with 3 ml of trypsin and put in an incubator for 3 minutes to allow the trypsin to detach the cells from the flask surface.

Following trypsinization, the cells in the flask were moved to a 15 ml falcon tube suspended in 5 ml of DMEM F12. After that, the Falcon tube was centrifuged at 1500 rpm for 5 minutes. Consequently, a pellet containing the collected cells formed at the bottom of the tube.

In a freezing medium, the cell pellet was thoroughly resuspended. The resuspended cells were separated into 1 mL cryovials to ensure even distribution. For the first 4 hours, the cryovials holding the cells were stored in a -20°C freezer. Following this first chilling period, the cryovials were moved and kept at -80°C in a long-term storage facility. This ensured that the cells would be preserved for future use.

Cell counting

A serological pipette was used to completely remove the old medium from the flask, which was carefully observed under a light microscope. The cells were then treated with 3 ml of 2X trypsin-EDTA and incubated for 3 minutes in the incubator. 6 ml of medium was added back into the flask after confirming the successful separation

of cells from the flask surface under a light microscope and ensuring no cells remained attached.

The cells were gently washed off the flask surface before being transferred to 15 ml falcon tubes. The falcon tubes were then centrifuged for 5 minutes at 1500 rpm. The supernatant was gently removed using a pipette, taking care not to disturb the resulting cell pellet. To resuspend the cells,19 ml medium was added. The falcon tube was securely closed and inverted several times to ensure the cells were distributed evenly throughout the medium. 50µl of the cell solution was transferred to a microcentrifuge tube, and 50µl of trypan blue solution was added to determine cell viability. To ensure proper mixing, the mixture was pipetted thoroughly. A Neubauer slide was used for cell counting, and 10µl of the cell trypan blue solution was added to both wells. Under a light microscope, viable cells were counted within 8 squares, and the number of cells in each square was averaged. The number of cells per mL was calculated by multiplying this value by the dilution factor 2.

3.5. Determination of Cytotoxicity by MTT Method

MTT assay measures cellular metabolic activity to assess cell viability, cell proliferation and cytotoxicity, and cell activation and cell proliferation in response to growth factors, cytokines and nutrients. This colorimetric analysis is mainly based on the reduction of 3-(4,5-dimethylthiazol-2-yl)-2,5-diphenyltetrazolium bromide, a yellow tetrazolium salt, into purple-colored formazan crystals by metabolically active cells. Living cells contain NADPH-dependent oxidoreductase enzymes that reduce MTT to formazan (153). The purple crystals formed are dissolved in DMSO. The darker the solution, the greater the number of viable, metabolically active cells. The amount of formazan produced is directly proportional to the number of viable cells. The absorbance was then measured at 570 nm by spectrophotometer.

Pre-assay preparation

Weigh out 15 mg of 3-(4,5-dimethylthiazol-2-yl)-2,5-diphenyltetrazolium bromide, dissolve in 3 ml of PBS and complete to 30 ml with 27 ml of medium. This way, 0.5 mg/ml of MTT solution is prepared. The prepared solution should be stored in the dark and be stable for 24 hours.

Assay protocol

Cell seeding was carried out in a 96-well plate, with 20,000 cells in 100 μl of the medium. The cells were then allowed to incubate at 37°C with 5% CO_2 for 24 hours, allowing them to adhere to the plate surface and proliferate. After carefully removing the medium containing the cells, a fresh medium containing different concentrations of application substances (including control with no substance) was added to the wells. The plate was placed back into the incubator for another 24 hours at 37°C with 5% CO_2. For the experiment, serial dilutions of aluminum hydroxide, $Al(OH)_3$ (ranging from 0-2500 μM), metformin hydrochloride (ranging from 0-1000 μM), naltrexone hydrochloride (ranging from 0-150 μM), and dihydrolipoic acid (ranging from 0-100 μM) were prepared by dissolving them in the respective medium and added to each well accordingly.

At the end of the incubation period, the treatment solutions were aseptically removed, and 100μl of MTT solution was added to each well. The MTT solution is light-sensitive, so the experiments were conducted in a dark environment. The plates with the MTT solution were then incubated for 3 hours. After the incubation, the MTT solution was carefully removed from the wells. To dissolve the purple-colored formazan crystals that formed due to the reaction, 150 μl of DMSO was added to each well and mixed on a plate shaker for 5-10 minutes. Finally, the absorbance values of the wells were measured at 570 nm using a spectrophotometer or a plate reader.

Calculating the results

The experiments were repeated several times at different concentrations to ensure accurate and reliable results for each substance. The optical density (OD) values obtained from the control group's cells were averaged to create a baseline value representing 100% cell viability. Using this as a baseline, the inhibitory concentration 20 (IC20), inhibitory concentration 30 (IC30), and inhibitory concentration 50 (IC50) values for the experimental groups were calculated as percentages of the cell viability of the control group.

The IC20 value represents the concentration of substances that results in a 20% decrease in cell viability. In contrast, the IC50 value represents the concentration of substances that results in a 50% decrease in cell viability. These values provide

important insights into the efficacy and impact of the substances on cell viability, allowing for comparisons and determination of inhibitory effects.

3.6. Alzheimer's disease modelling in SH-SY5Y cell line

Neuroblastoma cells have become a common tool for studying AD in laboratory settings. These cells are derived from embryonic neuronal cells in neuroblastoma cancer and can remain undifferentiated until activated. These cells resemble juvenile cholinergic neurons in their undifferentiated state. However, with induction, they can grow into fully-fledged cholinergic cells. AD is characterized by decreased acetylcholine levels caused by increased acetylcholinesterase activity in the brain's hippocampus. Neuroblastoma cells enable researchers to explore these unique aspects of Alzheimer's disease while facilitating medication development efforts. Neuroblastoma cells can be directed to develop into several types of neuronal cells, including cholinergic or dopaminergic neurons, by using differentiation agents such as retinoic acid or phorbol esters.

Furthermore, neuroblastoma cells have been used to investigate Alzheimer's disease-related events, such as the effect of glyceraldehyde on Alzheimer's pathogenesis. The cells display lower $A\beta$ levels of enhanced tau phosphorylation. It has elucidated the mechanisms underlying the prevention of A pathology by inhibiting GSK-3β.

3.7. Preparation of xenobiotics stock solutions and dilutions

Aluminum

362μM Aluminum hydroxide: 127μl Al (OH)$_3$ were added to 45ml DMEM F12

Metformin:

1,000μM Metformin hydrochloride stock solution: 1.27mg metformin HCl were dissolved in 1.27ml of DPBS, then completed by 6.40ml DMEM-F12.

100μM concentration: Dilute stock solution with DMEM F12 (1:10).

10μM concentration: (i) Dilute 100μM concentration with DMEM F12 (1:10) (ii) in another falcon dilute 100μM concentration with DIFFM1 (1:10).

0.25µM concentration: (i) Dilute 10uM concentration with DIFFM1(1:40). (ii) in another falcon dilute 10µM concentration with DMEM F12 (1:40).

Naltrexone

100000ng/ml Naltrexone hydrochloride stock solution: 0.69mg naltrexone dissolved in 6.9ml DMEM F12.

1000ng/ml concentration: Dilute stock solution with DMEM F12 (1:10).

100ng/ml concentration: (i) Dilute 1000ng/ml concentration with DMEM F12 (1:10) (ii) in another falcon dilute 1000ng/ml concentration with DIFFM1 (1:10).

2.5 ng/ml concentration: (i) Dilute 100ng/ml concentration with DIFFM1(1:40). (ii) in another falcon dilute 100ng/ml concentration with DMEM F12 (1:40).

Dihydrolipoic acid

1500µM Dihydrolipoic acid stock solution: 2.5ml DMEM F12 added to 17.47µl dihydrolipoic acid.

500µM concentration: Dilute stock solution with DMEM F12 (1:3).

100µM concentration: (i) Dilute 500µM concentration with DMEM F12 (1:10) (ii) in another falcon dilute 500µM concentration with DIFFM1 (1:10).

0.1µM concentration: (i) Dilute 100µM concentration with DIFFM1(1:40). (ii) in another falcon dilute 100µM concentration with DMEM F12 (1:40).

3.8. Study groups and differentiation modeling

The following study groups were planed (Table 3.1) within the scope of this thesis. Incubation time was applied as 7 days for all analyzes in all groups. According to the results obtained from MTT experiments, IC20 doses were used for Al and concentrations that did not change cell viability and reflected the plasma concentration of each chemical used for naltrexone, metformin and dihydrolipoic acid. For each group, 3 flasks were assigned. At day zero, one million cells were seeded in each $75cm^2$ flask. Each flask was then labeled according to study groups. The flasks were incubated at 37°C, 5% CO_2 for 24 hours. After the incubation period, the protocol of differentiation and exposure was followed according to Table 3.2.

Table 3.1. Study groups.

Control (n=3):	Control cells were grown in a growth medium, and medium change was done every 48 hours. If the flask was more than 80% confluent, subculturing with the same number of cells was performed.
Al group (n=3):	Al group was exposed to Al(OH)$_3$ (362 μM).
Neuroprotective group (n=3):	Nal group was exposed to naltrexone (2.5 ng/ml).
	Met group was exposed to metformin (0.25μM).
	DHL group was exposed to dihydrolipoic acid (0.1 μM).
Al-Neuroprotective group (n=3):	Al-Nal group was exposed to naltrexone (2.5 ng/ml) + Al (362 μM).
	Al-Met group was exposed to metformin (0.25μM) + Al (362 μM).
	Al-DHL group was exposed to dihydrolipoic acid (0.1 μM) + Al (362 μM).
AD group (n=3):	Cells were differentiated by exposure DIFFM1 + DIFFM2
AD-Algroup (n=3):	Differentiated cells + Al (362 μM)
AD-Neuroprotective group (n=3):	Differentiated cells + naltrexone (2.5 ng/ml)
	Differentiated cells + metformin (0.25μM)
	Differentiated cells + dihydrolipoic acid (0.1 μM)
AD-Al-Neuroprotective (n=3):	Differentiated cells + Al (362 μM) + naltrexone (2.5 ng/ml)
	Differentiated cells + Al (362 μM) + metformin (0.25μM)
	Differentiated cells + Al (362 μM) + dihydrolipoic acid (0.1 μM)

Table 3.2. AD modeling and treatment

Study groups	Day 1	Day 2	Day 3	Day 4	Day 5	Day 6	Day 7
Control	Observation	Growth Medium	Observation	Subculture	Observation	Growth Medium	Pellet Removal
Neuroprotective	Observation	Observation	Neuroprotective	Observation	Observation	Observation	Pellet Removal
Al	Al	Observation	Observation	Observation	Observation	Observation	Pellet Removal
Al-Neuroprotective	Al	Observation	Neuroprotective	Observation	Observation	Observation	Pellet Removal
AD	DIFFM1	Observation	Observation	DIFFM2	Observation	Observation	Pellet Removal
AD-Al	DIFFM1+Al	Observation	Observation	DIFFM2+ Al+ Neuroprotective	Observation	Observation	Pellet Removal
AD-Al-Neuroprotective	DIFFM1+Al	Observation	Neuroprotective	DIFFM2+ Al+ Neuroprotective	Observation	Observation	Pellet Removal
AD-Neuroprotective	DIFFM1	Observation	Neuroprotective	DIFFM2+ Al+ Neuroprotective	Observation	Observation	Pellet Removal

On the first day, DIFFM1 and DMEM F12 medium were kept in a 37°C water bath for 1 hour before usage. Retinoic acid, which would be added to DIFFM1, was measured and kept in a dark place. Retinoic acid was added to DIFFM1 right before adding this medium to proper flasks. Al(OH)$_3$ was prepared at the concentration of 362μM. The old media were aspirated from the flasks, according to Table 3.2. To the flask labeled as Al, 9ml, DMEM-F12 containing 362μM, Al(OH)$_3$ was added. 9 ml

DIFFM1 with retinoic acid was added to AD and AD-neuroprotective flasks. To AD-Al and AD-Al-neuroprotective flasks, 9 ml containing retinoic acid and $Al(OH)_3$ (362μM) was added. The other groups were observed under a microscope.

On the second day, all the flasks were observed under a microscope. Old media was replaced with fresh and warm DMEM F12 in the control and neuroprotective group flasks.

On the third day, the proper concentration of each neuroprotective chemical was prepared in 1 ml of fresh and warm medium and added to the proper flask. The medium used to prepare the neuroprotective concentration was the same as the medium in the flasks.

On the fourth day, the medium in the flasks under differentiation protocol was completely replaced with fresh and warm DIFFM2. Besides having retinoic acid, this medium contained 2.5 ng/ml BDNF. Moreover, proper concentration of neuroprotective and Al was added to the medium according to the group configuration. The other groups were observed under a microscope.

On days 5 and 6, the flasks were carefully observed under a microscope; on the 7th day, the cell pellets were removed for further pathway analysis.

3.9. Cell lysis

Cells were treated with trypsin-EDTA after being treated with the required chemicals for 24 hours. A 3 mL solution of 2X trypsin-EDTA was added to the cells and incubated for 3 minutes. The cells were seen to detach from the flask surface under a light microscope, verifying that all cells were eliminated. The flask was filled with 6 mL of media to collect the cells. After being rinsed from the flask surface, the cells were transferred to 15 mL falcon tubes. After centrifuging the tubes at 1500 rpm for 5 minutes, the supernatant was carefully removed without disturbing the particle. Three washes of pre-chilled PBS were performed on the pellet. The pellet was resuspended in 1 mL of cold PBS before being transferred to 1.5 mL eppendorf tubes. The tubes were placed in a -80°C freezer for at least 30 minutes. The frozen cells were thawed by incubating the tubes in a 37°C water bath and vortexed once. This cycle of freeze-thaw was performed three times. The lysate was centrifuged at 15,000 rpm for 10 minutes at 2-8°C after the final thawing. The supernatant containing the desired

cellular components was carefully collected. The lysate was split into tiny aliquots and frozen at -80°C for future usage to guarantee long-term storage and integrity.

3.10. Fluorometric Intracellular ROS

The fluorometric intracellular ROS assay provides a sensitive, one-step fluorometric measurement to detect intracellular ROS in living cells following 1-hour incubation. ROS reacts with a cell-permeable sensor to form a fluorometric product proportional to the amount of ROS present. The amount of ROS is determined by measuring the fluorescence intensity of the product formed.

Assay Protocol

On the day of pallet removal, 10000 cells in 90μl per well from each study group were seeded in a black 96-well plate. The cell culture plate is incubated overnight in an incubator (37°C, 5% CO_2). Then, take 20 μl of the ROS determination reagent prepared at a 500X concentration. Dissolve it in 10 ml of assay buffer to obtain the master reaction mixture. Add 100 μl of the master reaction mix to each well. Incubate for 30 minutes to 1 hour at 37°C in the incubator. After the incubation period, measure the fluorescence values of the solutions in each well using excitation and emission wavelengths of 540 nm and 570 nm, respectively.

Calculation of results

The ROS amount calculated for the control wells is accepted as 100%, and the other wells' ROS amounts are calculated relative to the control.

3.11. Protein Determination

The methodology takes advantage of Coomassie® dye's natural ability to undergo color alteration when bound to proteins in an acidic environment, similar to the widely used Bradford method for protein quantification. When the dye binds, its maximum absorption wavelength shifts from 465 nm to 595 nm, accompanied by a significant change in color from brown to blue. The amount of protein may be estimated by measuring the absorbance at 595 nm since the absorbance value is directly proportional to the protein quantity.

Pre-assay Preparations

To ensure optimal performance, all the vials included in the kit were properly warmed to room temperature prior to commencing the assay. Following this, thorough mixing was achieved by vortexing the contents, and a brief centrifugation step was performed to ensure proper settling.

Sample dilutions, working Reagents and Standard preparations were meticulously prepared per the manufacturer's instructions (Cataloge No: 10005020). These steps were undertaken to maintain accuracy and reliability throughout the assay process.

Assay Protocol

The assay was done precisely according to manufacturer instructions: The samples were diluted with distilled water at a ratio of 1:5. A volume of 100 μl of the standard or diluted sample was added to the appropriate wells of a 96-well plate. In each well, 100 μl of assay reagent was added. The plate was incubated for 5 minutes at room temperature. The absorbance of the contents in each well was read at 595 nm using a spectrophotometer.

Calculation of results

A standard curve was plotted to calculate the protein amount of each sample. The results were reported as μg/ml (Figure 3.1.).

y = 0.0006x + 0.0386
$R^2 = 0.9963$
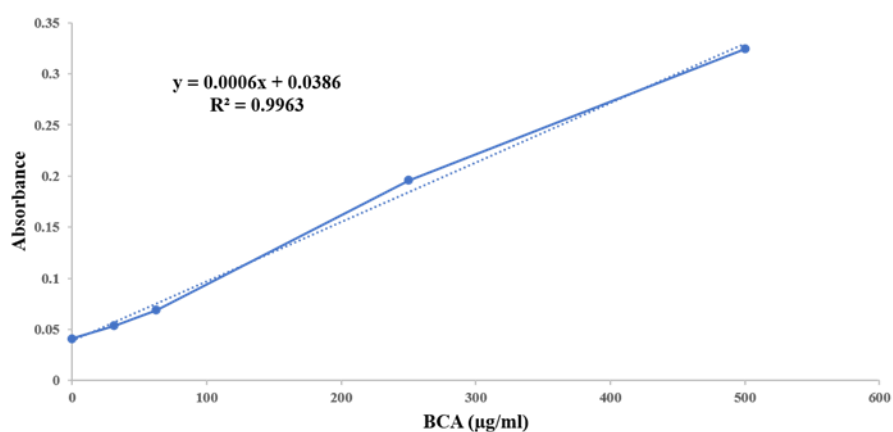
Figure 3.1. Protein calibration curve.

3.12. Protein Carbonyl Colorimetric Assay

Protein carbonylation is the most common and usually irreversible oxidative alteration of proteins. This alteration is chemically stable and crucial for carbonylated protein storage and detection. Many biochemical and analytical approaches for measuring protein carbonylation have been developed over the last thirty years. The most successful approach is the protein carbonyl (PCO) derivatization using 2,4-dinitrophenylhydrazine (DNPH) and subsequent spectrophotometric analysis. Because DNPH can react with carbonyl to form an adduct that absorbs at 366 nm, this test enables for global determination of PCO concentration.

Pre-assay Preparations

To ensure optimal performance, all the vials included in the kit were properly warmed to room temperature prior to commencing the assay. Following this, thorough mixing was achieved by vortexing the contents, and a brief centrifugation step was performed to ensure proper settling.

The hydrochloric Acid (HCl) 2.5M, 2,4-dinitrophenylhydrazine (DNPH), trichloroacetic acid (TCA) 20%, trichloroacetic acid (TCA) 10% and Ethyl acetate were meticulously prepared in accordance with the instructions provided by the manufacturer (Cataloge No: 10005020). These steps were undertaken to maintain accuracy and reliability throughout the assay process.

Assay Protocol

The assay was conducted precisely following the manufacturer's instructions: Two Eppendorf tubes were labeled for each sample, one as the sample and the other as the control. To each tube, 75 µl of the sample was added. To the sample Eppendorf tube, 300 µl of DNPH was added, while to the control Eppendorf tube, 300 µl of 2.5M HCl was added. The tubes were incubated for 1 hour in the dark at room temperature, with intermittent vortexing every 15 minutes. Following the incubation, 375 µl of 20% TCA was added to each Eppendorf tube, and the tubes were kept on ice for 5 minutes. Subsequently, they were centrifuged for 10 minutes at 15,000 rpm, and the supernatant was discarded. Next, 375 µl of 10% TCA was added to each Eppendorf tube, and the tubes were kept on ice for 5 minutes. They were centrifuged again for 10 minutes at 15,000 rpm, and the supernatant was discarded. 375 µl of a 1:1 mixture of ethyl acetate and ethanol was added to each Eppendorf tube. The tubes were vortexed and then

centrifuged for 10 minutes at 15,000 rpm. The supernatant was removed. The pellets in the Eppendorf tubes were resuspended with 200 µl of guanidine hydrochloride by vortexing. The tubes were then centrifuged at 15,000 rpm for 10 minutes. From the resulting supernatant, 150 µl was transferred to two wells of a 96-well plate. The absorbance of the contents in the wells was measured at a wavelength of 370 nm using a plate reader.

Calculating the results

I subtracted the average absorbance of controls from samples (CA). Then the following equation to calculate the protein carbonyl was used:

$\{(CA)/(0.011\mu M-1)\}$ (200µl/75µl) = protein carbonyl (nmol/ml)

3.13. GSH (Glutathione) ELISA Assay

The Competitive-ELISA concept is used in this kit. This kit includes a pre-coated micro-ELISA plate with GSH. During the reaction, GSH in the sample or standard competes for GSH-specific sites on the Biotinylated Detection Ab. Surplus conjugate and unbound sample or standard are washed away, and each microplate well is treated with Avidin-Horseradish Peroxidase (HRP) conjugate. Then, in each well, a TMB substrate solution is applied. When stop solution is added to the enzyme-substrate reaction, the color changes from blue to yellow. 450 nm wavelength were used to measure the OD. The concentration of GSH in the tested samples may be determined by comparing the samples' OD to the standard curve.

Pre-assay Preparations

To ensure optimal performance, all the vials included in the kit were properly warmed to room temperature prior to commencing the assay. Following this, thorough mixing was achieved by vortexing the contents, and a brief centrifugation step was performed to ensure proper settling.

The standard dilution, wash buffer, biotinylated detection antibody working solution, and HRP conjugate working solution were meticulously prepared per the manufacturer's instructions (Cataloge No: E-EL-0026). These steps were undertaken to maintain accuracy and reliability throughout the assay process.

Assay Protocol

The assay was done precisely according to manufacturer instructions: To each assigned well, 50 µl of the sample or standard and 50 µl of biotinylated detection antibody working solution were added. The plate was covered and incubated in a 37°C incubator for 45 minutes. After the 45-minute incubation, the plate was washed three times with the wash buffer, ensuring complete removal of any excess wash buffer. Subsequently, 100 µl of HRP Conjugate working solution was. After covering, the plate was kept in a 37°C incubator for 30 minutes. The plate was washed five times with the wash buffer, ensuring thorough removal of any excess wash buffer. Next, 90 µl of the substrate was added to the plate. The plate was covered, kept away from light, and placed in a 37°C incubator for 15 minutes to allow for the substrate reaction to occur. 50 µl of the stop solution was added to the plate to halt the reaction. Finally, the absorbance of the contents in the plate was measured at 450 nm using a spectrophotometer.

Calculating the results

The absorbance value of the blank well is subtracted from the absorbance values of the standard and sample wells. The standard curve is obtained using the 4-parameter algorithm with the Molecular Devices-Softmax® program. GSH levels in the samples are calculated using the standard curve equation. Results are expressed µg/mg (Figure 3.2.).
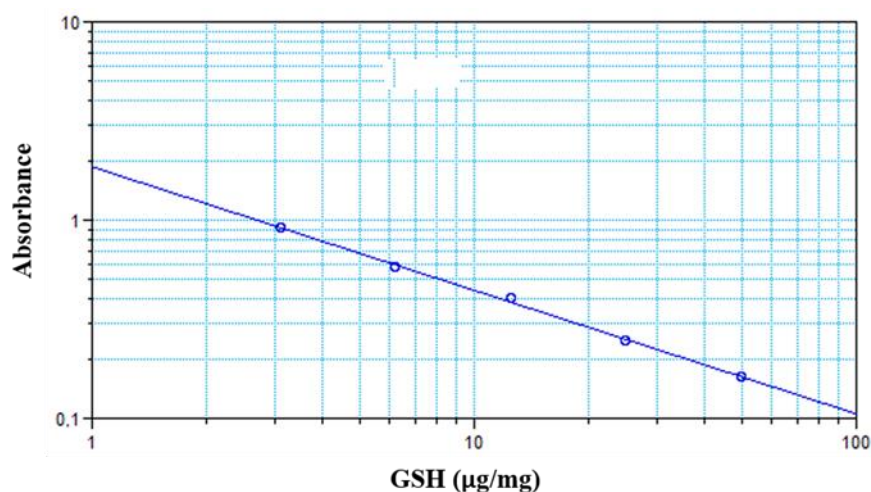

Figure 3.2. GSH calibration curve.

3.14. Lipid Peroxidation (TBARS) Assay

It is based on the colorimetric measurement of the malondialdehyde (MDA) – Thiobarbituric acid (TBA) complex formed by naturally occurring MDA and TBA reaction by lipid peroxidation under high temperature and acidic conditions.

Pre-assay Preparations

To ensure optimal performance, all the vials included in the kit were properly warmed to room temperature prior to commencing the assay. Following this, thorough mixing was achieved by vortexing the contents, and a brief centrifugation step was performed to ensure proper settling.

The thiobarbituric acid, TBA-acetic acid, TBA sodium hydroxide, TBA-malondialdehyde, TBA SDS solution and color reagent were meticulously prepared by the instructions provided by the manufacturer (Cataloge No: 10009055). These steps were undertaken to maintain accuracy and reliability throughout the assay process.

Assay Protocol

The assay was done precisely according to manufacturer instructions: First, it was ensured that all reagents, solutions, and samples were at room temperature. Tubes were labeled for both the samples and standards. In the sample tubes, 50 µl of the tested sample and 50 µl of a 5 µM standard solution were added to each sample tube. Separate tubes designated for standards were filled with 100 µl of the appropriate standard solutions. To each tube, 4 ml of the color reagent was added, and the tubes were securely capped. They were then placed in boiling water and incubated for 60 minutes. After the boiling step, the tubes were carefully transferred from the boiling water to an ice bath and cooled for 10 minutes. Following the cooling period, the tubes were centrifuged at 1600 rpm for 10 minutes to separate any precipitates or debris. Once centrifugation was complete, the tubes were allowed to cool completely at room temperature for approximately 30 minutes. Next, 150 µl of the supernatant from each tube was taken and poured into the appropriate wells of a 96-well plate.

Calculating the results

The samples' MDA levels are calculated using the standard curve obtained from the absorption values of the standard solutions. Results are expressed in nmol/mg protein (Figure 3.3.).
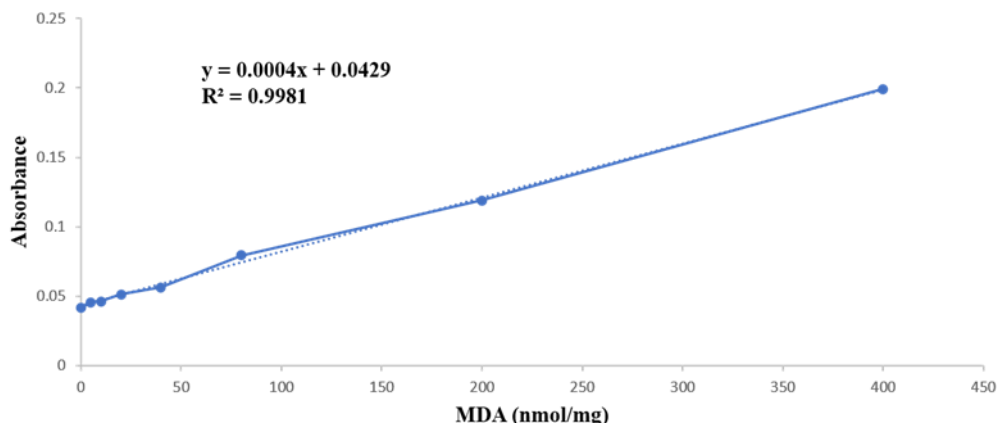
Figure 3.3. MDA calibration curve.

3.15. Human Glycogen Synthase Kinase 3 Beta (GSK-3β) ELISA Assay

It is a sandwich Elisa kit with a precoated microplate with a Human GSK-3β antibody. The Human GSK-3β in the sample or standard attached to this antibody. By administrating HRP and substrate, color develops, and the intensity of the color is measured.

Pre-assay Preparations

To ensure optimal performance, all the vials included in the kit were properly warmed to room temperature prior to commencing the assay. Following this, thorough mixing was achieved by vortexing the contents, and a brief centrifugation step was performed to ensure proper settling.

The standard dilution, wash buffer, biotinylated detection antibody working solution, and HRP conjugate working solution were meticulously prepared per the manufacturer's instructions (Cataloge No: E-EL-H2000). These steps were undertaken to maintain accuracy and reliability throughout the assay process.

Assay Protocol

The assay was conducted precisely per the manufacturer's instructions: A volume of 100 µl of the sample or standard was added to the designated plate, and the plate was covered. It was then placed in a 37°C incubator for a duration of 90 minutes. After incubation, the liquid was discarded, and 100 µl of the Biotinylated detection antibody working solution was added to the plate. The plate was covered again and placed in a 37°C incubator for 60 minutes. Following the second incubation, the plate

was washed three times with the wash buffer, ensuring complete removal of any excess wash buffer. Subsequently, 100 µl of the HRP conjugate working solution was added to the plate. The plate was covered and incubated for 30 minutes at 37°C. The plate was washed five times with the wash buffer, ensuring thorough removal of any excess wash buffer. A volume of 50 µl of the stop solution was added to the plate to stop the reaction. The absorbance of the contents in the plate was measured at 450 nm using a spectrophotometer.

Calculation of result

The absorbance value of the blank well is subtracted from the absorbance values of the standard and sample wells. The standard curve is obtained using the 4-parameter algorithm with the Molecular Devices-Softmax® program. GSK-3β levels in the samples are calculated using the standard curve equation. Results are expressed in ng/mg. (Figure 3.4.).
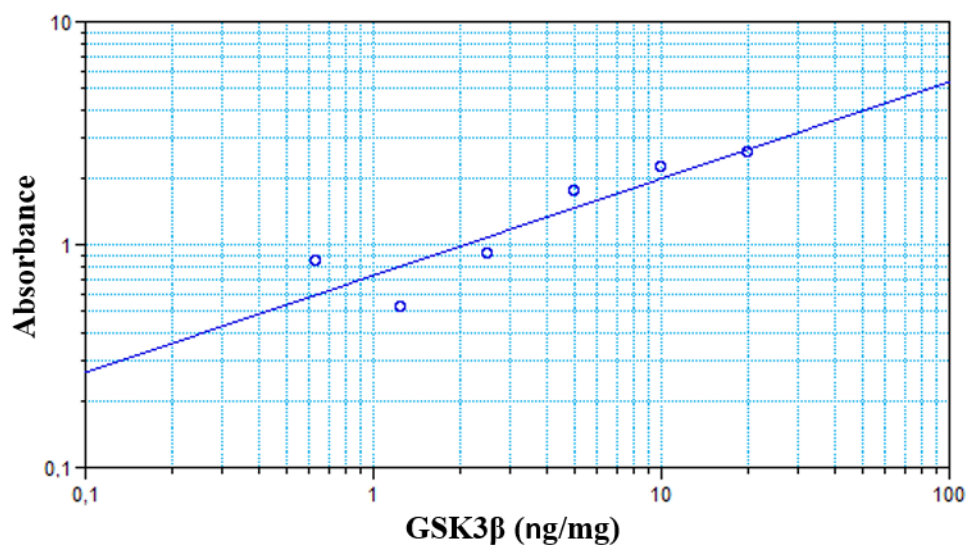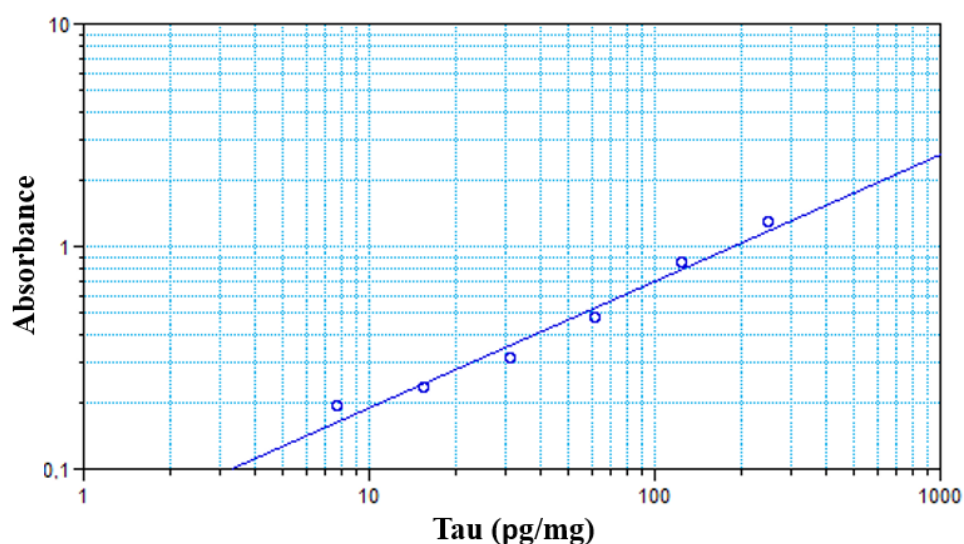

Figure 3.4. GSK-3β calibration curve.

3.16. Human MAPτ (Microtubule Associated Protein Tau/Tau Protein) ELISA Assay

It is a sandwich Elisa kit, with a precoated microplate with Human MAPτ antibody. The Human MAPτ in the sample or standard attaches to this antibody. By administrating HRP, substrate color develops, and the intensity of color is measured.

Pre-assay Preparations

To ensure optimal performance, all the vials included in the kit were properly warmed to room temperature prior to commencing the assay. Following this, thorough mixing was achieved by vortexing the contents, and a brief centrifugation step was performed to ensure proper settling.

The standard dilution, wash buffer, biotinylated detection antibody working solution, and HRP conjugate working solution were meticulously prepared per the manufacturer's instructions (Cataloge No: E-EL-H0948). These steps were undertaken to maintain accuracy and reliability throughout the assay process.

Assay Protocol

The assay was performed precisely following the instructions provided by the manufacturer: The assigned plate was carefully filled with 100 µl of the sample or standard. The plate was then placed in a 37°C incubator for 90 minutes for proper incubation. After the 90-minute incubation period, the liquid in the plate was discarded. Subsequently, 100 µl of the Biotinylated detection antibody working solution was added to the same plate, ensuring a secure seal. The plate was then returned to the 37°C incubator for 60 minutes to facilitate binding. To ensure a thorough washing step, the plate was rinsed three times with wash buffer, ensuring the complete removal of any excess wash buffer with each rinse. After washing, 100 µl of the HRP Conjugate working solution was added to the plate. The plate was securely covered and placed back into the 37°C incubator for 30 minutes. The plate was subjected to another round of washing by rinsing it five times with wash buffer, ensuring thorough removal of any excess wash buffer. Subsequently, 90 µl of the substrate reagent was added to the plate, ensuring a proper seal. The plate was then placed in a dark environment within the 37°C incubator for 15 minutes for the proper substrate reaction.

50 µl of the stop solution was added to the plate to halt the reaction. Finally, the absorbance was measured at 450 nm to obtain the desired readings, and the results were analyzed accordingly.

Calculation of result

The absorbance value of the blank well is subtracted from the absorbance values of the standard and sample wells. The standard curve is obtained using the 4-parameter algorithm with the Molecular Devices-Softmax® program. Tau levels in the samples are calculated using the standard curve equation. Results are expressed in pg/mg. (Figure 3.5.).

Figure 3.5. Tau calibration curve

3.17. Human RAC-alpha serine/threonine-protein kinase (AKT1) ELISA Assay

It is a sandwich Elisa kit with a precoated microplate with an AKT1 antibody. The AKT1 in the sample or standard attach to this antibody. By administrating HPR and substrate, color develops, and the intensity of color is measured.

Pre-assay Preparation

To ensure optimal performance, all the vials included in the kit were properly warmed to room temperature prior to commencing the assay. Following this, thorough mixing was achieved by vortexing the contents, and a brief centrifugation step was performed to ensure proper settling.

The standard dilution and wash buffer were meticulously prepared following the instructions provided by the manufacturer (Cataloge No: MBS2883458). These steps were undertaken to maintain accuracy and reliability throughout the assay process.

Assay Protocol

The assay was meticulously conducted in strict adherence to the manufacturer's instructions: Prior to starting the assay, it was ensured that all reagents, solutions, and samples were at room temperature. Standards were added to the designated wells of a 96-well plate, each receiving 50 µl of the appropriate standard solution. Subsequently, 50 µl of streptavidin-HRP was added to the standard wells. Sample wells were prepared by adding 40 µl of the sample, followed by adding 10 µl of anti-AKT1 antibody and 50 µl of streptavidin-HRP to each sample well. The plate was covered with a sealer and placed in a 37°C incubator for 60 minutes, allowing for proper incubation. After the incubation period, the plate was washed five times with wash buffer, ensuring complete removal of the wash buffer from the plate by tapping it on paper towels. Subsequently, 50 µl of substrate solution A and 50 µl of substrate solution B were added to each well. The plate was again covered with a sealer and kept in the dark for 10 minutes at 37°C to facilitate the reaction.

50 µl of stop solution was added to each well to stop the reaction. The absorbance of the contents in the wells was then measured at 450 nm using a spectrophotometer.

Calculation of results

The absorbance value of the blank well is subtracted from the absorbance values of the standard and sample wells. The standard curve is obtained using the 4-parameter algorithm with the Molecular Devices-Softmax® program. AKT levels in the samples are calculated using the standard curve equation. Results are expressed in ng/mg. (Figure 3.6.).
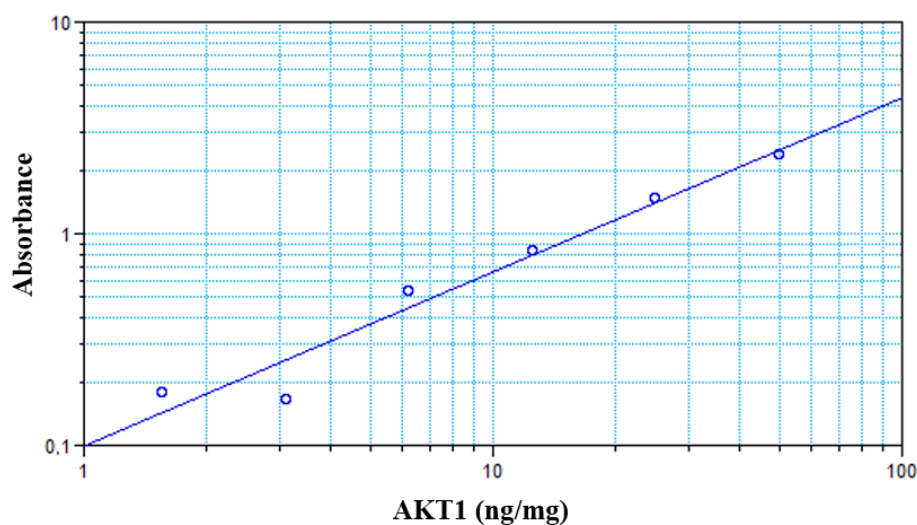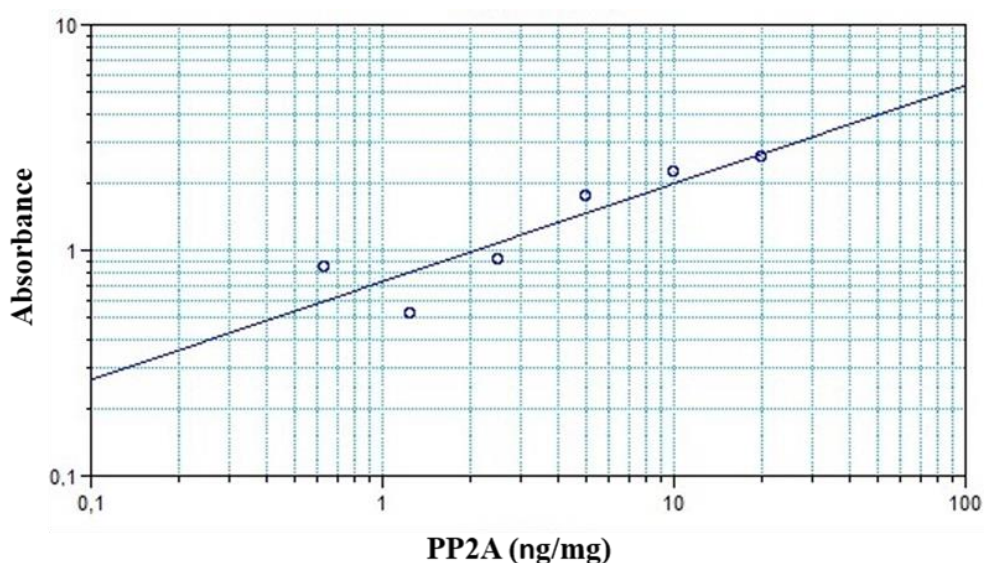
Figure 3.6. AKT calibration curve.

3.18. Human Protein Phosphatase 2A (PP2A) ELISA Assay

It is an Elisa kit with a precoated microplate with a PP2A antibody. The PP2A in the sample or standard attach to this antibody. By administrating HPR and substrate color develops, and the intensity of color is measured.

Pre-assay Preparation

To ensure optimal performance, all the vials included in the kit were properly warmed to room temperature prior to commencing the assay. Following this, thorough mixing was achieved by vortexing the contents, and a brief centrifugation step was performed to ensure proper settling. The standard dilution and wash buffer were meticulously prepared following the instructions provided by the manufacturer (Cataloge No: E6870Hu). These steps were undertaken to maintain accuracy and reliability throughout the assay process.

Assay Protocol

The assay was meticulously performed following the instructions provided by the manufacturer: It was ensured that all reagents, solutions, and samples were at room temperature before starting the assay. Standards were added to the designated wells of a 96-well plate, with each well receiving 50 µl of the appropriate standard solution. Following that, 50 µl of streptavidin-HRP was added to the standard wells. Sample wells were prepared by adding 40 µl of the sample, followed by adding 10 µl of anti-

PP2A antibody and 50 µl of streptavidin-HRP to each sample well. The plate was covered with a sealer to ensure proper sealing and incubated in a 37°C incubator for 60 minutes. After the incubation, the plate was washed five times with wash buffer, ensuring thorough removal of the wash buffer by tapping the plate on paper towels. Subsequently, 50 µl of substrate solution A and 50 µl of substrate solution B were added to each well. The plate was again covered with a sealer and placed in the dark within a 37°C incubator for 10 minutes to facilitate the reaction. To halt the reaction, 50 µl of stop solution was added to each well. The absorbance of the contents in the wells was then measured at 450 nm using a spectrophotometer.

Calculation of results

The absorbance value of the blank well is subtracted from the absorbance values of the standard and sample wells. The standard curve is obtained using the 4-parameter algorithm with the Molecular Devices-Softmax® program. PP2A levels in the samples are calculated using the standard curve equation. Results are expressed in ng/mg. (Figure3.7.).

Figure 3.7. PP2A calibration curve.

3.19. Human Serine/threonine-protein phosphatase PP1-alpha catalytic subunit (PPP1CA) ELISA Assay

The microplate is pre-coated with APP1αC antibody. The enzyme-substrate reaction will cause color change in the presence of APP1αC, biotin, and avidin conjugated enzyme. The color change will be read at 450nm using a spectrophotometer.

Pre-assay Preparation

To ensure optimal performance, all the vials included in the kit were properly warmed to room temperature prior to commencing the assay. Following this, thorough mixing was achieved by vortexing the contents, and a brief centrifugation step was performed to ensure proper settling.

The standard dilution, Detection Reagent A and B and wash buffer were meticulously prepared in accordance with the instructions provided by the manufacturer (Cataloge No: MBS9428821). These steps were undertaken to maintain accuracy and reliability throughout the assay process.

Assay Protocol

The assay was meticulously performed following the instructions provided by the manufacturer: A volume of 100 µl from both the standards and samples was added to the desired wells. The plate was covered and placed in a 37°C incubator for a duration of 120 minutes to allow for proper incubation. After the 120-minute incubation period, the liquid in the wells was discarded. Subsequently, 100 µl of detection reagent A was added to each well. The plate was covered again and placed in a 37°C incubator for 60 minutes to facilitate the detection process. Following the incubation with detection reagent A, the wells were washed three times with wash buffer. 100 µl of detection reagent B was added to each well. Covered plate placed in a 37°C incubator for an additional 60 minutes. The wells were washed five times with wash buffer. Any remaining wash buffer was removed, and 90 µl of substrate solution was added to each well. The plate was covered and kept in the dark within a 37°C incubator for 30 minutes to allow for the substrate reaction to occur. To halt the reaction, 50 µl of stop solution was added to each well. Finally, the absorbance of the contents in the wells was measured at 450 nm using a spectrophotometer.

Calculation of results

The absorbance value of the blank well is subtracted from the absorbance values of the standard and sample wells. The standard curve is obtained using the 4-parameter algorithm with the Molecular Devices-Softmax® program. PPP1AC levels in the samples are calculated using the standard curve equation. Results are expressed in ng/mg. (Figure 3.8.).
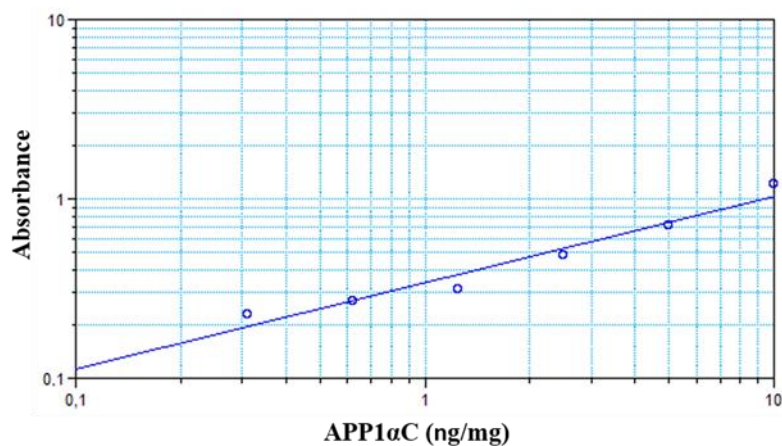

Figure 3.8. PPP1AC calibration curve.

3.20. Human Protein Wnt-5a ELISA Assay

It is an Elisa kit with a precoated microplate with a Wnt-5a antibody. The Wnt-5a in the sample or standard is attached to this antibody. By administrating HPR and substrate color develops, and the intensity of color is measured.

Pre-assay Preparation

To ensure optimal performance, all the vials included in the kit were properly warmed to room temperature prior to commencing the assay. Following this, thorough mixing was achieved by vortexing the contents, and a brief centrifugation step was performed to ensure proper settling.

The standard dilution, Detection Reagent A and B and wash buffer were meticulously prepared per the manufacturer's instructions (Cataloge No: MBS2886311). These steps were undertaken to maintain accuracy and reliability throughout the assay process.

Assay Protocol

The assay was meticulously performed following the instructions provided by the manufacturer: It was ensured that all reagents, solutions, and samples were at room temperature before starting the assay. A volume of 100 µl from either the standard or sample was added to each well. The plate was covered and placed in a 37°C incubator for a duration of 2 hours to allow for proper incubation. After the 2-hour incubation period, the liquid in the wells was discarded. Subsequently, 100 µl of detection reagent A was added to each well. The plate was covered again and kept in a 37°C incubator for 1 hour to facilitate detection. Following the incubation with detection reagent A, the wells were washed three times with wash buffer. Any remaining wash buffer was eradicated. Then, 100 µl of detection reagent B was added to each well. The plate was covered and kept in a 37°C incubator for an additional 1 hour. The wells were washed five times with a wash buffer. Any remaining wash buffer was eradicated. Subsequently, 90 µl of substrate solution was added to each well. The plate was covered and kept in the dark at a 37°C incubator for 20 minutes to allow for the substrate reaction to occur. To halt the reaction, 50 µl of stop solution was added to each well. Finally, the absorbance of the contents in the wells was measured at 450 nm using a spectrophotometer.

Calculation of results

The absorbance value of the blank well is subtracted from the absorbance values of the standard and sample wells. The standard curve is obtained using the 4-parameter algorithm with the Molecular Devices-Softmax® program. Wnt-5a levels in the samples are calculated using the standard curve equation. Results are expressed in ng/mg. (Figure 3.9.).
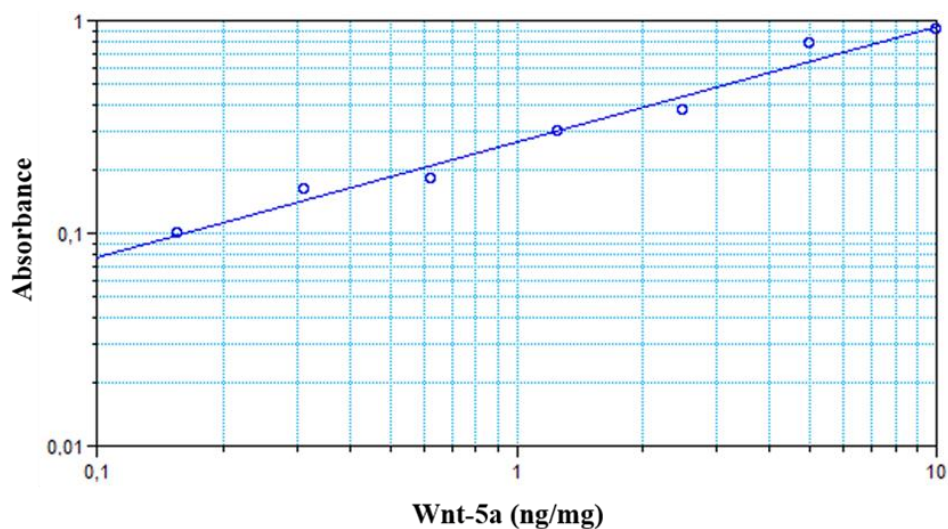
Figure 3.9. Wnt-5a calibration curve.

3.21. Antioxidant Assay (TAOC)

The principle of the assay is to decline or inhibit the formation of the oxidized products in the test environment. Production of (2,2'-azino-bis (3-ethylbenz-thiazoline-6-sulfonic acid) radical named ABTS•+ shows blue-green color when the absorbance is measured at 820, 650 and 734 nm. The suppression of ABTS•+ synthesis is proportionate to antioxidant concentration.

Pre-assay Preparation

To ensure optimal performance, all the vials included in the kit were properly warmed to room temperature prior to commencing the assay. Following this, thorough mixing was achieved by vortexing the contents, and a brief centrifugation step was performed to ensure proper settling.

The Trolox (2.25 mM) stock, standard dilution, wash buffer, Antioxidant Assay Buffer, Chromogen, Metmyoglobin, and Hydrogen peroxide were meticulously prepared following the instructions provided by the manufacturer (Cataloge No: 709001). These steps were undertaken to maintain accuracy and reliability throughout the assay process. The samples were diluted in the 1:2 ratio.

Assay protocol

In the wells designated for standards, 10 µl of the appropriate standards, 10 µl of metmyoglobin and 150 µl of chromogen, were added. In the wells designated for

the sample, a volume of 10 µl of the sample, 10 µl of metmyoglobin and 150 µl of chromogen, were added. To initiate the reaction, 40 µl of H_2O_2 was quickly added to each well. The plate was covered and placed on a shaker, and the contents were shaken for 5 minutes to ensure thorough mixing. Following shaking, the absorbance was measured at either 750 nm or 405 nm, depending on the specifications of the assay.

Calculation of results

Plot the standard curve using standard absorbance and concentration, then calculate the sample TAOC using the curve. (Figure 3.10.).

$y = -0.42x + 0.524$
$R^2 = 0.945$
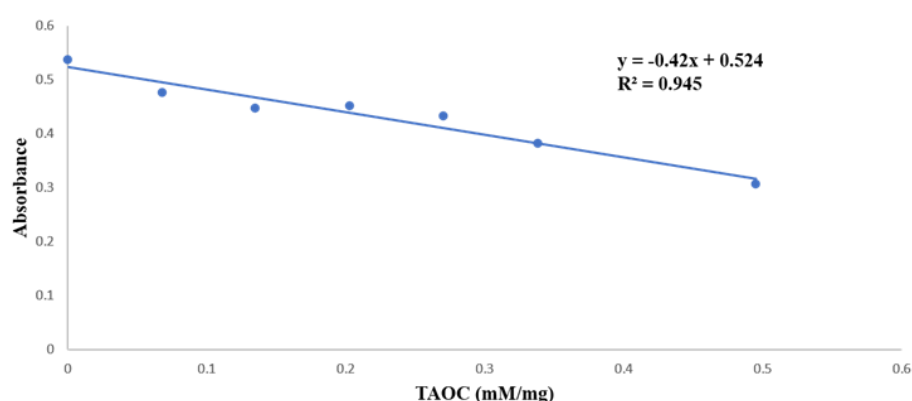
Figure 3.10. TAOC calibration curve.

3.22. Human CTNNβ1(Catenin, Beta 1) ELISA Assay

It is an Elisa kit with a precoated microplate with CTNNβ1 antibody. The CTNNβ1 in the sample or standard attach to this antibody. By administrating HPR and substrate color develops, and the intensity of color is measured.

Pre-assay Preparation

To ensure optimal performance, all the vials included in the kit were properly warmed to room temperature prior to commencing the assay. Following this, thorough mixing was achieved by vortexing the contents, and a brief centrifugation step was performed to ensure proper settling.

The standard dilution, Biotinylated Detection Ab Working Solution, HRP Conjugate Working Solution and wash buffer were meticulously prepared per the manufacturer's instructions (Cataloge No: E-EL-H0666). These steps were undertaken to maintain accuracy and reliability throughout the assay process.

Assay Protocol

The assay was done precisely according to manufacturer instructions: A volume of 100 µl of either the sample or standard was added to the assigned well. The plate was then covered and placed in a 37°C incubator for 90 minutes. After the 90-minute incubation period, the liquid in the well was discarded. Next, 100 µl of the Biotinylated detection antibody working solution was added to the same well. The plate was covered again and kept in a 37°C incubator for 60 minutes. Following the incubation with the Biotinylated detection antibody, the well was washed three times with the wash buffer, ensuring the complete removal of any excess wash buffer. Subsequently, 100 µl of the HRP Conjugate working solution was added to the plate. The plate was covered and kept in a 37°C incubator for 30 minutes. The plate was washed five times with the wash buffer, ensuring thorough removal of any excess wash buffer. Next, 90 µl of the substrate was added to the plate. The plate was covered, kept away from light, and placed in a 37°C incubator for 15 minutes to allow for the substrate reaction to occur. 50 µl of the stop solution was added to the plate to halt the reaction. Finally, the absorbance of the contents in the plate was measured at 450 nm using a spectrophotometer.

Calculation of results

The absorbance value of the blank well is subtracted from the absorbance values of the standard and sample wells. The standard curve is obtained using the 4-parameter algorithm with the Molecular Devices-Softmax® program. Wnt-5a levels in the samples are calculated using the standard curve equation. Results are expressed in ng/mg. (Figure 3.11.).
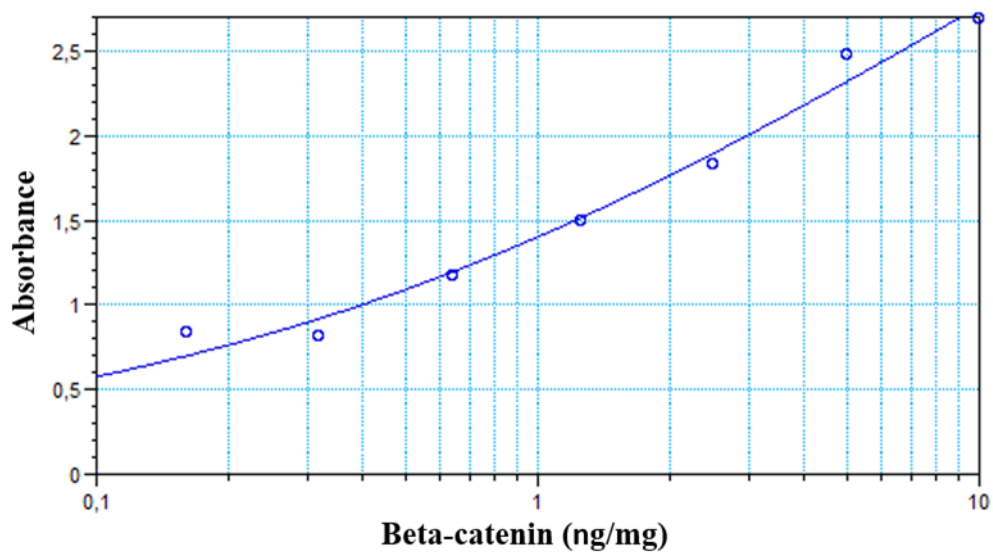
Figure 3.11. Beta-catenin calibration curve.

3.23. Statistical Analysis

The results were expressed as mean ± standard deviation (SD). GraphPad Prism® (version 8.2.1, GraphPad Software, San Diego, CA, USA) was used for statistical analysis. ANOVA analyzed the results, and the Mann-Whitney U test made pairwise comparisons. $p < 0.05$ were accepted as statistically significant.

4. RESULTS

4.1. Cell viability

SH-SY5Y cell viability was compared to the control group, and inhibitory concentrations 50, 30, and 20 (IC50, IC30, and IC20) were calculated following aluminum treatment.

The vitality of SH-SY5Y cells reduced dose-dependently when Al concentrations increased from 0 to 2500 μM (Figure 4.1.). The computed IC50, IC30, and IC20 values were 2201 μM, 975 μM, and 362 μM, respectively. Aluminum at a concentration of 362 μM (IC20) was utilized in all subsequent studies.
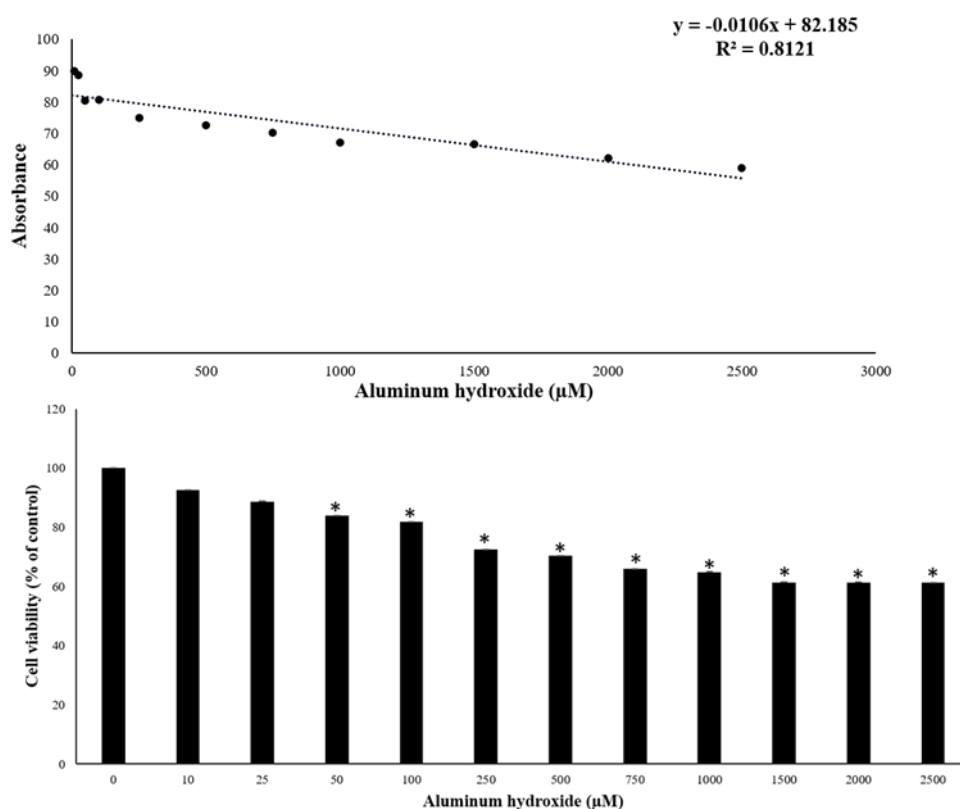
Figure 4.1. Cell viability was observed at different concentrations of aluminum.

*p < 0.001 represents a significant difference between control and individual treatment.

The viability of SH-SY5Y cells was reduced with increasing naltrexone dosages, as seen in figure 4.2. For naltrexone, the IC50, IC30, and IC20 values were discovered to be 23 μM, 15 μM, and 11 μM, respectively. It should be noted that naltrexone plasma concentrations have been observed to range from 1 to 3 ng/ml (154).

Instead of using lethal dosages, a concentration of 2.5 ng/ml was used in all tests to represent everyday exposure levels.
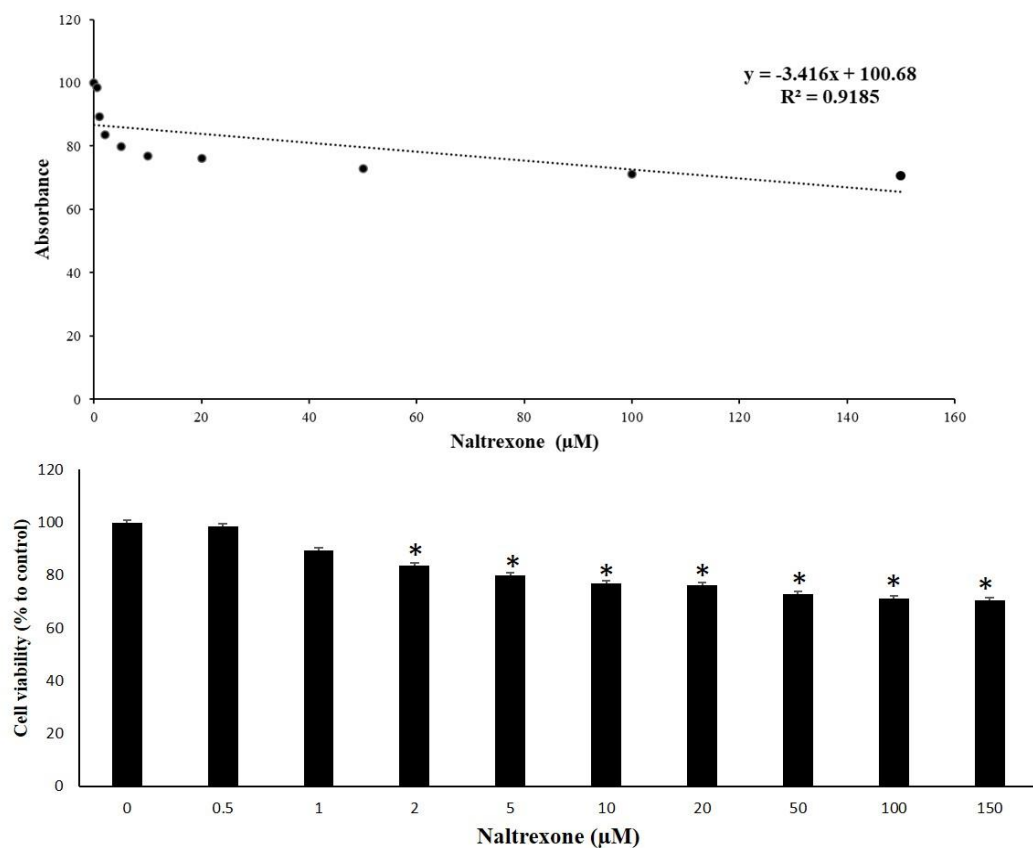

Figure 4.2. Cell viability was observed at different concentrations of naltrexone.

*p < 0.05 represents a significant difference between control and individual treatment. **p < 0.01 represents a significant difference between control and individual treatment.

IC50, IC30 and IC20 were -19.05 µM, -27.17 µM and -31.23 µM respectively. Figure 4.3. shows that increasing the doses of DHLA boosted the vitality of SH-SY5Y cells. The plasma concentration of DHLA has been observed to be 8.1 µM as the 0 to 5 µM doses did not show any toxicity, and considering the plasma concentration of DHLA, 0.1 µM dose were chosen throughout the studies rather than high concentrations so that the outcomes would be representative of exposure in daily life.
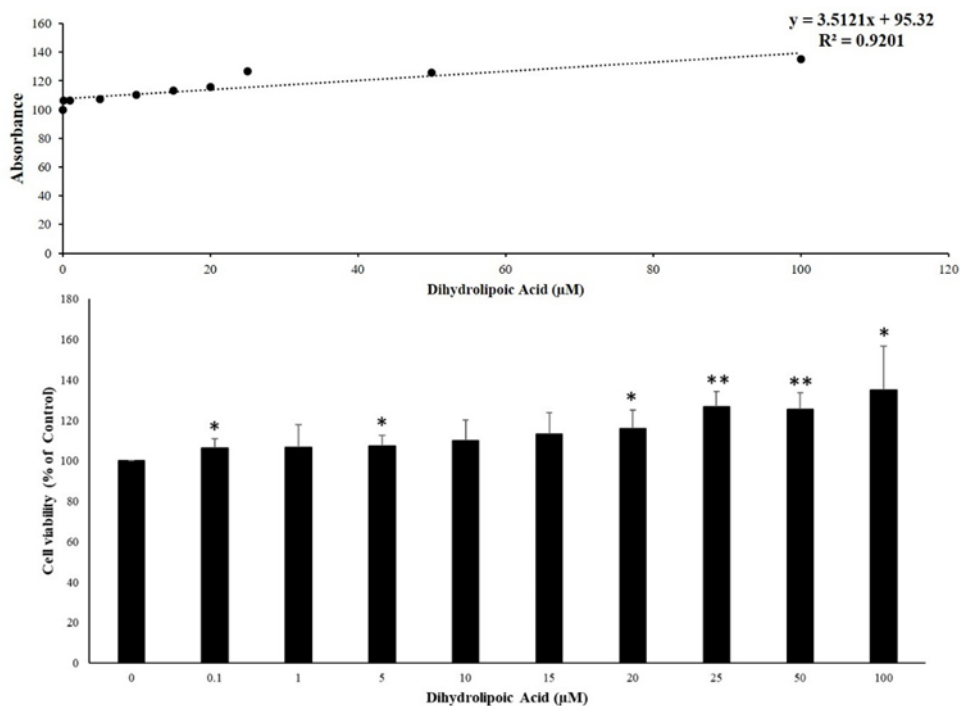
Figure 4.3. Cell viability was observed at different concentrations of dihydrolipoic acid.

*p < 0.05 represents a significant difference between control and individual treatment. **p < 0.01 represents a significant difference between control and individual treatment.

IC50, IC30 and IC20 were 14.47 µM, 8.84 µM and 6.02 µM respectively. Figure 4.4. shows that increasing the doses of metformin decreased the vitality of SH-SY5Y cells. The literature review regarding the plasma concentration of metformin has revealed no consistency in the bioavailability of metformin. Thus 0.25µM concentration was chosen for this study.
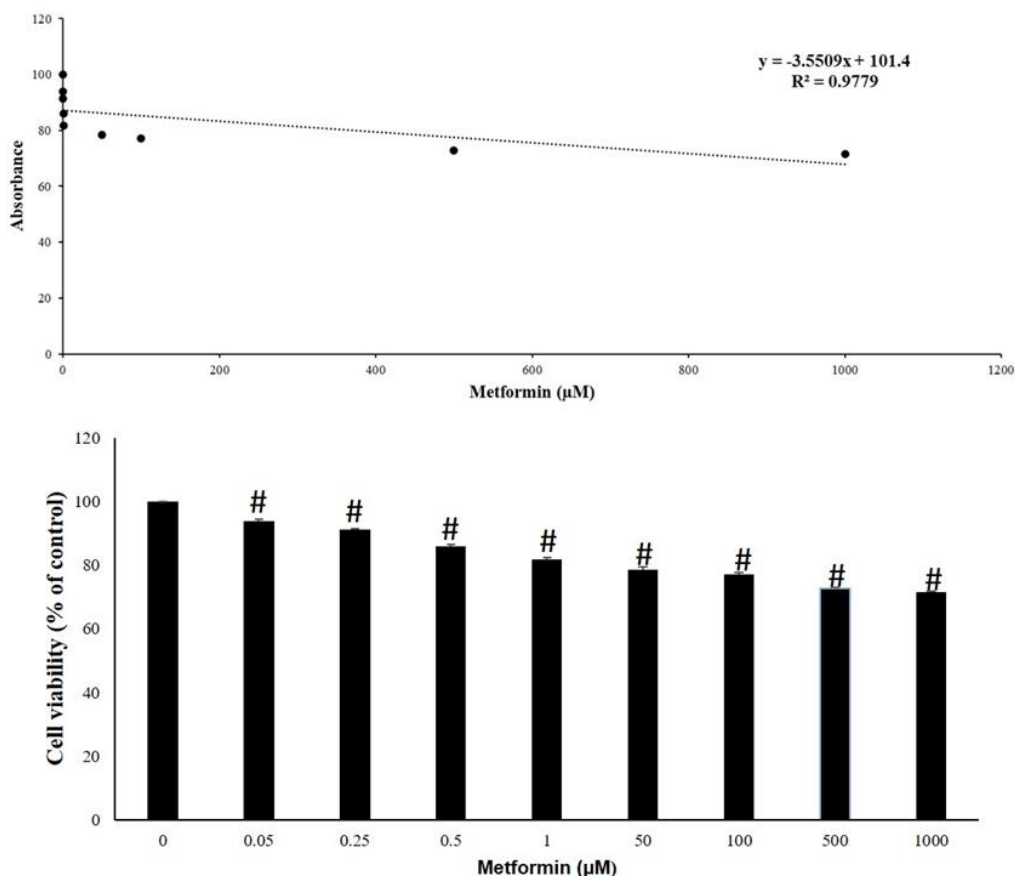
Figure 4.4. Cell viability was observed at different concentrations of metformin

#p < 0.001 represents a significant difference between control and individual treatment.

4.2. Findings of Naltrexone

4.2.1. ROS

ROS levels in the Al, AD and AD-Al groups were almost increased 2.5-fold versus the control. Exposure to Al increased the ROS production in the AD model by 1-fold. Treatment with naltrexone caused a significant decrease in ROS levels, especially in the AD-Al-Nal group; the drop is almost 3-fold, and for AD-Nal and Al-Nal groups, it is 2-fold compared to AD-Al, AD and Al groups, respectively (p < 0.001). The reactive oxygen species levels are shown in figure 4.5.
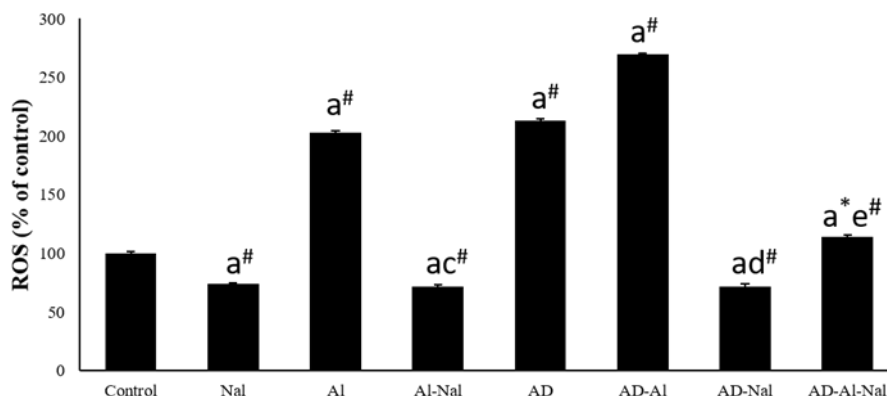
Figure 4.5. Intracellular ROS levels of study groups.

ROS: reactive oxygen species. The amount of intracellular ROS produced by the control cells was assumed to be 100%, and the amount of ROS produced by the other cells was calculated as % compared with the control. (a) Significant from the control group (c) Significant from the Al group (d) Significant from the AD group (e) Significant from the AD-Al group. #p <0.001.

4.2.2. Oxidative stress parameters

Figures 4.6, 4.7, 4.8 and 4.9 present an overview of the oxidative stress indicators. Except for the naltrexone group, glutathione levels varied throughout the groups as compared to the control group. Notably, the AD-Al group had the lowest GSH level, most likely attributable to the cells' reaction to oxidative stress (p<0.001). Al exposure in the AD-Al group resulted in a substantial 1-fold decrease in GSH levels compared to the AD group (p<0.001). The naltrexone-treated groups, on the other hand, showed a considerable increase in GSH levels, with a nearly 1-fold (30%) in AD-Nal and 4-fold in AD-Al-Nal compared to the AD and AD-Al groups, respectively (all, p<0.001). Furthermore, the GSH level in Al-Nal was about 1.3-fold higher than in the Al group (p<0.001) (Figure 4.6.).
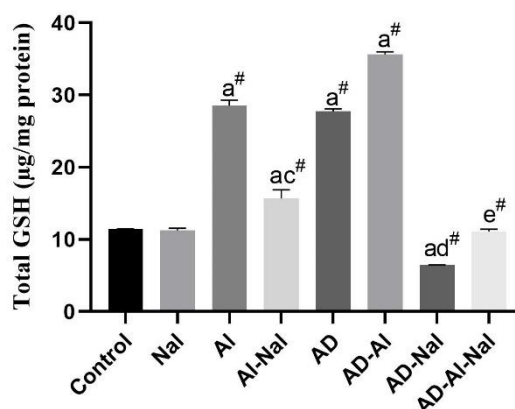
Figure 4.6. Glutathione levels.

(a) Significant from control group (b) Significant from Nal group (c) Significant from Al group (d) Significant from AD group (e) Significant from AD-Al group. #p < 0.001.

Malonaldehyde values, which indicate lipid peroxidation, were higher in the Al group (p<0.001) compared to the control group. Al exposure in the AD-Al group further elevated MDA levels, worsening AD. However, naltrexone therapy lowered MDA levels in the AD-Al-Nal group by 5.4-fold (p<0.001). Similarly, AD-Nal had a 2.5-fold lower MDA level than the AD group (p<0.001) (Figure 4.7.). The Al-Nal group displayed a remarkable 3.8-fold (285%) drop in MDA levels, demonstrating naltrexone's powerful ability to inhibit lipid peroxidation.
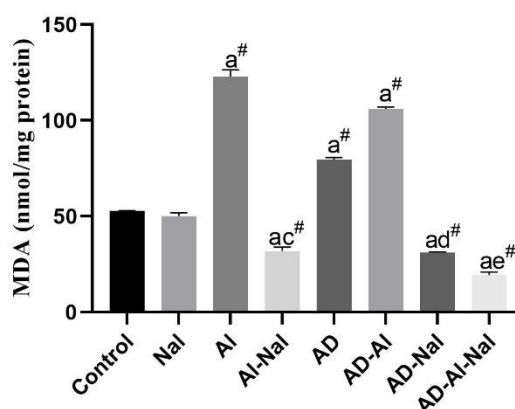

Figure 4.7. Malondialdehyde levels.

(a) Significant from control group (b) Significant from Nal group (c) Significant from Al group (d) Significant from AD group (e) Significant from AD-Al group. #p < 0.001.

Protein oxidation in all groups differed considerably from the control group. When the AD group was treated with Al (AD-Al), there was a 32% increase in protein

oxidation. The capacity of naltrexone to decrease carbonyl groups associated with protein oxidation was established. The AD-Al-Nal group had the lowest carbonyl group levels, almost 10-fold lower, demonstrating that naltrexone significantly inhibited protein oxidation (p<0.001). Furthermore, compared to the Al group, Al-Nal had a 2.5-fold reduction in carbonyl groups (p<0.001). Compared to the AD group, AD-Nal had a 5-fold decrease in carbonyl groups (Figure 4.8.).
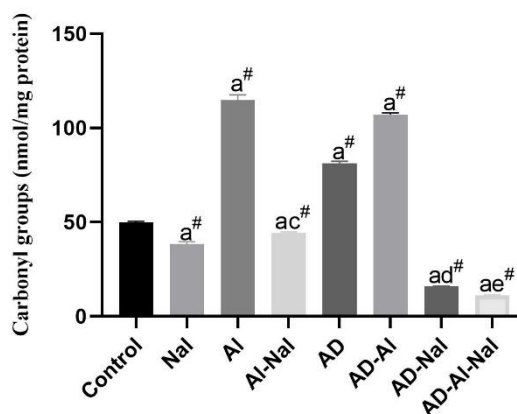

Figure 4.8. Protein carbonyl levels.

(a) Significant from control group (b) Significant from Nal group (c) Significant from Al group (d) Significant from AD group (e) Significant from AD-Al group. #p < 0.001.

The research groups' total antioxidant capacity (TAOC) values are shown in figure 4.9. Notably, the Al and AD groups had considerably lower TAOC levels than the others, showing that enhanced oxidative stress leads to Al toxicity and AD pathogenesis. The addition of naltrexone to the media, on the other hand, significantly increased the antioxidant capacity of the cells. TAOC levels rose 3.4-fold in the Al-Nal group, 4-fold in the AD-Al-Nal group, and 3.3-fold in the AD-Nal group compared to the Al, AD-Al, and AD groups, respectively (p<0.001).
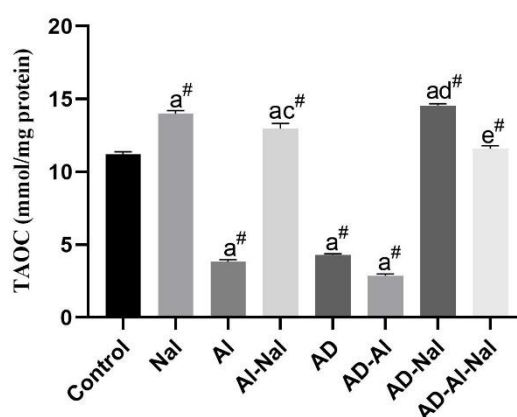
Figure 4.9. Total antioxidant capacity levels.

(a) Significant from control group (b) Significant from Met group (c) Significant from Al group (d) Significant from AD group (e) Significant from AD-Al group. #p < 0.001.

4.2.3. GSK-3β pathway

The AD-Al (282%), Al (179%), and AD (138%) groups had the highest levels of GSK-3β among all groups, substantially greater than the control group (p<0.001). However, naltrexone treatment decreased GSK-3β activity (Figure 4.10.). When compared to the AD-Al, AD, and Al groups, we found a 3.8-fold (74%) drop in GSK-3β levels in the AD-Al-Nal group, a 1.9-fold (48%) decrease in AD-Nal, and a 1.7-fold (43%) decrease in Al-Nal (p<0.001).
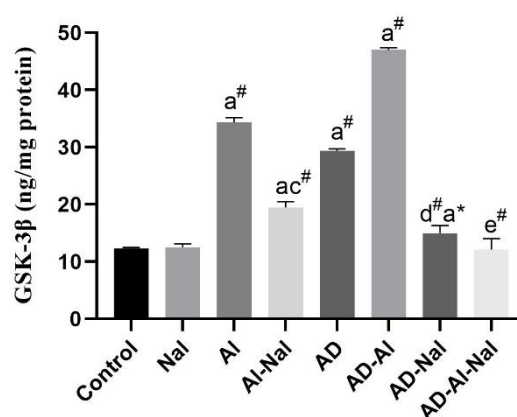

Figure 4.10. Glycogen synthase kinase-3 beta levels

(a) Significant from control group (b) Significant from Nal group (c) Significant from Al group (d) Significant from AD group (e) Significant from AD-Al group. *p < 0.05 and #p < 0.001.

The Al and AD-Al groups had the lowest PP2A levels ($p<0.001$). However, the PP2A levels in the naltrexone groups increased ($p<0.001$) (Figure 4.11.). Compared to the AD-Al, AD, and Al groups, the PP2A levels in the AD-Al-Nal, AD-Nal and Al-Nal groups rose 6.2-fold, 2.8-fold, and 2-fold, respectively ($p<0.001$).
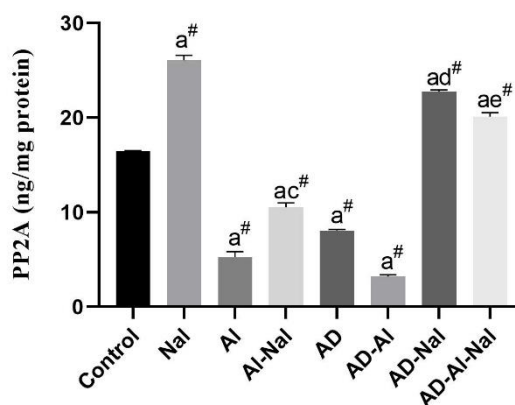

Figure 4.11. Protein phosphatase 2A levels.

(a) Significant from control group (b) Significant from Nal group (c) Significant from Al group (d) Significant from AD group (e) Significant from AD-Al group. *$p < 0.05$ and #$p < 0.001$.

There were differences in PPP1CA levels between the groups. PPP1CA levels were lowest in the Al and AD-Al groups, and naltrexone treatment boosted PPP1CA levels fourfold in the Al-Nal and AD-Al-Nal groups ($p<0.001$) (Figure 4.12.). When comparing the AD and AD-Al groups, Al exposure resulted in a 40% drop in PPP1CA levels.
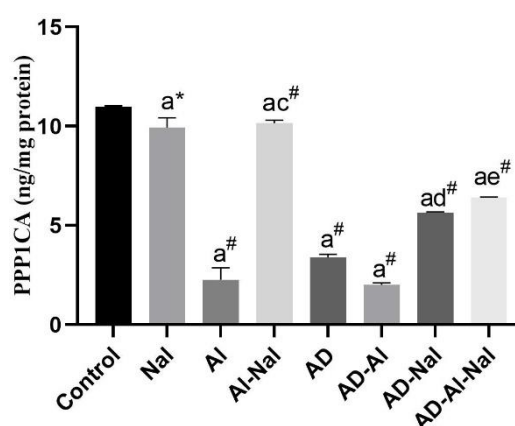
Figure 4.12. Serine/threonine-protein phosphatase levels.

(a) Significant from control group (b) Significant from Nal group (c) Significant from Al group (d) Significant from AD group (e) Significant from AD-Al group. $*p < 0.05$ and $\#p < 0.001$.

The Al, AD, and AD-Al groups had the lowest Akt levels ($p<0.001$). Al exposure exacerbated the AD state by reducing Akt levels in the AD-Al group by 49%. The presence of naltrexone, on the other hand, boosted Akt activation. Akt levels rose 341% (4.4-fold) in the AD-Al-Nal group, 269% (3.6-fold) in the AD-Nal group, and 179% (2.7-fold) in the Al-Nal group as compared to the AD-Al, AD, and Al groups. Increased Akt activity in the presence of naltrexone and lower GSK-3β levels may contribute to naltrexone's neuroprotective effects (Figure 4.13.).
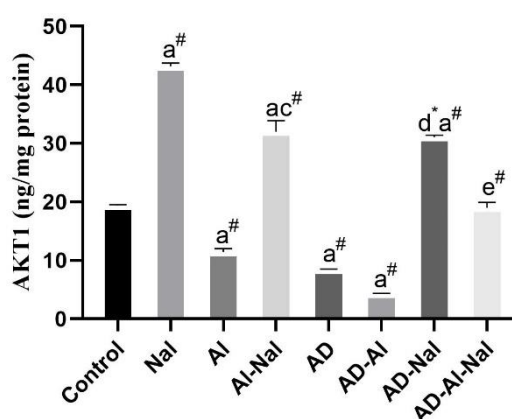

Figure 4.13. Alpha serine/threonine-protein kinase levels.

(a) Significant from control group (b) Significant from Nal group (c) Significant from Al group (d) Significant from AD group (e) Significant from AD-Al group. $*p < 0.05$ and $\#p < 0.001$.

Tau protein levels in the AD, Al, and AD-Al groups were considerably higher than in the control group (p<0.001). Compared to the AD group, the AD-Al group had a nearly 1.2-fold (28%) rise in tau levels, showing the function of Al in raising tau, which is an essential feature of AD. Compared to the other groups, the Al group had the most outstanding tau level, suggesting that Al alone can boost tau synthesis in cells. Tau levels, on the other hand, were considerably lower in the naltrexone-treated groups. The reduction was 1.5-fold in the AD-Nal group and 5.6-fold in the AD-Al-Nal group compared to the AD and AD-Al groups, respectively (p<0.001) (Figure 4.14.).
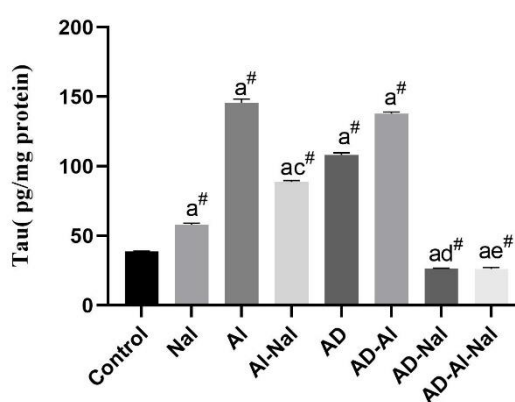

Figure 4.14. Tau levels.

(a) Significant from control group (b) Significant from Nal group (c) Significant from Al group (d) Significant from AD group (e) Significant from AD-Al group. *p < 0.05 and #p < 0.001.

4.2.4. Wnt/ β-catenin pathway

The Al, AD-Al, AD, and AD-Nal groups exhibited lower Wnt protein levels than the control group. Notably, the AD-Nal group showed a significant increase of 2-fold (109%) in Wnt levels compared to the AD group (p<0.05). Conversely, the Wnt activity in the Al-Nal group was approximately 3.5-fold (250%) higher than that of the Al group (p<0.001). In the AD-Al-Nal group, it was nearly 2.5-fold (158%) higher than the AD-Al group (p<0.001) (Figure 4.15.A).

Regarding β-catenin levels, the Al, AD-Al, AD, and AD-Nal groups demonstrated decreases compared to the control group. However, in the AD-Nal group, β-catenin levels were slightly higher (1.1-fold, 17%) than those in the AD group (p<0.001). Remarkably, the AD-Al-Nal group exhibited a substantial increase of 5.5-

fold (450%) compared to the AD-Al group. The Al-Nal group displayed a 3-fold (209%) increase compared to the Al group (Figure 4.15.B).
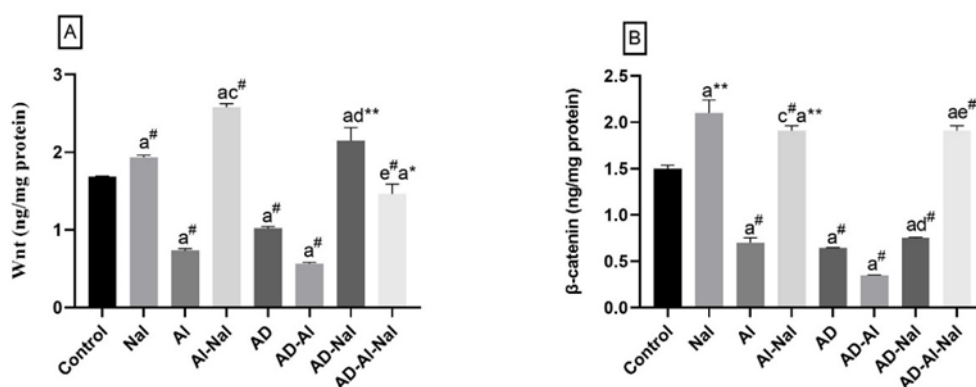

Figure 4.15. Alterations in the Wnt/β-catenin pathway in the study groups

[A] Wnt levels, and [B] β- catenin levels. (a) Significant from control group (b) Significant from Met group (c) Significant from Al group (d) Significant from AD group (e) Significant from AD-Al group. $*p < 0.05$ and $\#p < 0.001$.

4.3. Findings of Dihydrolipoic acid

4.3.1. ROS

ROS levels are shown in figure 4.16. The ROS level was compared between groups, and the results are reported as follows: the AD, AD-Al, and Al ROS levels are 2.1(170%), 2.6 (114%), and 2-fold (104%) higher than the control group, respectively. 25% increase has been measured in the AD-Al compared to the AD group. Treatment with DHLA, a potent antioxidant, decreased ROS levels in the AD-DHLA (142%, 2.9-fold), AD-Al-DHLA (183%, 2.4-fold), and Al-DHLA (130%, 3.3-fold) groups significantly compared to AD, AD-Al, and Al groups (all, (p<0.001).
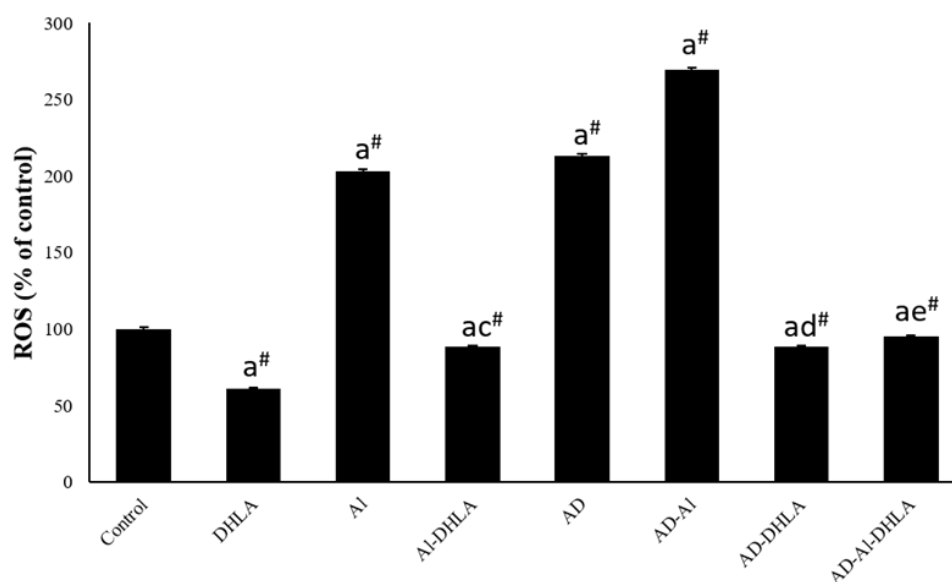
Figure 4.16. Intracellular ROS levels of study groups.

ROS: reactive oxygen species. The amount of intracellular ROS produced by the control cells was assumed as 100%, and the amount of ROS produced by the other cells was calculated as % compared with the control. (a) Significant from control group (c) Significant from Al group (d) Significant from AD group (e) Significant from AD-Al group. #p <0.001.

4.3.2. Oxidative stress parameters

The oxidative stress parameters are presented in figures 4.17, 4.18, 4.19 and 4.20. Among the groups, the Al group exhibited the highest level of GSH compared to the control group (p < 0.001). This increase in GSH levels in the Al group is likely a response to oxidative insult. However, treatment with DHLA, a potent antioxidant,

significantly reduced GSH levels in the AD-Al, Al, and AD groups (all, $p < 0.001$). Notably, the AD-Al-DHLA group showed a 96% (28-fold) reduction. The Al-DHLA group showed a 79% (5.4-fold) decrease. AD-DHLA group showed 86% (7-fold) in GSH levels compared to the AD-Al group, the Al group and the AD group, respectively ($p < 0.001$) (Figure 4.17.).

Figure 4.17. Glutathione levels.

(a) Significant from control group (b) Significant from DHLA group (c) Significant from Al group (d) Significant from AD group (e) Significant from AD-Al group. #$p < 0.001$.

The total antioxidant capacity (TAOC) levels of the study groups are presented in figure 4.18. The TAOC level varied among the groups. The TAOC level was significantly lower in the AD-Al, AD, and Al groups compared to the control group ($p < 0.001$). However, groups co-exposed to DHLA and Al showed significantly higher TAOC levels than the AD-Al and Al groups (all, $p < 0.001$) due to the protective mechanism of DHLA. The AD-DHLA group exhibited a 5.6-fold (469%) increase in TAOC level, while the AD-Al-DHLA group showed a 5.8-fold (487%) increase compared to the AD and AD-Al groups.

Figure 4.18. The total antioxidant capacity levels.

(a) Significant from control group (b) Significant from DHLA group (c) Significant from Al group
(d) Significant from AD group (e) Significant from AD-Al group. $\#p < 0.001$.

Protein oxidation levels in all groups showed significant differences compared to the control group. The protein carbonyl levels in the AD-DHLA group were significantly lower than in the AD group (77% reduction, $p < 0.001$). The AD-DHLA group had the lowest protein carbonyl levels compared to all other groups. Regardless of the chemicals in the cell culture, the addition of DHLA protected cells against protein oxidation (Figure 4.19.).

Figure 4.19. Protein carbonyl levels.
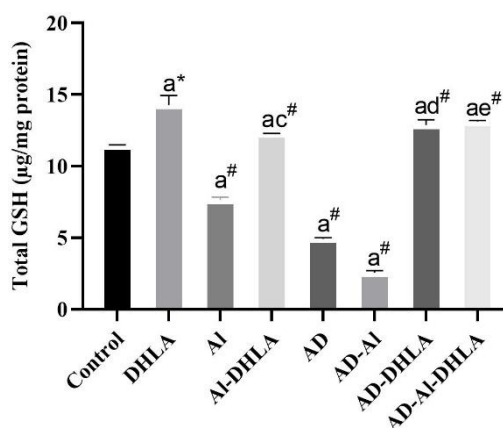
(a) Significant from control group (b) Significant from DHLA group (c) Significant from Al group
(d) Significant from AD group (e) Significant from AD-Al group. $\#p < 0.001$.

As a potent antioxidant, DHLA significantly reduced the production of MDA when added to the environment. The MDA levels in the Al, AD-Al, and AD groups

were significantly higher than in the control group ($p < 0.001$). Treatment with DHLA in the AD and Al groups resulted in an almost four-fold reduction in lipid peroxidation (Figure 4.20.). DHLA effectively protects cells from lipid peroxidation and protein oxidation caused by Al toxicity.

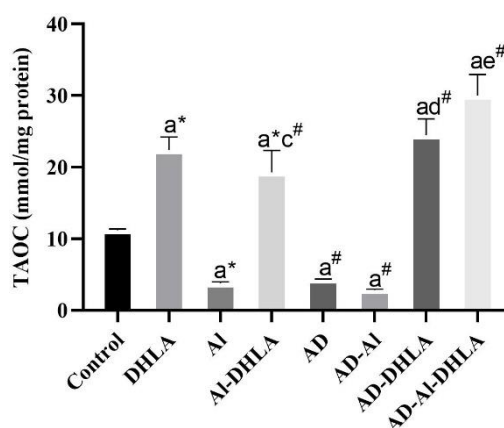**Figure 4.20.** Malonaldehyde levels.

(a) Significant from control group (b) Significant from DHLA group (c) Significant from Al group
(d) Significant from AD group (e) Significant from AD-Al group. $\#p < 0.001$.

4.3.3. GSK3-β pathway

Among the study groups, the AD-Al group exhibited the highest levels of GSK-3β. Similarly, Al exposure increased GSK-3β levels in cells. GSK-3β levels were significantly higher in the Al, AD, and AD-Al groups compared to the control group, showing an almost three-fold increase ($p < 0.001$). Al added to the AD model increased the GSK-3β by 60%, indicating the exacerbating effect of Al. In the DHLA-treated groups, GSK-3β levels decreased to almost half those in the AD-Al, AD, and Al groups (Figure 4.21.).
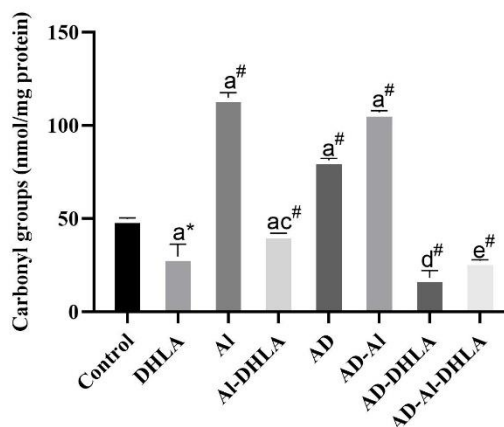
Figure 4.21. Glycogen synthase kinase-3 beta levels.

(a) Significant from control group (b) Significant from DHLA group (c) Significant from Al group
(d) Significant from AD group (e) Significant from AD-Al group. *$p < 0.05$ and #$p < 0.001$.

PP2A levels were higher in the DHLA and AD-DHLA groups compared to the control group ($p < 0.01$ and $p < 0.001$, respectively). However, in the AD-Al and Al groups, PP2A levels decreased significantly compared to the control group ($p < 0.001$). Notably, the AD-Al-DHLA and AD-DHLA groups showed a 295% (3.9-fold) and 252% (3.5-fold) increase in PP2A levels compared to the AD-Al and AD groups, respectively ($p < 0.001$ for both comparisons). Comparing the Al group with the Al-DHLA group, DHLA treatment resulted in a two-fold (103%) increase in PP2A levels (Figure 4.22.).

Figure 4.22. Protein phosphatase 2A levels.
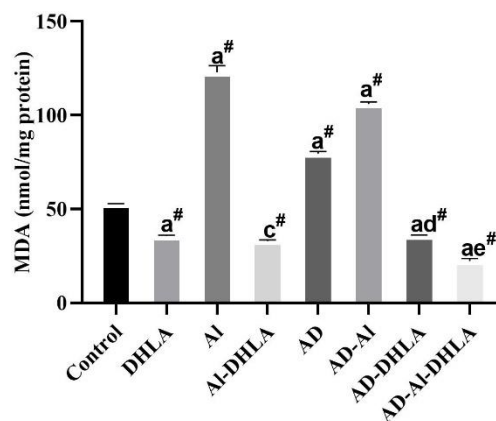
(a) Significant from control group (b) Significant from DHLA group (c) Significant from Al group
(d) Significant from AD group (e) Significant from AD-Al group. *$p < 0.05$ and #$p < 0.001$.

PPP1CA levels decreased in most study groups compared to the control group ($p < 0.001$, $p < 0.01$ for the DHLA group). However, DHLA-treated groups demonstrated increased PPP1CA levels, with the AD-Al-DHLA, AD-DHLA, and Al-DHLA groups showing an approximately one-fold increase compared to the control group (Figure 4.23.).

Figure 4.23. Serine/threonine-protein phosphatase levels.

(a) Significant from control group (b) Significant from DHLA group (c) Significant from Al group (d) Significant from AD group (e) Significant from AD-Al group. *p < 0.05 and #p < 0.001.

Tau levels, which are important pathophysiological hallmarks of AD, were increased in our cell culture model of AD. The Al, AD-Al and AD groups exhibited tau levels almost three times higher than the control group ($p < 0.001$). However, in the DHLA-treated groups, tau levels were significantly reduced ($p < 0.001$). Specifically, the AD-Al-DHLA group showed an almost 85% decrease in tau levels compared to the AD-Al group (Figure 4.24.).
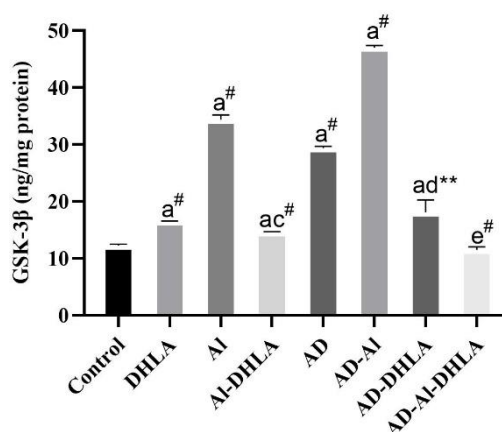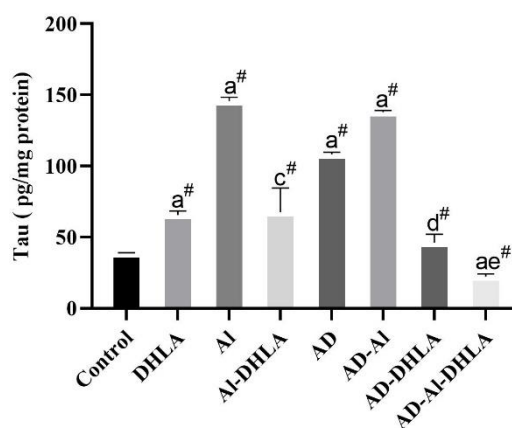
Figure 4.24. Tau levels.

(a) Significant from control group (b) Significant from DHLA group (c) Significant from Al group
(d) Significant from AD group (e) Significant from AD-Al group. *$p < 0.05$ and #$p < 0.001$.

Akt levels were significantly reduced in the AD and AD-Al groups compared to the control group ($p < 0.01$). Conversely, the DHLA group demonstrated the highest Akt level, exhibiting a remarkable four-fold increase compared to the control group ($p < 0.001$). Furthermore, the DHLA-treated groups displayed a significant elevation in Akt levels. The AD-Al-DHLA group exhibited a 4.4-fold (348%) increase, the AD-DHLA group showed a 4.7-fold (371%) increase, and the Al-DHLA group demonstrated a 3.5-fold (257%) increase when compared to their respective untreated groups (Figure 4.25.).
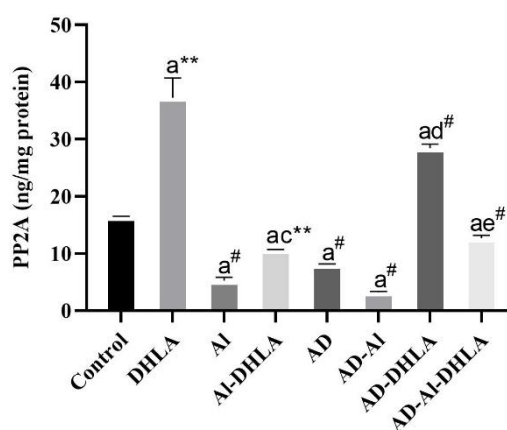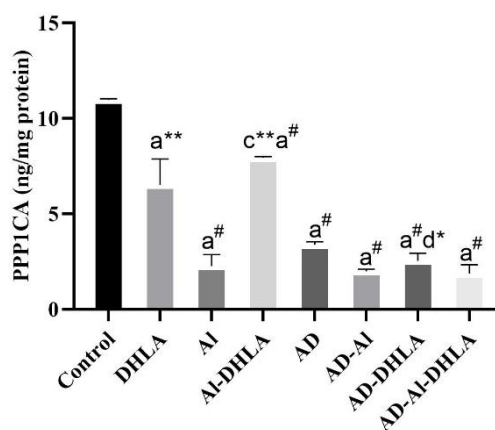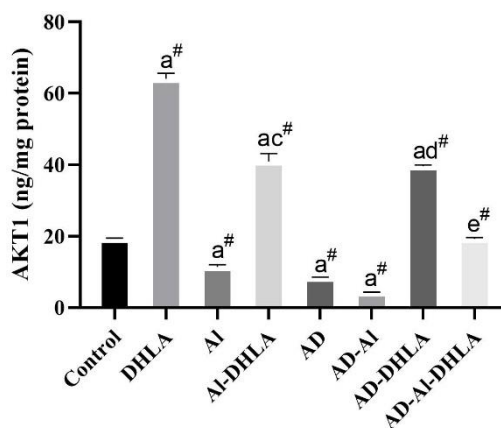

Figure 4.25. Alpha serine/threonine-protein kinase levels.

(a) Significant from control group (b) Significant from DHLA group (c) Significant from Al group
(d) Significant from AD group (e) Significant from AD-Al group. *$p < 0.05$ and #$p < 0.001$.

4.3.4. Wnt/ β-catenin pathway

Wnt protein levels were lower in the Al, AD, and AD-Al groups. However, the AD-DHLA and Al-DHLA groups exhibited a significant increase in Wnt levels, showing an almost 3-fold increase compared to the AD and a 6-fold increase compared to Al groups. Furthermore, when compared to the control group, the Wnt protein level was significantly higher in the DHLA ($p < 0.01$), Al-DHLA ($p < 0.01$), and AD-DHLA groups ($p < 0.001$) (Figure 4.26.A). All groups, except for the AD-Al-DHLA and Al-DHLA groups, demonstrated decreases in β-catenin levels compared to the control group. Specifically, the AD-Al and AD groups exhibited an almost four-fold reduction in β-catenin levels compared to control (Figure 4.26.B). Conversely, in the AD-DHLA and Al-DHLA groups, β-catenin levels were 1-fold and 4.5-fold higher than in the AD and Al groups, respectively ($p < 0.01$) (Figure 4.26.B).
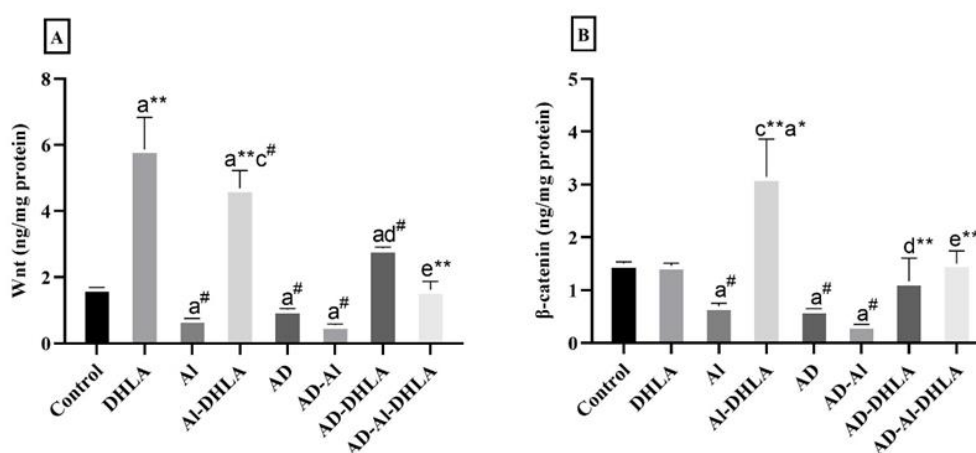
**Figure 4.26.** Alterations in the Wnt/β-catenin pathway in the study groups.

[A] Wnt levels, and [B] β- catenin levels. (a) Significant from control group (b) Significant from DHLA group (c) Significant from Al group (d) Significant from AD group (e) Significant from AD-Al group. *$p < 0.05$ and #$p < 0.001$.

4.4. Findings of Metformin

4.4.1. ROS

The ROS levels are given in Figure 4.27. For all the groups except the AD-Al-Met, the ROS level was significantly higher than the control (all, $p < 0.001$). Metformin treatment is the most obvious in reducing the ROS level in AD-Met by

almost 9-fold compared to the AD group. The ROS level declined, followed by Al-Met by 250% (3.4-fold) compared to the Al group. However, comparing the control group to the metformin group, the decline was just 35 %.
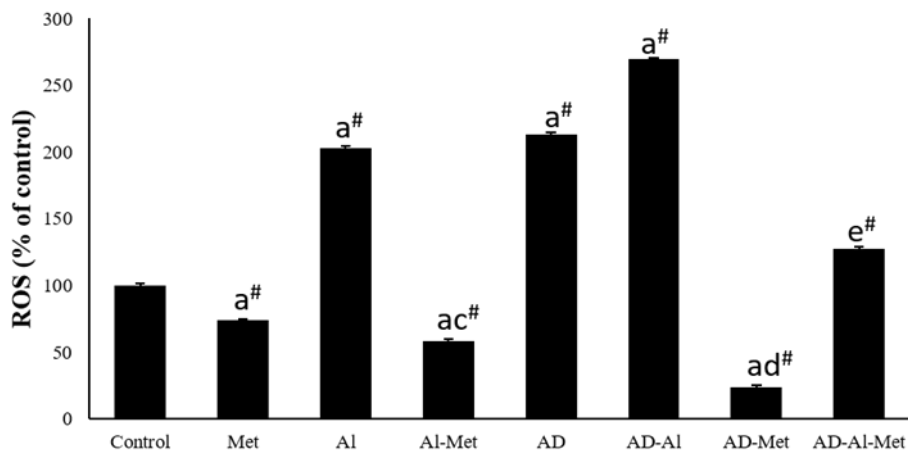
Figure 4.27. Intracellular ROS levels of study groups.

ROS: reactive oxygen species. The amount of intracellular ROS produced by the control cells was assumed as 100%, and the amount of ROS produced by the other cells was calculated as % compared with the control. (a) Significant from control group (c) Significant from Al group (d) Significant from AD group (e) Significant from AD-Al group. #p <0.001.

4.4.2. Oxidative stress parameters

The figures 4.28, 4.29, 4,30 and 4.31 give an in-depth look at the oxidative stress parameters. Notably, the AD-Al-Met, Al-Met, and AD-Met groups did not vary from the control group. The AD-Al group, on the other hand, had the greatest GSH levels, indicating a cellular response to oxidative damage (p <0.001). The AD-Al group, which had chronic Al exposure, had a 1.3-fold increase in GSH levels compared to the AD group (p <0.001). In contrast, metformin-treated groups had significantly lower GSH levels, with a fall of roughly 2.5-fold (61%) in AD-Met and 3-fold (67%) in AD-Al-Met compared to the AD and AD-Al groups, respectively (all, p <0.001). Furthermore, as compared to the Al group, the GSH level in Al-Met reduced about 2.3-fold (58%) (p <0.001) (Figure 4.28.).

Figure 4.28. Glutathione levels.

(a) Significant from control group (b) Significant from Met group (c) Significant from Al group (d) Significant from AD group (e) Significant from AD-Al group. #p < 0.001.

MDA levels were higher in the Al group (p <0.001) than in the control group. Al exposure in the AD-Al group increased MDA levels much more, aggravating the state of AD. However, metformin therapy significantly lowered MDA levels in the AD-Al-Met group by 2.7-fold (64%) (p <0.001). Similarly, AD-Met reduced MDA levels by half (49%) when compared to the AD group (p <0.001) (Figure 4.29.). The Al-Met group had a stunning 4.7-fold drop (80%) in MDA levels, demonstrating metformin's powerful ability to prevent lipid peroxidation.

Figure 4.29. Malondialdehyde levels.

(a) Significant from control group (b) Significant from Met group (c) Significant from Al group (d) Significant from AD group (e) Significant from AD-Al group. #p < 0.001.

Protein oxidation in all groups differed considerably from the control group. When the AD group was treated with Al (AD-Al), there was a 32% increase in protein oxidation. On the other hand, metformin revealed its capacity to decrease carbonyl groups linked with protein oxidation. When compared to the Al group, Al-Met had a 3.7-fold (74%) reduction in carbonyl groups (p <0.001). Compared to the AD group, AD-Met had a 4.6-fold (79%) drop-in carbonyl groups (Figure 4.30.). The AD-Al-Met group had the greatest reduction in carbonyl groups, with a 6-fold reduction (84%) compared to the AD-Al group.

Figure 4.30. Protein carbonyl levels.

(a) Significant from control group (b) Significant from Met group (c) Significant from Al group (d) Significant from AD group (e) Significant from AD-Al group. #p < 0.001.

TAOC values of the research groups are shown in figure 4.31. Notably, the Al and AD groups had considerably lower TAOC levels than the others, showing that enhanced oxidative stress leads to Al toxicity and AD pathogenesis. However, adding metformin to the media significantly increased the antioxidant capacity of the cells. TAOC levels rose 4.4-fold (343%) in the Al-Met group, 3.7-fold (270%) in the AD-Al-Met group, and 2.3-fold (134%) in the AD-Met group compared to the Al, AD-Al, and AD groups, respectively (p <0.001).

Figure 4.31. Total antioxidant capacity levels.

(a) Significant from control group (b) Significant from Met group (c) Significant from Al group (d) Significant from AD group (e) Significant from AD-Al group. #p < 0.001.

4.4.3. GSK-3β pathway

The AD-Al (282%), Al (179%), and AD (138%) groups had the highest levels of GSK-3β among all groups, substantially greater than the control group (p<0.001). However, metformin treatment decreased GSK-3β activity (Figure 4.32.). When compared to the AD-Al, AD, and Al groups, we found a 4-fold (75%) drop in GSK-3β levels in the AD-Al-Met group, a 2.6-fold (62%) decrease in AD-Met, and a 3.2-fold (69%) decrease in Al-Met (p<0.001).
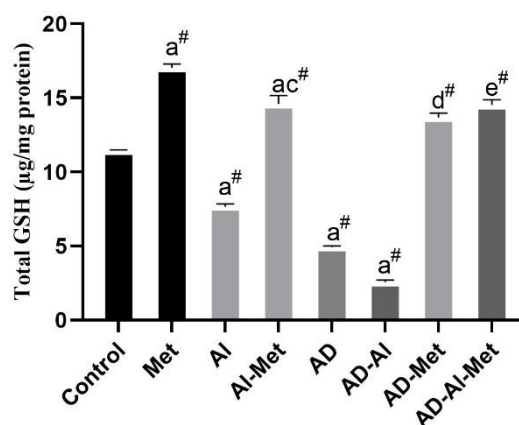
Figure 4.32. Glycogen synthase kinase 3 beta levels.

(a) Significant from control group (b) Significant from Met group (c) Significant from Al group (d) Significant from AD group (e) Significant from AD-Al group. $*p < 0.05$ and $\#p < 0.001$

The Al and AD-Al groups had the lowest PP2A levels ($p<0.001$). However, the PP2A levels in the metformin groups increased ($p<0.001$) (Figure 4.33.). Compared to the AD-Al, AD, and Al groups, the PP2A levels in the AD-Al-Met, AD-Met and Al-Met groups rose 8.3-fold, 3.1-fold, and 2.5-fold, respectively ($p<0.001$).
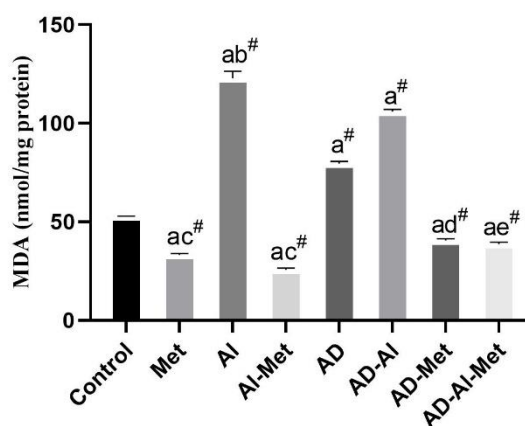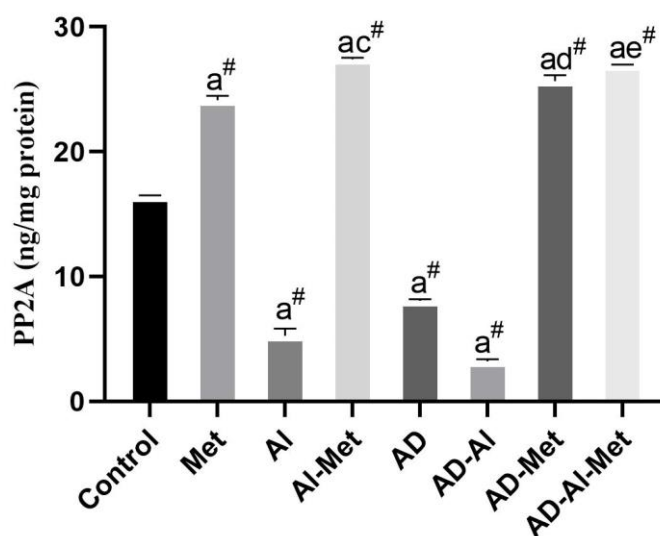
Figure 4.33. Protein phosphatase 2A levels.

(a) Significant from control group (b) Significant from Met group (c) Significant from Al group (d) Significant from AD group (e) Significant from AD-Al group. $*p < 0.05$ and $\#p < 0.001$.

There were differences in PPP1CA levels between the groups. PPP1CA levels were lowest in the Al and AD-Al groups, and metformin treatment boosted PPP1CA levels four-fold in the Al-Met and AD-Al-Met groups (p<0.001) (Figure 4.34.). When comparing the AD and AD-Al groups, Al exposure resulted in a 40% drop in PPP1CA levels.
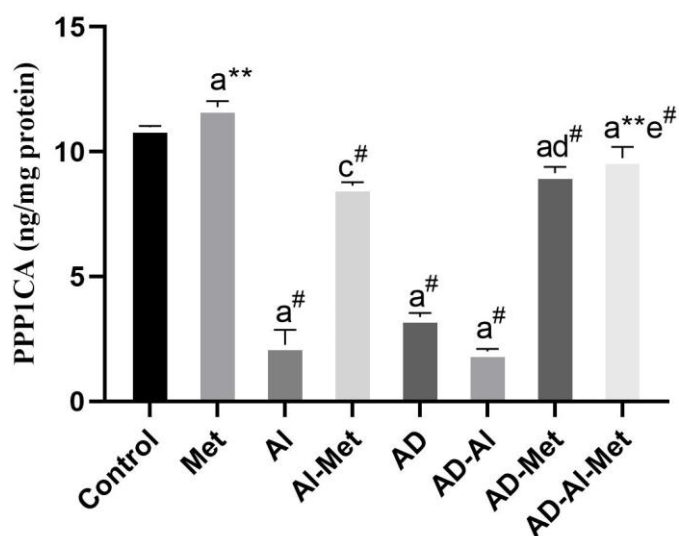
Figure 4.34. Serine/threonine-protein phosphatase levels.

(a) Significant from control group (b) Significant from Met group (c) Significant from Al group (d) Significant from AD group (e) Significant from AD-Al group. *$p < 0.05$ and #$p < 0.001$

The Al, AD, and AD-Al groups had the lowest Akt levels ($p<0.001$). Al exposure exacerbated the AD state by reducing Akt levels in the AD-Al group by 49%. The presence of metformin, on the other hand, boosted Akt activation. Akt levels rose 346% (4.4-fold) in the AD-Al-Met group, 193% (2.9-fold) in the AD-Met group, and 116% (2.1-fold) in the Al-Met group as compared to the AD-Al, AD, and Al groups (Figure 4.35.).
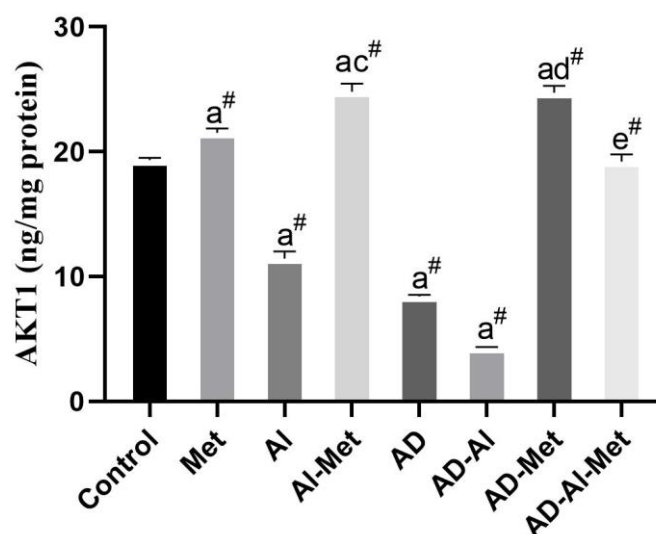
Figure 4.35. Alpha serine/threonine-protein kinase levels.
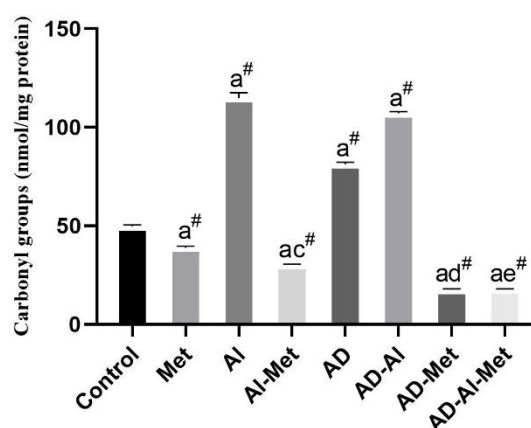
(a) Significant from control group (b) Significant from Met group (c) Significant from Al group (d) Significant from AD group € Significant from AD-Al group. $*p < 0.05$ and $\#p < 0.001$.

Tau protein levels in the AD, Al, and AD-Al groups were considerably higher than in the control group ($p<0.001$). When compared to the AD group, the AD-Al group had a nearly 1.2-fold (28%) rise in tau levels, showing the function of Al in raising tau, which is an essential feature of AD. Compared to the other groups, the Al group had the greatest tau level, suggesting that Al alone can boost tau synthesis in cells. Tau levels, on the other hand, were considerably lower in the metformin-treated groups. The reduction was 3.3-fold in the AD-Met group and 4.8-fold in the AD-Al-Met group compared to the AD and AD-Al groups, respectively ($p<0.001$) (Figure 4.36.).
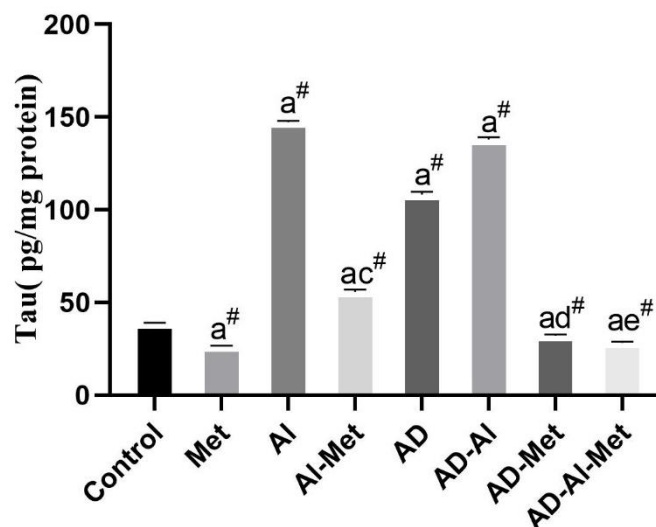
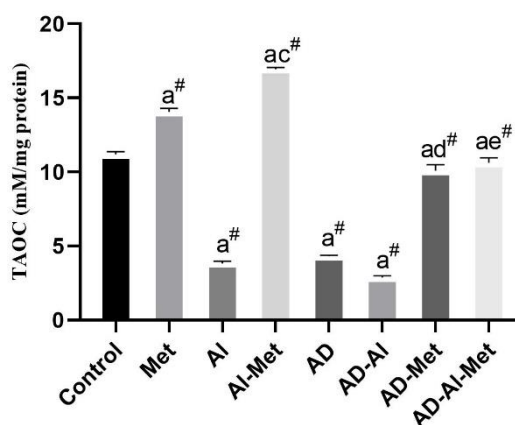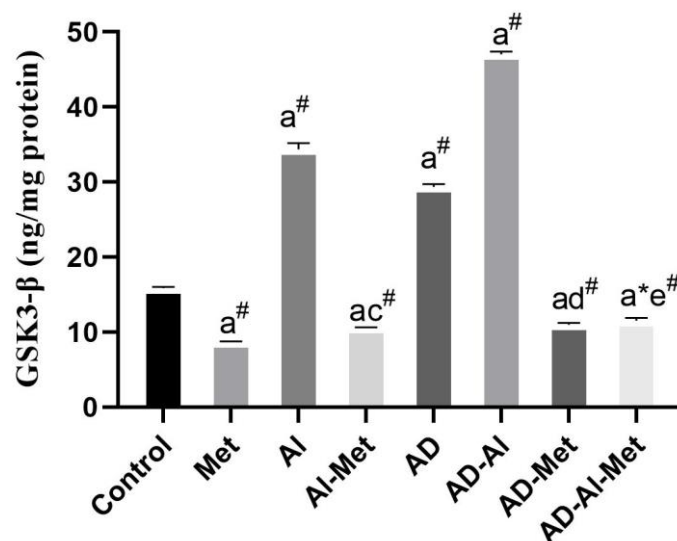**Figure 4.36.** Tau levels.

(a) Significant from control group (b) Significant from Met group (c) Significant from Al group (d) Significant from AD group (e) Significant from AD-Al group. $*p < 0.05$ and $\#p < 0.001$

4.4.4. Wnt/ β-catenin pathway

The Al, AD-Al, and AD groups exhibited lower Wnt protein levels than the control group. Notably, the Al-Met group showed a significant increase of 3.3-fold (237%) in Wnt levels compared to the Al group (p<0.001). Conversely, the Wnt activity in the AD-Al-Met group was approximately 3.4-fold (243%) higher than that of the AD-Al group (p<0.001). In the AD-Met group, it was nearly 2-fold (89%) higher than the AD group (p<0.05) (Figure 4.37.A).

Regarding β-catenin levels, the Al, AD-Al and AD groups demonstrated decreases compared to the control group. However, in the AD-Met group, β-catenin levels were 3-fold higher (201%) than in the AD group (p<0.001). Remarkably, the AD-Al-Met group exhibited a substantial increase of 5.4-fold (447%) compared to the AD-Al group. The Al-Met group displayed a 3.2-fold (224%) increase compared to the Al group (Figure 4.37.B).
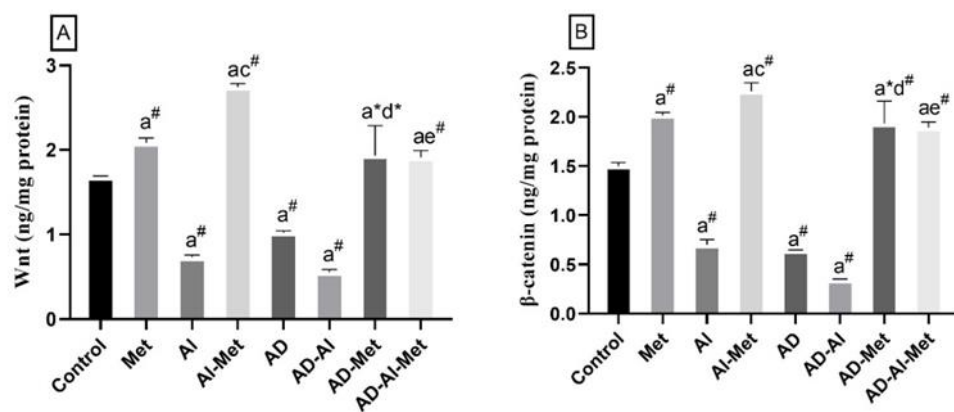
**Figure 4.37.** Alterations in the Wnt/β-catenin pathway in the study groups.

[A] Wnt levels, and [B] β- catenin levels. (a) Significant from control group (b) Significant from Met group (c) Significant from Al group (d) Significant from AD group (e) Significant from AD-Al group. *p < 0.05 and #p < 0.001.

5. DISCUSSION

5.1. SH-SY5Y differentiated in vitro model

The application of in vitro model systems has brought about substantial advancements in the fields of neuroscience and neurotoxicology. Cultivated cells offer a highly effective environment for investigating the activity of proteins and the molecular processes that govern certain incidents. These models play a significant role in enhancing our understanding of the underlying mechanisms of illnesses and infections, as well as contributing to the early evaluation of the effectiveness of drugs.

This thesis focuses on the SH-SY5Y cell line derived from the parental neuroblastoma SK-N-SH cell line. The SH-SY5Y cell line has been well recognized as an in vitro neuronal model, with many applications in the study of neurodegeneration (155), neurotrauma (156), developmental neurotoxicity (Attoff et al., 2020) and neurite outgrowth (157).

The differentiation of SH-SY5Y cells into various phenotypes depends on the specific therapy employed. The differentiation agents well recognized in the literature include phorbol esters and retinoic acid (158). Growth factors such as BDNF, nerve growth factor (NGF), and neuregulins have also been identified as important regulators of differentiation (159). The less often used elements include the Vitamin D metabolite 1,25-dihydroxycholecalciferol (VitD3) and cholesterol, as shown by previous studies (160,161).

Our model introduces an improved in vitro model of human neurons, whereby SH-SY5Y neuroblastoma cells are induced to exhibit durable neuronal shape by adding RA and BDNF. The aforementioned cells display distinct characteristics typical of fully developed neurons, such as synaptic structures and the ability to transport vesicles along axons. Significantly, the expression of tau protein attains levels comparable to those observed in the fully developed human brain, comprising the mature isoforms. The novel methodology for in vitro differentiation described in this study has significant implications for several areas of neuroscientific research, particularly in the context of AD. During the differentiation process, SH-SY5Y cells undergo a cessation of proliferation, undergo an extension of long neurites, and exhibit the expression of markers characteristic of neurons. The differentiation process, when

combined with BDNF, leads to the dispersion of tau protein within neurons, which coexists with tubulin along neurites. The development of important proteins linked with AD, such as APP and Aβ, has been extensively acknowledged in SH-SY5Y cells (162,163). Thus, the differentiated SH-SY5Y model we designed here is appropriate for studying AD and its molecular mechanisms.

Our established in vitro model, centered on differentiated SH-SY5Y cells, presents a promising platform for unraveling the intricate molecular underpinnings of AD. Through meticulous exploration, we have brought to light compelling evidence of dysregulation in pivotal pathways, underscoring the relevance of our model in the AD research landscape.

Evidently, our findings spotlight the aberrant behavior of the GSK-3β/Akt and Wnt/β-catenin pathways within our cellular milieu. This dysregulation is a tangible reflection of the intricate turmoil that characterizes AD pathogenesis. The disarray within these pathways echoes the disruptions witnessed in the intricate choreography of AD-affected brains, thus substantiating the utility of our in vitro system for dissecting their dynamics. The GSK-3β/Akt pathway emerges as a critical player in the array of disrupted molecular pathways. This pathway is pivotal in integrating signals related to synaptic neurotransmission within cells. Moreover, it influences various essential processes like neuronal cell growth, movement, and adaptability (164,165).

In parallel, the substantial decline in the activity of PP2A adds another layer of authenticity to our model's representation of AD-associated intricacies (166). As a kinase known to play a central role in the phosphorylation of tau protein, PP2A's diminishing presence within our model mirrors the well-documented alterations witnessed in AD-impacted neurons. Notably, the reduction in PPP1AC, a crucial actor responsible for the methylation of the PP2A, C-terminus (167), enhances the plausibility of our model's relevance in capturing the nuances of tau-related dysfunctions that hallmark AD.

The CNS relies on the intricate workings of the Wnt pathway to govern various crucial aspects of neuronal activity. This intricate web of functions encompasses neuronal differentiation, neurogenesis, the establishment of synapses, and the safeguarding of neurons (168–170). Beyond its role in synapse formation, Wnt

proteins exhibit the capacity to influence neurotransmission both before and after synapse formation, as indicated by studies (112). A pivotal participant in the Wnt signal transduction cascade is β-Catenin, which controls cell fate determination throughout developmental processes. Absent Wnt ligands, cytosolic β-catenin encounters rapid phosphorylation by GSK-3β, culminating in its degradation through the proteasome route (171). Upon Wnt ligand binding to Frizzled receptors, the Dishevelled protein (Dvl) is activated, inhibiting GSK-3β and the consequent stabilization of β-catenin. This liberated β-catenin forms complexes within the nucleus alongside members of the T-cell factor/lymphoid enhancer factor (TCF/LEF) transcription factor family, thereby governing the expression of Wnt target genes that sustain neuron survival and plasticity, crucial for maintaining neuronal integrity (118).

Within the context of AD, the hyperphosphorylation of tau is mediated by GSK-3β. Activation of the Wnt/β-catenin signaling pathway, which suppresses GSK-3β activity, emerges as a mechanism that mitigates tau phosphorylation and the formation of neurofibrillary tangles (172). Our investigation culminated in noteworthy findings, demonstrating reduced levels of β-catenin alongside heightened GSK-3β expression and diminished Wnt activity. This compellingly implies that the differentiated SH-SY5Y cell line is a robust in vitro model to scrutinize Wnt signaling within the context of AD.

The SH-SY5Y cell line, a recurrent choice in studies scrutinizing the Wnt/β-catenin pathway, has yielded crucial insights. Perturbing endogenous Wnt expression resulted in cellular demise and the hindrance of cell growth (173). Notably, suppressing Wnt activity exacerbated the neurotoxic impact of paraquat and maneb on SH-SY5Y cells, underscoring the neuroprotective role of Wnt signaling (174). In an additional exploration, the SH-SY5Y cell line, engineered to express wild-type and mutant Presenilin 1 (PS1), was harnessed to dissect the interaction between PS1 and β-catenin. Uemura et al. (175) revealed that PS1 positively governs the nuclear translocation of β-catenin following RA treatment, consequently leading to an elevation in cellular cyclin D1 levels. Further investigations involving a dopaminergic model of SH-SY5Y cells sought to uncover the protective influence of exogenous Wnt1 in PD. Their findings unveiled the inhibition of the Wnt/β-catenin pathway

following a 24-hour exposure to 6-hydroxydopamine, characterized by a decline in β-catenin levels and an increase in GSK-3β activity (176).

Cellular oxidative stress, stemming from either excessive ROS production or inadequate antioxidant defense mechanisms, can lead to detrimental cellular effects, including damage to proteins, lipids, and DNA and activation of apoptotic pathways. This phenomenon is particularly relevant in the context of neurodegenerative diseases such as AD, where accumulating oxidative damage has been implicated (177). Our in vitro model, tailored to simulate AD conditions, exhibited nearly threefold higher ROS production compared to undifferentiated cells, underscoring an imbalance in the cellular antioxidant system. The heightened ROS levels could potentially destabilize lipid membrane, affecting integrity and fluidity (178). Measurement of MDA, a by-product of lipid peroxidation, served as a marker for oxidative stress, with these reactive molecules capable of triggering tau phosphorylation, intracellular calcium pathway disruption, and apoptosis (177).

Concomitant with ROS, protein oxidation occurs through ROS-protein interactions, leading to structural distortion and protein aggregation (179). Our study demonstrated elevated carbonyl group levels, indicative of protein oxidation. Furthermore, mitochondrial DNA and protein damage resulting from ROS can impede energy production, exacerbating ROS generation cyclic and ultimately resulting in apoptosis (180). Notably, the antioxidant system's compromised functionality in AD contributes to an exponential increase in oxidative stress indicators. GSH, a critical endogenous antioxidant responsible for ROS neutralization and cellular redox balance, has been implicated in AD pathology. Reduced brain GSH levels, observed in various animal studies, are linked to intensified oxidative stress-related brain damage, particularly impacting neurons (181). However, our study revealed augmented GSH levels, which could potentially be attributed to early-phase GSH overactivity in response to escalated ROS levels. Varied postmortem findings in GSH content across different studies underscore the need to assess the GSH/GSSG ratio at various stages of AD to delineate its role during each phase (182–184).

Notably, oxidative stress has been associated with the neurotoxic oligomerization of Aβ peptides and tau tangles (185). While some studies, such as that by Pienkowska et al. (186), link elevated GSH levels to tau overexpression in

neuroblastoma cells; our findings suggest that increased tau levels in differentiated cells are a consequence of enhanced ROS production and mitochondrial dysfunction (187). These contrasting results underscore the complex interplay between oxidative stress, GSH levels, and tau pathology in the context of AD.

5.2. Aluminum Toxicity

Our current understanding of Al's non-essential nature doesn't eliminate Al's possibility to instigate or catalyze biomolecular reactions or hinder or decelerate biochemical processes. A challenge posed by Al lies in its strong affinity for participating in biochemical reactions, particularly through robust binding with oxygen-based functional groups (31). Al easily crosses the BBB, accumulating predominantly in neurons within structures like senile plaques, NFTs, Lewy bodies, and lipofuscin, each of which contains components strongly prone to binding with Al (188). The rate at which Al ions reach their target is crucial to neurotoxicity. Various animal-based studies have highlighted that an increased transport rate corresponds to heightened neurotoxicity (189). In humans, Al-induced encephalopathy represents the acute form of Al neurotoxicity, accompanied by various anomalous processes, including alterations in tau protein processing (190) and Al deposition in neurons, glia, and choroid epithelium (188). Acute toxicity disrupts the brain's microenvironment due to BBB disturbances. Al's transfer across the barriers occurs via transferrin, thereby interfering with iron transport. This disturbance in transferrin cycling disrupts the Fenton reaction, leading to imbalanced oxidative stress within the brain.

In our study, the differentiated and undifferentiated SH-SY5Y cells were exposed to 362μM Al for 7 days. This period will mimic chronic exposure to Al to explore its neurotoxic effects. The evaluation under the microscope has shown that chronic exposure to Al increases the death of cells. Exposure to Al resulted in a drastic increase in ROS levels in cells. The production rate of ROS in the differentiated cells was worsened than in undifferentiated ones, showing Al's capability to produce more ROS and exacerbating the AD situation. Animal studies exposed to Al chronically reported increased oxidative stress production in the brain (191,192). One of the reasons behind this may be Al change in metals, iron and copper homeostasis. Metal dyshomeostasis correlates with the initiation and progress of various human

neurodegenerative diseases. However, whether or not this correlation is a causing effect remains largely unknown. Metal dyshomeostasis has also been observed in Al-treated cells and Al-induced animal models (193). Iron and copper, present in various cell compartments, act as pro-oxidant metals. Al enhances the pro-oxidant potential of this transition (194). In Al-treated flies, the amount of Fe is reported to be increased dramatically (193).

When the creation of ROS exceeds the capabilities of detoxification and repair processes, it initiates oxidative damage to proteins, DNA, and phospholipids. This disruption affects the process of mitochondrial oxidative phosphorylation, ultimately leading to cellular damage and death. The brain is an organ that exhibits a high metabolic demand for oxygen, rendering it vulnerable to alterations in oxygen radicals. The aforementioned extremely reactive free radicals engage in chemical reactions with nucleic acids, proteins, and lipids, resulting in permanent harm to cellular structures (195) . Cells, when subjected to ideal growth circumstances, are able to sustain a fundamental level of ROS that are generated as by-products during the fundamental metabolic pathways. Nevertheless, when exposed to Al, the formation of ROS significantly amplifies, leading to a disruption in the redox equilibrium and an escalation in oxidative stress (193).

The occurrence of oxidative cellular damage induced by ROS is typically accompanied by an elevation in lipid peroxide levels, leading to a decrease in membrane fluidity. MDA, a byproduct resulting from the degradation of lipid peroxides, has been widely employed as a measure for assessing the magnitude of lipid peroxidation (196). In the current study, it was shown that the concentration of MDA exhibited a statistically significant increase following exposure to Al treatment. The findings of our study align with the research conducted by other scholars (197,198). Elevated malondialdehyde levels were seen in rats that were exposed to Al, lead, and phenolic chemicals. Additionally, research has indicated that exposure to Al has been found to increase lipid peroxidation in liposomes, resulting in changes to membrane fluidity (199). In their study, Golub et al. (200) reported the absence of any alterations in lipid peroxidation levels in rats that were subjected to Al exposure.

GSH, as part of the non-enzymatic antioxidant, in the presence of increased ROS due to Al, showed increased activity in differentiated and undifferentiated SH-

SY5Y cells. GSH, a tripeptide synthesized within virtually all animal cells, is the most important cellular-reducing sulfhydryl-containing agent. It performs various metabolic functions, including detoxifying free radicals, metals and electrophilic compounds (201). The increase in GSH in our results may be due to the GSSG/GSH ratio imbalance. Al may deplete the GSH-related enzymes, which means an increase in GSH level. Another possible mechanism behind increased GSH would be its role as a metal chelator, which means increased GSH confronting Al (202). In oxaliplatin-treated mice, Al was accumulated in the dorsal root ganglia (DRG), and accumulated Al in DRG or other organs aggravated oxaliplatin-induced neuropathic pain. GSH acts as a metal chelator, removing Al and relieving neuropathy (203). Rizvi et al. (198) reported that SH-SY5Y cells exposed to different Al concentrations showed depletion in the antioxidant system, which decreased the GSH levels. In another study, Al and zinc-induced acute toxicity in rats were investigated. In this study, GSH may reduce the oxidant capacity increased by Al administration and may have a tolerant role on the accumulated serum Al levels (204). However, Öztürk et al. (205) did not find increased levels of total GSH in the Al-treated undifferentiated SH-SY5Y cells. Animals exposed to Al displayed notable reductions in reduced and oxidized GSH levels and diminished glutathione reductase activity in different rat brain regions (206).

Al neurotoxicity is increasingly recognized as a significant risk factor for AD development. The potential connection lies in its influence on key markers like tau protein and Aβ, both hallmarks of AD pathology. Our research sheds light on these connections by revealing that exposure to Al prompts notable changes in these factors. Our findings highlight that exposure to 362μM of Al for just a week increases tau levels in affected cells. This increase in tau protein aligns with the widely accepted notion that elevated tau is a crucial factor in AD progression.

Furthermore, our investigations indicate that Al exposure also leads to an elevation in Aβ levels. The accumulation of Aβ and aggregation into plaques are fundamental drivers of AD pathology. Central to the mechanism underlying Al-induced neurotoxicity is the GSK-3β and Akt signaling pathways. Prolonged Al exposure disrupts the delicate balance between these pathways, exacerbating AD risk.

It is worth mentioning that GSK-3β plays a pivotal role in the modulation of tau phosphorylation (5). The findings of our investigation indicate a positive

correlation between elevated levels of GSK-3β and an increase in tau hyperphosphorylation. The heightened phosphorylation status of tau has been linked in the formation of NFTs, which are recognized as a characteristic feature of AD pathogenesis. The regulation of tau activity is often contingent upon the process of phosphorylation and dephosphorylation. The phenomenon of hyperphosphorylation observed in AD is attributed to an in equilibrium between the activities of kinases, which add phosphate groups to proteins, and phosphatases, which remove phosphate groups from proteins (207). Neuronal injury is caused by a variety of neurotoxins, which act by dephosphorylating Akt at Ser473 and GSK-3β at Ser9. This process is linked to a reduction in Akt activity and an increase in GSK-3β activity. In the setting of aluminum-induced neurotoxicity in rats, previous studies have shown that a decrease in Akt activity, coupled with an increase in GSK-3β activity, leads to elevated levels of hyperphosphorylated tau. This, in turn, negatively impacts cognitive processes and memory (62,208,209).

Furthermore, our research highlights the significance of PP2A in this context. PP2A, responsible for the phosphorylation of tau, acts as a counterbalance to the effects of kinases like GSK-3β (166). As underscored in our research, the discernible reduction in PP2A levels undermines the brain's capacity to regulate tau phosphorylation, thereby intensifying the accumulation of hyperphosphorylated tau variants. Notably, the impairment of PPP1CA, a crucial contributor to PP2A functionality, further contributes to the disruption of tau homeostasis. Reports by Parekh et al. (210) and J. Walton (211) have indicated that rats PP2A activity is inhibited in Al-induced AD in rats, leading to elevated tau levels.

Research has shown that diminishing GSK-3β activity and boosting PP2A activity can mitigate tau hyperphosphorylation and cognitive impairment (104). These observations find support in numerous post-mortem studies conducted on AD patients' brains, which demonstrated that neurons bearing tangles were linked to reduced PP2A activities due to increased phosphorylation at Tyr307 and elevated GSK-3β levels (212,213). Nonetheless, a few studies have reported that certain phosphorylated tau residues in AD patients' brains are not influenced by the actions of PP2A and GSK-3β (214,215).

Broadening our perspective, we postulated that the disruption of the Wnt/β-catenin pathway might significantly contribute to the mechanism of aluminum-induced neurotoxicity. This signaling pathway plays a pivotal role in safeguarding neural integrity and synaptic adaptability, with its dysregulation having implications for neurodegenerative disorders such as AD (112,216). Our ongoing investigation proposes that chronic exposure to aluminum disrupts Wnt signaling, thereby compromising neuroprotective mechanisms and potentially aggravating the underlying pathogenesis of AD. Notably, excessive activation of GSK-3β suppresses the Wnt/β-catenin pathway; its inhibition results in elevated GSK-3β activity, instigating β-catenin's degradation. Significantly, the GSK-3β/β-catenin interplay has been linked to neuronal viability, neurodegeneration, and cognitive consolidation (217). Intriguingly, the Wnt/β-catenin pathway is closely intertwined with oxidative stress in AD (217,218). Elevated GSK-3β activity curtails canonical Wnt signaling, amplifying β-catenin phosphorylation and rendering it susceptible to proteasomal degradation (219).

Several investigations underscore the potential interrelation between aluminum-induced neurotoxicity and the Wnt signaling pathway. Notably, studies have indicated that Al-exposed osteoblasts display diminished proliferation due to the downregulation of Wnt/β-catenin pathways. These findings reveal decreased expression of Wnt3a, receptor Frizzled (Fzd2), low-density lipoprotein receptor-related protein 5 (LRP5), β-catenin, Transcription factor 4 (TCF-4), cyclin D1, and c-Myc mRNA, collectively leading to Wnt/β-catenin signaling pathway inactivation, potentially mediated by the reduction in Wnt3a (220–222). In an AD model involving rats exposed to Al over 6 weeks, enhanced Aβ deposition, diminished cholinergic activity, and impaired GSK-3β/Wnt/β-catenin pathways were observed (223). Another study employing an aluminum-induced AD model reported compromised spatial learning, memory, and GSK-3β/Wnt/β-catenin signaling pathways (224).

5.3. Naltrexone

As far as we know, this is the first study investigating the effects of naltrexone, a Mu receptor antagonist, on the GSK-3β and Wnt pathways. We hypothesised that a non-toxic concentration of naltrexone might regulate the GSK-3β and Wnt signaling pathways. Regulation of these pathways would reduce tau hyperphosphorylation, increase neurogenesis and reduce neuroinflammation in Al toxicity and AD disease. We found that naltrexone minimized oxidative stress, elevated GSH levels, activated the Wnt pathway, and inhibited the GSK-3β pathway.

Wnt signaling is essential for neurogenesis in the adult brain and neuronal growth, maturation, differentiation, and proliferation. Impaired Wnt signaling pathways are linked to increased Aβ, decreased β-catenin levels, and increased production of the GSK-3 enzyme, implying a direct link to AD pathogenesis (225). Wnt5a is an innate factor that regulates neurogenesis in the adult brain's hippocampus. Treatment with Wnt5a restores normal neuronal differentiation and proliferation in Wnt5a knockout mice (226). Our study found that naltrexone increased Wnt pathway activity while decreasing GSK-3β activity. As a result, naltrexone may be a promising candidate for stimulating neurogenesis by activating Wnt signaling. However, a study by Hyman and colleagues (227) stated that the administration of 100 mg/kg/day of naltrexone to 17 Alzheimer's patients had no improvement in their cognitive deficits or memory. Ip et al. (228), used a psoriasis tissue model to test naltrexone-containing dermal formulation. The biochemical experiments reported that naltrexone decreases β-catenin activity. However, we have shown that naltrexone increased the activity of β-catenin, thus activating the Wnt signaling pathway. These different results may be due to the different cell types.

Chronic exposure to Al in mice has been shown to cause bone loss and osteoporosis by dysregulating the Wnt signaling. Wnt signaling is crucial for bone regeneration and remodeling during bone development (221,222). Our study found that naltrexone exposure improved the Wnt signaling pathway in Al-treated groups. This suggests that naltrexone may be a potential therapeutic option to promote bone restoration and development in individuals with Al-induced bone impairment.

Exposure to Al has been reported to cause neuroinflammation by increased oxidative stress, impaired ion hemostasis and increased proinflammatory cytokines

and increased lipid peroxidation (229–231). Exposure to Al in our study did also increase oxidative stress parameters significantly. The imbalance in the antioxidant activity in the groups was restored by exposure to naltrexone. This medication has shown to improve inflammation by preventing cytokine and superoxide release (232,233).

Neuroinflammation is another cause of AD (234). An increase in intracellular ROS levels and oxidative damage are modified by hyperphosphorylated tau and Aβ plaques. The dysregulated Wnt signaling also interferes with the immune response to inflammation in the central nervous system (235). Recently, researchers proposed using low-dosage naltrexone as an analgesic and anti-inflammatory in Crohn's disease, multiple sclerosis, fibromyalgia and psoriasis Vulgaris (236,237). Low-dose naltrexone upregulates endogenous encephalin and endorphin levels and positively regulates Mu opioid receptor (238). In the current study, naltrexone was shown to have an anti-inflammatory effect at 2.5 ng/ml by increasing Wnt signaling, decreasing hyperphosphorylated tau, and acting as an anti-inflammatory agent.

GSK-3β activity in the hippocampus of AD patients is linked to hyperphosphorylated tau, NFTs, and an impaired autophagy system (239,240). GSK-3β also contributes to neuroinflammation by regulating the expression and release of harmful cytokines from glial cells, thereby directly increasing neuronal death (241). GSK-3β inhibiting compounds have been proposed to reduce Aβ, increase neurogenesis, and decrease the production of neurofibrillary tangles (5) The effect of naltrexone on GSK-3β levels in the differentiated SH-SY5Y cell line was demonstrated in this study. We revealed that naltrexone significantly decreased the activity of this pathway. Besides that, by inhibiting GSK-3β, naltrexone reduced the production of hyperphosphorylated tau. More research is needed to determine the effects of naltrexone in AD patients, particularly its effect on autophagy stimulation.

In addition to GSK-3β, phosphatase downregulation has been linked to tau aggregation and phosphorylation (242). One of these phosphatases that are dysregulated in AD is PP2A. It is a heterotrimeric phosphatase with structural subunits A, B, and C. Inactivation of PP2A is linked to GSK3-β mediated dysregulation (243). PP2A activators could treat Alzheimer's disease by reducing hyperphosphorylated tau and treating spatial memory deficits. Our findings shed light on the dysregulation of

PP2A and PPP1CA in Alzheimer's disease, and naltrexone may be able to regulate these proteins, lowering tau phosphorylation and spatial memory dysfunction. Another important player in controlling tau phosphorylation besides GSK-3 and PP2A are Akt. The harmonized activity between these molecular mechanisms decreases tauopathies. Growth factors and insulin play as Akt/GSK-3 regulators, which in term decrease tau phosphorylation (166). Naltrexone action on the Akt is increasing its activity which in results will decrease the activity of GSK-3β and decrease the tau phosphorylation and delay the progression of AD.

5.4. Dihydrolipoic acid

The results of our study indicate that cells exposed to DHLA alleviated the neurotoxic effects caused by Al in both differentiated and undifferentiated SH-SY5Y cell lines. Several studies indicated DHLA as a metal chelator, antioxidant, radical scavenger, and anti-inflammatory agent (244–246). Both α-LA and DHLA have also been proposed to have neuroprotective effects and can be an option for treating AD (247–250). However, very little data were published about the ability of α-LA to reduce possible damage caused by Al, whereas no data is available for DHLA (246,251).

In our study, Al-exposed cells treated by DHLA showed a significant decline in ROS and oxidative stress due to this compound's ability to neutralize the free radicals and metal chelation. In one study, it is stated that DHLA lowers the redox activity of transition metal ions but does not remove them from the active site of enzymes (252). In another study, it is suggested that relative to the Fe^{3+}/Fe^{2+} reduction with ascorbate, DHLA can fully inhibit the formation of hydroxyl (•OH) radicals but not with superoxide (O^{2-}) (253). Al is transported to the brain by the iron transporter transferrin, which means that there will be an increased rate of free circulation iron (5). This iron induces lipid peroxidation. As DHLA has a metal-chelating effect, it protects against iron-induced lipid peroxidation (254).

The overproduction of ROS and oxidative stress have detrimental effects on cell structures and contribute to AD development. ROS can react with sugars, DNA, and lipids, producing reactive aldehydes and carbonyl derivatives (255). Measurement of protein carbonylation is considered a useful method to assess the extent of oxidative

damage to proteins associated with oxidative stress, physiological disorders, neurodegeneration, Alzheimer's disease, and ageing (255,256). The increased oxidative stress parameters with a significant increase in carbonyl groups and MDA was observed in our study. Also, exposure to Al in AD groups doubled the oxidative stress effect, thus exacerbating the adverse effects in these groups. Antioxidant act as free radical scavengers or boosters of body antioxidant systems and have shown promise in mitigating oxidative stress in AD, offering potential therapeutic avenues (257). α-LA considerably reduces oxidative stress by limiting lipid and protein oxidation and significantly inhibits free radical production (258) In this study, the oxidative stress level of AD groups treated with DHLA significantly decreased, showing the importance of antioxidants in treatment regimes.

Our study's findings are consistent with prior studies revealing that Al exposure causes tau protein aggregation (259–261). This aggregation is thought to be caused by increased oxidative stress, mitochondrial malfunction, and a disruption in iron homeostasis (262). However, the precise mechanism behind this process is unknown.

Oxidative stress may directly interact with GSK-3β and cause tau phosphorylation and the development of neurofibropathy (263). Under pathological conditions, ROS disrupts tau's normal function, causing it to engage with cyclin-dependent protein kinase-5 and GSK-3β kinases, resulting in hyperphosphorylation. As a result, it loses its capacity to connect to microtubules and accelerates microtubule depolymerization, disrupting neuronal signal conduction. Su et al. (2010) demonstrated that persistent oxidative stress increases tau phosphorylation in M17 neuroblastoma cells and plays an important role in nerve fiber disease *in vivo*. Additionally, ROS inhibits PP2A activity, allowing GSK-3β to be activated. Our experiments align with previous results (265). Our study highlighted that the presence of DHLA reduced oxidative stress. Consequently, the PP2A and PP1AC activity was regulated, reducing tau and GSK-3β.

The Akt pathway supports neuronal survival, whereas its blockage causes neuronal death. Akt has a wide range of biological effects, mostly by boosting the phosphorylation of Bax (one of the Bcl-2 family's apoptotic promoters), mammalian target of rapamycin (mTOR), GSK-3β, and other downstream substrates (266).

Downregulation of Akt with increased GSK-3β activity is linked to brain dysfunction and neuropathophysiological alterations. GSK-3β, in its active state, translocate from the cytoplasm to the nucleus and causes apoptotic effects (267). Zhu et al. (268) demonstrated that/GSK-3β/β-catenin signaling pathway activation mitigates neuronal apoptosis triggered by Aβ. In the present study, exposure to Al has caused a decrease in Akt level and increased GSK-3β activity. In contrast, treatment by DHLA significantly increased the Akt and decreased the GSK-3β, showing that Al exposure dysregulates GSK-3β/Akt pathway. Our results are consistent with the findings of Huang et al. (2017) which reported that one of the pathways behind Al toxicity in the PC12 cell line is the change in Akt/GSK-3β pathway.

Wnt signaling is important in the nervous system, from early patterning to higher functions such as synaptic plasticity and memory in the adult brain. Several Wnt pathway components, like Wnt ligands (Wnt2, Wnt4, and Wnt9a), as well as transcription factors lymphoid enhancer-binding factor 1 (Lef1) and transcription factor 3 (Tcf3), are down-regulated in the elderly rodent brain. Wnt3 and Wnt3a expression in the *dentate gyrus* area of the hippocampus decreases between 1 and 22 months of age. Furthermore, there is a distinct decrease in canonical Wnt signaling in the hippocampus of elderly rats where disheveled segment polarity protein 2 (Dvl2), Axin2, and nuclear β-catenin are downregulated by age (269). Reduced Wnt signaling increases GSK-3β activity, contributing to tau hyperphosphorylation. GSK-3β overexpression in the brain induces neurodegeneration and learning impairments (269,270). The Wnt signaling pathway was impaired in our AD groups, indicating decreased Wnt activity as a possible mechanism involved in AD development. The reported increased activity of GSK-3β in our study is evidence to conclude that Wnt signaling has been suppressed in AD.

Along with AD groups, a decrease in the Wnt signaling pathway was also observed in cells exposed to Al. This may indicate that an impaired Wnt signaling pathway might be an underlying mechanism behind the neurotoxicity of Al. Treatment with DHLA, especially in the AD and Al groups, improved Wnt signaling. As a result, DHLA reduced the activity of GSK-3β, and Wnt signaling improved in all DHLA-treated cells.

5.5. Metformin

Numerous studies have demonstrated that insulin resistance contributes to advancing two primary clinical characteristics of AD, Aβ and NFTs (271,272). Brain insulin levels and their binding to the insulin receptor decline with ageing and are significantly lower in the brains of individuals with AD than those without the condition (273). AD patients exhibit reduced CSF insulin and insulin resistance levels to prolonged peripheral hyperinsulinemia and decreased insulin transport across the BBB (274). Moreover, the buildup of Aβ oligomers can impede the self-phosphorylation of the insulin receptor (IR). These oligomers can also notably diminish the levels and functioning, resulting in the loss of dendritic structures and synaptic connections (275). Chronic hyperinsulinemia has also been reported in impaired memory and cognition (276).

Insulin resistance triggers microglial activation and inflammation, involving changes in microglial characteristics and responses. This condition shares a common molecular feature with AD, which is elevated levels of AGEs. When AGEs bind to cellular receptors, they promote tau hyperphosphorylation through GSK-3β activation and activate the NF-κB pathway, producing pro-inflammatory cytokines (274). Pro-inflammatory cytokines contribute to an elevation in the accumulation of Aβ. This, in turn, amplifies the influx of calcium ions, resulting in heightened tau phosphorylation mediated by GSK-3 and suppression of IR tyrosine kinase signaling. Elevated calcium levels stimulate the activation of Ca^{2+}-Akt, which subsequently phosphorylates IRs, thereby exerting a negative regulatory influence on insulin receptors within the brain (277). As previously discussed, insulin resistance leads to the generation of ROS. This heightened oxidative stress results in the deactivation of the Akt pathway, concurrently triggering the activation of GSK-3 downstream and, consequently, leading to the excessive phosphorylation of the tau protein (278,279). The accumulation of Aβ and the excessive phosphorylation of tau play a role in a self-reinforcing mechanism that worsens insulin resistance. This mechanism is driven by heightened oxidative stress, neurotoxicity, and impaired synaptic function (280).

Mice with diabetes and advanced age serve as a compelling model for investigating nerve damage, showcasing many neuropathological traits reminiscent of AD. These traits encompass diminished Akt activity, neuronal depletion, the buildup

of tau protein, and the overactivation of GSK-3β. In this context, metformin, known for its anti-diabetic properties, emerges as a promising therapeutic avenue. It holds the potential to be harnessed in the realms of ageing and neurodegenerative conditions, offering a means to mitigate or alleviate these detrimental effects. A recent study by Chen et al. (281) showcased metformin's remarkable potential in mitigating oxidative stress and reducing Aβ accumulation in the hippocampus of db/db mice. Additionally, Li et al. (282) highlighted metformin's capacity to enhance brain bioenergetics and improve cognitive function in non-diabetic mice. Building upon these pivotal insights, our investigation delved into how metformin impacts SH-SY5Y cells. Our results yield promise, demonstrating that metformin exposure significantly reduced oxidative stress levels and a noteworthy amelioration of AD. It is worth noting that sub-chronic exposure to Al in mice has been documented to disrupt glucose metabolism, consequently inducing alterations in brain energy metabolism and exacerbating the toxic effects of Al. This disruption ultimately results in insufficient ATP synthesis, neuronal demise, and a decline in cognitive function. However, Song et al. (283) observed that metformin could effectively alleviate the energy metabolism disorder and cognitive impairment induced by Al exposure.

In the investigation conducted by Li et al. (284), they employed the SH-SY5Y cell line exposed to Aβ as an AD model. Their findings indicated that metformin treatment not only halted apoptosis but also orchestrated the regulation of autophagy. Additionally, metformin contributed to a reduction in intracellular calcium levels and a decrease in the presence of ROS. These effects were attributed to the attenuation of neurotoxicity induced by excitatory amino acids and, possibly, the restoration of proper autophagy processes through autophagy regulation.

In the study by Binlateh et al. (285), exposure to metformin in SH-SY5Y cells increased ROS levels. However, a noteworthy contrast emerged in our research, as the group subjected to metformin treatment exhibited a significant decrease in ROS levels. Our research findings provide clear evidence that metformin effectively modulates the activity of Akt. Metformin is crucial in promoting neuronal survival by activating the Nrf2-HO-1 signaling pathway through the Akt pathway in SH-SY5Y, hence facilitating the induction of antioxidative characteristics (286).

One of the mechanisms contributing to the neuroprotective benefits of metformin involves its influence on GSK-3β and PP2A kinases. In vitro studies have consistently indicated that metformin has the potential to reduce tau phosphorylation through these pathways (287–289). In addition to in vitro investigations, a few in vivo studies have demonstrated metformin's anticancer properties by modulating these pathways (289). As our results underscore, metformin exhibited a dual impact on GSK-3β and PP2A levels, notably decreasing GSK-3β while increasing PP2A activity. This effect was consistent across both Al-exposed groups and the AD model, reducing tau phosphorylation. Within the context of AD, it is widely posited that insulin resistance plays a pivotal role by instigating the activation of GSK-3β, a kinase of significance. This activation, in turn, precipitates the aggregation of Aβ, setting in motion a cascade that triggers the hyperphosphorylation of tau proteins (290). This intricate sequence of events is central to our understanding of AD pathology.

To the best of our knowledge, the potential influence of metformin on the Wnt signaling pathway, which may underlie its neuroprotective effects, remains unexplored. Nevertheless, there have been limited investigations into how metformin modulates Wnt signaling in the contexts of cancer (291,292) and diabetes. Studies conducted on osteoblasts have provided intriguing insights, revealing that metformin can regulate Wnt signaling, reducing inflammation and apoptosis (293). Our research findings have contributed to the growing understanding of metformin's impact on Wnt signaling. In our study, metformin effectively regulated the Wnt pathway by diminishing GSK-3β activity and elevating beta-catenin levels. This dual action on GSK-3β and β-catenin subsequently enhanced Wnt signaling, facilitating neurogenesis and bolstering cell survival as key outcomes.

Numerous investigations have demonstrated that metformin's central mechanism of action primarily involves inhibiting mitochondrial complex I, also known as NADH (294–296). This particular complex is recognized for its significant contribution to the generation of ROS within cells(297). Well-documented research has established that the blockade of this complex results in a diminished production of reactive species stemming from a reduced flow of electrons originating from NADH plus H^+. Consequently, the evidence strongly suggests that metformin effectively lowers endogenous ROS levels within the mitochondria. Moreover, metformin was

able to reduce SOD, and CAT enzyme expression in rats. However, no difference in Gpx or GSH activity was reported (298).

Furthermore, in a study by Diniz Vilela et al. (298), it was observed that metformin could decrease the expression of SOD and CAT enzymes in rats, although no discernible difference in Gpx or GSH activity (299,300) was noted. Our investigation found that metformin significantly impacted both Al-exposed groups and AD-affected groups, which initially exhibited high ROS levels. Metformin treatment resulted in a substantial increase in total antioxidant capacity, a reduction in MDA and protein oxidation, and a notable elevation in GSH levels. These findings underscore the potent antioxidant properties of metformin. Reduced MDA levels have been reported in diabetic patients using metformin (299). Metformin also increases the Akt phosphorylation (300), as shown in the results, which plays a crucial role in preserving mitochondrial integrity and enhancing the capacity to withstand damage caused by inflammation and oxidative stress. In AD, reduced glucose metabolism and impaired glucose uptake by neurons have been reported to increase oxidative stress and Aβ plaques. Metformin administration has been shown to reduce oxidative stress and ROS damage in these cases. Metformin also induces autophagy by activating the AMPK pathway and reducing Aβ plaques (300).

6. CONCLUSION

The need for cell culture models that faithfully replicate fully developed human neurons is paramount in the field of neuroscience. While human neural crest stem cells hold promise in this regard, their application is riddled with challenges. Beyond ethical concerns, it's crucial to recognize their susceptibility to precise culturing conditions and their notable variability in culture. This study introduces an innovative strategy for inducing differentiation in a widely accessible human neuroblastoma cell line, transforming them into cells closely resembling mature human neurons in patients with Alzheimer's disease. The differentiation of SH-SY5Y cell lines through the application of retinoic acid and BDNF offers a reproducible and readily available methodology that is also cost-effective. These attributes render it highly suitable for investigating critical cellular structures and processes in the field of neuroscience. Notably, our model effectively captures two pivotal hallmarks of Alzheimer's disease: the formation of senile plaques and hyperphosphorylated tau. The cellular morphology remained consistent throughout the experiment, and cell survival rates were maintained as intended. While some researchers have argued against using SH-SY5Y in elucidating Alzheimer's disease's primary molecular mechanisms, our study has demonstrated that this cell line can fully express the specific molecular mechanisms targeted in our project.

Among the many risk factors associated with Alzheimer's disease, aluminum occupies a significant position due to its pervasive presence in our daily lives. Exposure to aluminum occurs readily and abundantly through commonplace sources such as household items, building construction materials, vaccines, and even drinking water. An alarming aspect is aluminum's ability to traverse the BBB and accumulate within the brain easily. Even minimal, chronic exposure to this metal elevates the risk of aluminum-induced neurotoxicity, a condition implicated in developing neurodegenerative diseases, including Alzheimer's. We also have shown that aluminum would show its neurotoxicity by dysregulating Wnt signaling and impairing the neurogenesis.

In the realm of scientific literature, researchers have predominantly employed aluminum chloride or aluminum malate as agents to investigate aluminum-induced toxicity. However, our investigation ventured into relatively uncharted territory by

utilizing aluminum hydroxide, an adjuvant commonly found in vaccines. This choice allowed us to reveal a crucial insight: irrespective of the specific aluminum compound employed, and there exists a concerning potential for the induction of neurodegenerative disorders and harm to the human body. Our findings underscore the significance of comprehensively assessing the impact of various aluminum formulations on health and the potential risks they may pose.

Naltrexone, an opioid antagonist, has recently garnered significant attention among researchers due to its potential as a neuroprotective agent. This interest arises from its ability to safeguard against neuroinflammation, particularly in lower doses than those typically used as an antidote. Remarkably, naltrexone has not undergone testing in any Alzheimer's disease models thus far, and our study is poised to serve as a crucial reference point for future investigations.

In our research, naltrexone displayed promising outcomes by effectively reducing oxidative stress within our model. This outcome holds the promise that forthcoming studies, both in animal models and later in clinical settings, may unveil new possibilities for applying this medication in neurodegeneration. Although more detailed, dose-dependent in vivo and in vitro studies are necessary to pinpoint the optimal form and dosage for administering this medication, our work has illuminated the path for future research endeavors.

The encouraging effects of naltrexone in diminishing tau protein levels, a hallmark feature in aluminum toxicity and Alzheimer's disease have opened up fresh avenues for exploring other elements within the GSK and Wnt signaling pathways. This revelation offers exciting prospects for further investigations into the intricate molecular mechanisms that underlie these conditions.

Our research findings have illuminated a compelling discovery: the direct addition of dihydrolipoic acid to the media can substantially mitigate the toxicity induced by aluminum. This intervention led to a dramatic reduction in oxidative stress and a noteworthy increase in total antioxidant capacity. These outcomes strongly suggest that incorporating this compound into the diet of individuals may serve as a protective measure against Alzheimer's disease or potentially ameliorate its symptoms.

Interestingly, dihydrolipoic acid can be readily administered through supplements, eliminating the need for the intermediate step of metabolizing α-lipoic

acid into dihydrolipoic acid. We propose that this approach could yield faster and more effective results. Despite being primarily recognized as an antioxidant, with its primary function centered on reducing ROS and oxidative stress, dihydrolipoic acid also exhibited a potent chelating effect. This ability to effectively mitigate the neurotoxic effects of aluminum highlights its multifaceted properties.

Surprisingly, there is a scarcity of information concerning the impact of this compound on various molecular pathways. Consequently, our project has not only shed light on its potential but has also opened up exciting new avenues for researching the influence of this antioxidant on different pathways, expanding our understanding of its broader effects.

Metformin, a widely recognized medication in the treatment of diabetes, has displayed encouraging potential in mitigating aluminum toxicity within our Alzheimer's disease model. While existing literature has offered limited insights into the impact of metformin on the Wnt signaling pathway, our research has illuminated a novel dimension. We have demonstrated that metformin possesses the capacity to engage this pathway, suggesting that its neuroprotective effects may be mediated through this intricate mechanism. Furthermore, metformin's interaction with GSK-3β holds promise in reducing two critical hallmarks of Alzheimer's disease: amyloid-beta aggregation and tau hyperphosphorylation. This multi-faceted role of metformin introduces a promising avenue for further exploration in the quest to combat this debilitating neurodegenerative condition.

Parallel in vivo and in vitro studies for all of these xenobiotics with different concentrations and incubation periods with different concentrations of aluminum will be the most important further study topics of this project. The exact phosphorylation site of the GSK-3β and β-catenin activated in aluminum toxicity would be another topic to investigate.

7. REFERENCES

1. Alasfar RH, Isaifan RJ. Aluminum environmental pollution: the silent killer. Environmental Science and Pollution Research. 2021;28(33):44587–97.

2. ATSDR. Toxicological Profile for Aluminum. In: ATSDR's Toxicological Profiles. CRC Press; 2008.

3. Inan-Eroglu E, Ayaz A. Is aluminum exposure a risk factor for neurological disorders? Journal of Research in Medical Sciences. 2018;23(1):51.

4. Sanajou S, Şahin G, Baydar T. Aluminium in cosmetics and personal care products. Journal of Applied Toxicology. 2021;41(11): jat.4228.

5. Sanajou S, Erkekoğlu P, Şahin G, Baydar T. Role of aluminum exposure on Alzheimer's disease and related glycogen synthase kinase pathway. Drug Chem Toxicol. 2023;46(3):510–22.

6. Wang Z, Wei X, Yang J, Suo J, Chen J, Liu X, et al. Chronic exposure to aluminum and risk of Alzheimer's disease: A meta-analysis. Neurosci Lett. 2016; 610:200–6.

7. Mendiola-Precoma J, Berumen LC, Padilla K, Garcia-Alcocer G. Therapies for Prevention and Treatment of Alzheimer's Disease. Biomed Res Int. 2016; 2016:1–17.

8. Breijyeh Z, Karaman R. Comprehensive Review on Alzheimer's Disease: Causes and Treatment. Molecules. 2020;25(24):5789.

9. Niu Q. Overview of the Relationship Between Aluminum Exposure and Health of Human Being. In: Advances in Experimental Medicine and Biology. Springer New York LLC; 2018:1–31.

10. Hardisson A, Revert C, Dailos González- Weller, Gutiérrez Á, Paz S, Rubio C. Aluminium Exposure Through the Diet. Food Sci Nutr. 2017;3(2):1–10.

11. Igbokwe IO, Igwenagu E, Igbokwe NA. Aluminium toxicosis: a review of toxic actions and effects. Interdiscip Toxicol . 2019;12(2):45–70.

12. Krewski D, Yokel R a, Nieboer E, Borchelt D, Cohen J, Harry J, et al. Human health risk assessment for aluminium, aluminium oxide, and aluminium hydroxide. J Toxicol Environ Health B Crit Rev. 2007;10 Suppl 1(1):1–269.

13. Hu X, He H. A Review of Cosmetic Skin Delivery. J Cosmet Dermatol. 2021 Mar 2; jocd.14037.

14. Yousef H, Sharma S. Anatomy, Skin (Integument), Epidermis. StatPearls. StatPearls Publishing; 2018.

15. Larese Filon F. Penetration of Metals Through the Skin Barrier. In: Metal Allergy. Cham: Springer International Publishing; 2018:67–74.

16. Exley C. Human exposure to aluminium. Environ Sci: Processes Impacts. 2013;15(10):1807–16.

17. Anane R, Bonini M, Creppy EE. Transplacental passage of aluminium from pregnant mice to fetus organs after maternal transcutaneous exposure. Hum Exp Toxicol.;16(9):501–4.

18. Flarend R, Bin T, Elmore D, Hem SL. A preliminary study of the dermal absorption of aluminium from antiperspirants using aluminium-26. Food and Chemical Toxicology. 2001;39(2):163–8.

19. Pineau A, Guillard O, Fauconneau B, Favreau F, Marty MH, Gaudin A, et al. In vitro study of percutaneous absorption of aluminum from antiperspirants through human skin in the Franz^{TM} diffusion cell. J Inorg Biochem. 2012; 110:21–6.

20. Sorenson JRJ, Campbell IR, Tepper LB, Lingg RD. Aluminum in the Environment and Human Health. Environ Health Perspect. 1974; 8:3–95.

21. Lee RE, von Lehmden DJ. Trace Metal Pollution in the Environment. J Air Pollut Control Assoc. 1973;23(10):853–7.

22. Exley C. Aluminium and iron, but neither copper nor zinc, are key to the precipitation of β-sheets of Aβ 42 in senile plaque cores in Alzheimer's disease. Journal of Alzheimer's Disease. 2006;10(2–3):173–7.

23. Wesdock JC, Arnold IMF. Occupational and Environmental Health in the Aluminum Industry. J Occup Environ Med. 2014 May;56(Supplement 5S): S5–11.

24. Liaquat L, Sadir S, Batool Z, Tabassum S, Shahzad S, Afzal A, et al. Acute aluminum chloride toxicity revisited: Study on DNA damage and histopathological, biochemical and neurochemical alterations in rat brain. Life Sci. 2019; 217:202–11.

25. Nie J. Exposure to Aluminum in Daily Life and Alzheimer's Disease. Adv Exp Med Biol. 2018; 1091:99–111.

26. Harris WR. Binding and transport of aluminum by serum proteins. Coord Chem Rev. 1996; 149:347–65.

27. Valkonen S, Aitio A. Analysis of aluminium in serum and urine for the biomonitoring of occupational exposure. Science of The Total Environment. 1997;199(1–2):103–10.

28. Chen B, Zeng Y, Hu B. Study on speciation of aluminum in human serum using zwitterionic bile acid derivative dynamically coated C18 column HPLC separation with UV and on-line ICP-MS detection. Talanta. 2010;81(1–2):180–6.

29. EFSA. Statement of EFSA on the Evaluation of a new study related to the bioavailability of aluminium in food. EFSA Journal. 2011;9(5):2157.

30. Ganrot R 0. Metabolism and Possible Health Effects of Aluminum. Vol. 65, Environmental Health Perspectives. 1986.

31. Exley C. The toxicity of aluminium in humans. Morphologie. 2016;100(329):51–5.

32. Dey M, Singh RK. Neurotoxic effects of aluminium exposure as a potential risk factor for Alzheimer's disease. Pharmacological Reports. 2022;74(3):439–50.

33. Tietz T, Lenzner A, Kolbaum AE, Zellmer S, Riebeling C, Gürtler R, et al. Aggregated aluminium exposure: risk assessment for the general population. Arch Toxicol. 2019;93(12):3503–21.

34. Bondy SC. Low levels of aluminum can lead to behavioral and morphological changes associated with Alzheimer's disease and age-related neurodegeneration. Neurotoxicology. 2016; 52:222–9.

35. Exley C, Price NC, Kelly SM, Birchall JD. An interaction of β-amyloid with aluminium in vitro. FEBS Lett. 1993;324(3):293–5.

36. Bondy SC, Truong A. Potentiation of beta-folding of β-amyloid peptide 25–35 by aluminum salts. Neurosci Lett. 1999;267(1):25–8.

37. Mirhashemi SM, Shahabaddin ME. Evaluation of aluminium, manganese, copper and selenium effects on human islets amyloid polypeptide hormone aggregation. Pakistan Journal of Biological Sciences. 2011;14(4):288–92.

38. Mirhashemi SM, Aarabi MH. To study various concentrations of magnesium and aluminium on amylin hormone conformation. Pakistan Journal of Biological Sciences. 2011;14(11):653–7.

39. Sakamoto T, Saito H, Ishii K, Takahashi H, Tanabe S, Ogasawara Y. Aluminum inhibits proteolytic degradation of amyloid β peptide by cathepsin D: A potential link between aluminum accumulation and neuritic plaque deposition. FEBS Lett. 2006;580(28–29):6543–9.

40. Exley C, Birchall JD. The cellular toxicity of Aluminium. journal of theorethical Biology. 1992; 159:83–98.

41. Mailloux RJ, Hamel R, Appanna VD. Aluminum toxicity elicits a dysfunctional TCA cycle and succinate accumulation in hepatocytes. J Biochem Mol Toxicol. 2006;20(4):198–208.

42. Capdevielle MC, Scanes CG. Effect of dietary acid or aluminum on growth and growth-related hormones in mallard ducklings (Anas platyrhynchos). Arch Environ Contam Toxicol. 1995;29(4):462–8.

43. Grewal P, Viswanathen VA. Liver Cancer and Alcohol. Clin Liver Dis. 2012;16(4):839–50.

44. Toyokuni S. Iron and carcinogenesis: from Fenton reaction to target genes. Redox Report. 2002;7(4):189–97.

45. Niemoeller OM, Kiedaisch V, Dreischer P, Wieder T, Lang F. Stimulation of eryptosis by aluminium ions. Toxicol Appl Pharmacol. 2006;217(2):168–75.

46. Yang X, Yu K, Wang H, Zhang H, Bai C, Song M, et al. Bone impairment caused by AlCl3 is associated with activation of the JNK apoptotic pathway mediated by oxidative stress. Food and Chemical Toxicology. 2018;116(600):307–14.

47. Yamanaka K, Minato N, Iwai K. Stabilization of iron regulatory protein 2, IRP2, by aluminum. FEBS Lett. 1999;462(1–2):216–20.

48. Anane R, Creppy EE. Lipid peroxidation as pathway of aluminium cytotoxicity in human skin fibroblast cultures: Prevention by superoxide dismutase+catalase and vitamins E and C. Hum Exp Toxicol. 2001;20(9):477–81.

49. Gonzalez MA, Alvarez MDL, Pisani GB, Bernal CA, Roma MG, Carrillo MC. Involvement of oxidative stress in the impairment in biliary secretory function induced by intraperitoneal administration of aluminum to rats. Biol Trace Elem Res. 2007;116(3):329–48.

50. D'Souza SP, Vijayalaxmi KK, Naik P. Assessment of genotoxicity of aluminium acetate in bone marrow, male germ cells and fetal liver cells of Swiss albino mice. Mutation Research/Genetic Toxicology and Environmental Mutagenesis. 2014 May 15; 766:16–22.

51. Lukiw WJ, LeBlanc HJ, Carver LA, McLachlan DRC, Bazan NG. Run-on gene transcription in human neocortical nuclei. Journal of Molecular Neuroscience.1998;11(1):67–78.

52. Nam SM, Kim JW, Yoo DY, Kim W, Jung HY, Hwang IK, et al. Additive or synergistic effects of aluminum on the reduction of neural stem cells, cell proliferation, and neuroblast differentiation in the dentate gyrus of high-fat diet-fed mice. Biol Trace Elem Res. 2014;157(1):51–9.

53. Nam SM, Kim JW, Yoo DY, Jung HY, Choi JH, Hwang IK, et al. Reduction of adult hippocampal neurogenesis is amplified by aluminum exposure in a model of type 2 diabetes. J Vet Sci. 2016;17(1):13–20.

54. Yang X, Huo H, Xiu C, Song M, Han Y, Li Y, et al. Inhibition of osteoblast differentiation by aluminum trichloride exposure is associated with inhibition of BMP-2/Smad pathway component expression. Food and Chemical Toxicology. 2016; 97:120–6.

55. Fogarty U, Perl D, Good P, Ensley S, Seawright A, Noonan J. A cluster of equine granulomatous enteritis cases: the link with aluminium. Vet Hum Toxicol. 1998;40(5):297–305.

56. De Chambrun GP, Body-Malapel M, Frey-Wagner I, Djouina M, Deknuydt F, Atrott K, et al. Aluminum enhances inflammation and decreases mucosal healing in experimental colitis in mice. Mucosal Immunology 2014 7:3. 2013;7(3):589–601.

57. Jangra A, Kasbe P, Pandey SN, Dwivedi S, Gurjar SS, Kwatra M, et al. Hesperidin and Silibinin Ameliorate Aluminum-Induced Neurotoxicity: Modulation of Antioxidants and Inflammatory Cytokines Level in Mice Hippocampus. Biol Trace Elem Res. 2015;168(2):462–71.

58. Johnson VJ, Sharma RP. Aluminum Disrupts the Pro-Inflammatory Cytokine/Neurotrophin Balance in Primary Brain Rotation-Mediated Aggregate Cultures: Possible Role in Neurodegeneration. Neurotoxicology. 2003;24(2):261–8.

59. Milnerowicz H, Ściskalska M, Dul M. Pro-inflammatory effects of metals in persons and animals exposed to tobacco smoke. Journal of Trace Elements in Medicine and Biology. 2015; 29:1–10.

60. AI P, V J, Y Z, WJ L. Systemic Inflammation in C57BL/6J Mice Receiving Dietary Aluminum Sulfate; Up-Regulation of the Pro-Inflammatory Cytokines IL-6 and

TNFα, C-Reactive Protein (CRP) and miRNA-146a in Blood Serum. J Alzheimers Dis Parkinsonism. 2017;07(06):1–6.

61. She Y, Wang N, Chen C, Zhu Y, Xia S, Hu C, et al. Effects of Aluminum on immune functions of cultured splenic T and B lymphocytes in rats. Biol Trace Elem Res. 2012;147(1–3):246–50.

62. Zhang H, Yang X, Qin X, Niu Q. Caspase-3 is Involved in Aluminum-Induced Impairment of Long-Term Potentiation in Rats Through the Akt/GSK-3β Pathway. Neurotox Res. 2016;29(4):484–94.

63. Netterlid E, Hindsén M, Siemund I, Björk J, Werner S, Jacobsson H, et al. Does Allergen-specific Immunotherapy Induce Contact Allergy to Aluminium? Acta Dermato Venereologica.2013; 93(1):50-56.

64. Chinoy N, Patel T. Effects of Sodium Fluoride and Aluminum Chloride on Ovary and Uterus of Mice and Their Reversal by Some Antidotes. Biology (Basel). 2001; 34:9–21.

65. Shahraki MR, Palan Mony EY, Zahedi Asl S, Sarkaki AR, Shahraki AR. Effects of aluminium chloride injection in lateral ventricle on serum gonadothropines, testosterone and spermatogenesis in rats. Journal of Medical Sciences. 2008;8(4):410–4.

66. Orihuela D. Aluminium effects on thyroid gland function: Iodide uptake, hormone biosynthesis and secretion. J Inorg Biochem. 2011;105(11):1464–8.

67. Zhang Q, Cao Z, Sun X, Zuang C, Huang W, Li Y. Aluminum Trichloride Induces Hypertension and Disturbs the Function of Erythrocyte Membrane in Male Rats. Biol Trace Elem Res. 2016;171(1):116–23.

68. Fu Y, Jia FB, Wang J, Song M, Liu SM, Li YF, et al. Effects of sub-chronic aluminum chloride exposure on rat ovaries. Life Sci. 2014;100(1):61–6.

69. Lukyanenko LM, Skarabahatava AS, Slobozhanina EI, Kovaliova SA, Falcioni ML, Falcioni G. In vitro effect of AlCl3 on human erythrocytes: Changes in membrane morphology and functionality. Journal of Trace Elements in Medicine and Biology. 2013;27(2):160–7.

70. Suwalsky M, Norris B, Villena F, Cuevas F, Sotomayor P, Zatta P. Aluminum fluoride affects the structure and functions of cell membranes. Food and Chemical Toxicology. 2004;42(6):925–33.

71. Vittori D, Nesse A, Pérez G, Garbossa G. Morphologic and functional alterations of erythroid cells induced by long-term ingestion of aluminium. J Inorg Biochem. 1999;76(2):113–20.

72. Skarabahatava AS, Lukyanenko LM, Slobozhanina EI, Falcioni ML, Orlando P, Silvestri S, et al. Plasma and mitochondrial membrane perturbation induced by aluminum in human peripheral blood lymphocytes. Journal of Trace Elements in Medicine and Biology. 2015; 31:37–44.

73. Vorbrodt AW, Trowbridge RS, Dobrogowska DH. Cytochemical study of the effect of aluminium on cultured brain microvascular endothelial cells. The Histochemical Journal. 1994;26(2):119–26.

74. Vota DM, Crisp RL, Nesse AB, Vittori DC. Oxidative stress due to aluminum exposure induces eryptosis which is prevented by erythropoietin. J Cell Biochem. 2012;113(5):1581–9.

75. Gitler AD, Dhillon P, Shorter J. Neurodegenerative disease: Models, mechanisms, and a new hope. DMM Disease Models and Mechanisms. 2017;10(5):499–502.

76. Lane CA, Hardy J, Schott JM. Alzheimer's disease. Eur J Neurol. 2018 Jan;25(1):59–70.

77. Dernegi A. Türkiye Alzheimer Derneği. 2021. Available from: https://www.alzheimerdernegi.org.tr/2020/08/29/turkiyede-600-000-aile-alzheimer-hastaligi-ile-mucadele-ediyor/

78. Association A. 2020 Alzheimer' s disease facts and figures. Alzheimers Dement. 2020;391–460.

79. OECD/European Union. Health at a Glance: Europe 2018. In 2018:108–9.

80. WHO. WHO. 2021. WHO EMRO | Dementia | Health topics. Available from: http://www.emro.who.int/health-topics/dementia/index.html

81. Cipriani G, Dolciotti C, Picchi L, Bonuccelli U. Alzheimer and his disease: a brief history. Neurological Sciences. 2011;32(2):275–9.

82. Pascual B, Masdeu JC. Tau, amyloid, and hypometabolism in the logopenic variant of primary progressive aphasia. Neurology. 2016;86(5):487–8.

83. Mendez MF. Early-Onset Alzheimer Disease. Neurol Clin. 2017;35(2):263–81.

84. Karran E, Strooper B De. The amyloid hypothesis in Alzheimer disease: new insights from new therapeutics. Nature Reviews Drug Discovery.2022;21(4): 306-318.

85. Skalny A V., Aschner M, Jiang Y, Gluhcheva YG, Tizabi Y, Lobinski R, et al. Molecular mechanisms of aluminum neurotoxicity: Update on adverse effects and therapeutic strategies. Adv Neurotoxicol. 2021; 5:1–34.

86. Lauretti E, Dincer O, Praticò D, Roda A, Serra-Mir G, Montoliu-Gaya L, et al. Glycogen synthase kinase-3 signaling in Alzheimer's disease. Biochim Biophys Acta Mol Cell Res. 2020;1867(5):118664.

87. Roda A, Serra-Mir G, Montoliu-Gaya L, Tiessler L, Villegas S. Amyloid-beta peptide and tau protein crosstalk in Alzheimer's disease. Neural Regen Res. 2022;17(8):1666–74.

88. Jagust W. Is amyloid-β harmful to the brain? Insights from human imaging studies. Brain. 2016;139(1):23.

89. Makin S. The amyloid hypothesis on trial. Nature. 2018;559(7715): S4–7.

90. Society A. Alzheimer Society of Canada. 2021. Risk factors for dementia | Alzheimer Society of Canada.

91. Kitagishi Y, Nakanishi A, Ogura Y, Matsuda S. Dietary regulation of PI3K/AKT/GSK-3β pathway in Alzheimer's disease. Alzheimers Res Ther. 2014;6(3):1–7.

92. Chen XQ, Mobley WC. Exploring the pathogenesis of Alzheimer disease in basal forebrain cholinergic neurons: Converging insights from alternative hypotheses. Front Neurosci. 2019;13(MAY):1–18.

93. Ferreira-Vieira TH, Guimaraes IM, Silva FR, Ribeiro FM. Alzheimer's Disease: Targeting the Cholinergic System. Curr Neuropharmacol. 2016; 14:101–15.

94. Hampel H, Mesulam MM, Cuello AC, Farlow MR, Giacobini E, Grossberg GT, et al. The cholinergic system in the pathophysiology and treatment of Alzheimer's disease. Brain. 2018;141(7):1917–33.

95. Sanabria-Castro A, Alvarado-Echeverría I, Monge-Bonilla C. Molecular pathogenesis of alzheimer's disease: An update. Ann Neurosci. 2017;24(1):46–54.

96. Hampel H, Mesulam MM, Cuello AC, Khachaturian AS, Vergallo A, Farlow MR, et al. Revisiting the Cholinergic Hypothesis in Alzheimer's Disease: Emerging Evidence from Translational and Clinical Research. J Prev Alzheimers Dis. 2019;6(1):2–15.

97. Hoffmeister L, Diekmann M, Brand K, Huber R. GSK3: A Kinase Balancing Promotion and Resolution of Inflammation. Cells. 2020;9(4):820.

98. Gu Y, Gao L, Han Q, Li A, Yu H, Liu D, et al. GSK-3β at the Crossroads in Regulating Protein Synthesis and Lipid Deposition in Zebrafish. Cells. 2019;8(3):205.

99. Beurel E, Grieco SF, Jope RS. Glycogen synthase kinase-3 (GSK3): Regulation, actions, and diseases. Pharmacol Ther. 2015; 148:114–31.

100. Jope RS, Cheng Y, Lowell JA, Worthen RJ, Sitbon YH, Beurel E. Stressed and Inflamed, Can GSK3 Be Blamed? Trends Biochem Sci. 2017;42(3):180–92.

101. Walz A, Ugolkov A, Chandra S, Kozikowski A, Carneiro BA, O'Halloran T V., et al. Molecular Pathways: Revisiting Glycogen Synthase Kinase-3β as a Target for the Treatment of Cancer. Clinical Cancer Research. 2017;23(8):1891–7.

102. Bhat R V., Andersson U, Andersson S, Knerr L, Bauer U, Sundgren-Andersson AK. The Conundrum of GSK3 Inhibitors: Is it the Dawn of a New Beginning? Perry G, Avila J, Moreira PI, Sorensen AA, Tabaton M, editors. Journal of Alzheimer's Disease. 2018;64(s1): S547–54.

103. Sayas CL, Ávila J. GSK-3 and Tau: A Key Duet in Alzheimer's Disease. Cells. 2021;10(4):721.

104. Toral-Rios D, Pichardo-Rojas PS, Alonso-Vanegas M, Campos-Peña V. GSK3β and Tau Protein in Alzheimer's Disease and Epilepsy. Front Cell Neurosci. 2020;14(March):1–9.

105. Ly PTT, Wu Y, Zou H, Wang R, Zhou W, Kinoshita A, et al. Inhibition of GSK3β-mediated BACE1 expression reduces Alzheimer-associated phenotypes. Journal of Clinical Investigation. 2013;123(1):224–35.

106. Peineau S, Nicolas CS, Bortolotto ZA, Bhat R V, Ryves WJ, Harwood AJ, et al. A systematic investigation of the protein kinases involved in NMDA receptor-dependent LTD: evidence for a role of GSK-3 but not other serine/threonine kinases. Mol Brain. 2009;2(1):22.

107. Zhang H, Han Y, Zhang L, Jia X, Niu Q. The GSK-3β/β-Catenin Signaling–Mediated Brain–Derived Neurotrophic Factor Pathway Is Involved in Aluminum-Induced Impairment of Hippocampal LTP In Vivo. Biol Trace Elem Res. 2021;199(12):4635–45.

108. Ng L, Kaur P, Bunnag N, Suresh J, Sung I, Tan Q, et al. WNT Signaling in Disease. Cells. 2019;8(8):826.

109. Rim EY, Clevers H, Nusse R. The Wnt Pathway: From Signaling Mechanisms to Synthetic Modulators. Annu Rev Biochem. 2022;91(1):571–98.

110. Jia L, Piña-Crespo J, Li Y. Restoring Wnt/β-catenin signaling is a promising therapeutic strategy for Alzheimer's disease. Mol Brain. 2019;12(1):104.

111. Zhang L, Yang X, Yang S, Zhang J. The Wnt/β-catenin signaling pathway in the adult neurogenesis. European Journal of Neuroscience. 2011;33(1):1–8.

112. McLeod F, Salinas PC. Wnt proteins as modulators of synaptic plasticity. Curr Opin Neurobiol. 2018; 53:90–5.

113. Sweeney MD, Sagare AP, Zlokovic B V. Blood–brain barrier breakdown in Alzheimer disease and other neurodegenerative disorders. Nature Reviews Neurology. 2018;14(3):133–50.

114. Okerlund ND, Cheyette BNR. Synaptic Wnt signaling-a contributor to major psychiatric disorders? J Neurodev Disord. 2011;3(2):162–74.

115. Godin JD, Poizat G, Hickey MA, Maschat F, Humbert S. Mutant huntingtin-impaired degradation of β-catenin causes neurotoxicity in Huntington's disease. EMBO J. 2010;29(14):2433–45.

116. Inestrosa NC, Montecinos-Oliva C, Fuenzalida M. Wnt Signaling: Role in Alzheimer Disease and Schizophrenia. Journal of Neuroimmune Pharmacology 2012;7(4):788–807.

117. L'Episcopo F, Tirolo C, Caniglia S, Testa N, Morale MC, Serapide MF, et al. Targeting Wnt signaling at the neuroimmune interface for dopaminergic neuroprotection/repair in Parkinson's disease. J Mol Cell Biol. 2014;6(1):13–26.

118. L'Episcopo F, Serapide MF, Tirolo C, Testa N, Caniglia S, Morale MC, et al. A Wnt1 regulated Frizzled-1/β-catenin signaling pathway as a candidate regulatory circuit controlling mesencephalic dopaminergic neuron-astrocyte crosstalk: Therapeutical relevance for neuron survival and neuroprotection. Mol Neurodegener. 2011;6(1):1–29.

119. L'Episcopo F, Tirolo C, Testa N, Caniglia S, Morale MC, Cossetti C, et al. Reactive astrocytes and Wnt/β-catenin signaling link nigrostriatal injury to repair in 1-methyl-4-phenyl-1,2,3,6-tetrahydropyridine model of Parkinson's disease. Neurobiol Dis. 2011;41(2):508–27.

120. Marchetti B. Wnt/β-Catenin Signaling Pathway Governs a Full Program for Dopaminergic Neuron Survival, Neurorescue and Regeneration in the MPTP Mouse Model of Parkinson's Disease. International Journal of Molecular Sciences 2018;19(12):3743.

121. Serafino A, Giovannini D, Rossi S, Cozzolino M. Targeting the Wnt/β-catenin pathway in neurodegenerative diseases: recent approaches and current challenges. Expert Opin Drug Discov. 2020;15(7):803–22.

122. Younger J, Parkitny L, McLain D. The use of low-dose naltrexone (LDN) as a novel anti-inflammatory treatment for chronic pain. Clin Rheumatol. 2014;33(4):451–9.

123. Van Bockstaele EJ, Qian Y, Sterling RC, Page ME. Low dose naltrexone administration in morphine dependent rats attenuates withdrawal-induced norepinephrine efflux in forebrain. Prog Neuropsychopharmacol Biol Psychiatry. 2008;32(4):1048–56.

124. Raffaeli W, Indovina P. Low-Dose Naltrexone to Prevent Intolerable Morphine Adverse Events: A Forgotten Remedy for a Neglected, Global Clinical Need. Pain Medicine (United States). 2015;16(6):1239–42.

125. Alzheimer Discovery. Low-dose Naltrexone. 2022:1-20.

126. Qu N, Meng Y, Handley MK, Wang C, Shan F. Preclinical and clinical studies into the bioactivity of low-dose naltrexone (LDN) for oncotherapy. Int Immunopharmacol. 2021; 96:107714.

127. Liu WM, Dalgleish AG. Naltrexone at low doses (LDN) and its relevance to cancer therapy. Expert Rev Anticancer Ther. 2022;22(3):269–74.

128. Dantzer R, Kelley KW. Twenty years of research on cytokine-induced sickness behavior. Brain Behav Immun. 2007;21(2):153–60.

129. Liao SL, Chen WY, Raung SL, Chen CJ. Neuroprotection of naloxone against ischemic injury in rats: role of mu receptor antagonism. Neurosci Lett. 2003;345(3):169–72.

130. Liu B, Du L, Kong LY, Hudson PM, Wilson BC, Chang RC, et al. Reduction by naloxone of lipopolysaccharide-induced neurotoxicity in mouse cortical neuron–glia co-cultures. Neuroscience. 2000;97(4):749–56.

131. Torres-Berrio A, Nava-Mesa MO. The opioid system in stress-induced memory disorders: From basic mechanisms to clinical implications in post-traumatic stress

disorder and Alzheimer's disease. Prog Neuropsychopharmacol Biol Psychiatry. 2019; 88:327–38.

132. Cai Z, Ratka A. Opioid System and Alzheimer's Disease. Neuromolecular Med. 2012;14(2):91–111.

133. Pomara N, Roberts R, Rhiew HB, Stanley M, Gershon S. Multiple, single-dose naltrexone administrations fail to effect overall cognitive functioning and plasma cortisol in individuals with probable Alzheimer's disease. Neurobiol Aging. 1985;6(3):233–6.

134. Lv Z, Guo Y. Metformin and Its Benefits for Various Diseases. Front Endocrinol (Lausanne). 2020;11.

135. Foretz M, Guigas B, Viollet B. Metformin: update on mechanisms of action and repurposing potential. Nat Rev Endocrinol. 2023;19(8):460–76.

136. Triggle CR, Mohammed I, Bshesh K, Marei I, Ye K, Ding H, et al. Metformin: Is it a drug for all reasons and diseases? Metabolism. 2022; 133:155223.

137. Saenz A, Fernandez-Esteban I, Mataix A, Ausejo Segura M, Roqué i Figuls M, Moher D. Metformin monotherapy for type 2 diabetes mellitus. In: Saenz A, editor. Cochrane Database of Systematic Reviews. Chichester, UK: John Wiley & Sons, Ltd; 2005.

138. Moses RG. Achieving glycosylated hemoglobin targets using the combination of repaglinide and metformin in type 2 diabetes: a reanalysis of earlier data in terms of current targets. Clin Ther. 2008;30(3):552–4.

139. Sundelin E, Jensen JB, Jakobsen S, Gormsen LC, Jessen N. Metformin Biodistribution: A Key to Mechanisms of Action? J Clin Endocrinol Metab. 2020;105(11):3374–83.

140. Elkind-Hirsch KE, Paterson MS, Seidemann EL, Gutowski HC. Short-term therapy with combination dipeptidyl peptidase-4 inhibitor saxagliptin/metformin extended release (XR) is superior to saxagliptin or metformin XR monotherapy in prediabetic women with polycystic ovary syndrome: a single-blind, randomized, pilot . Fertil Steril. 2017;107(1):253-260.e1.

141. Deng J, Peng M, Zhou S, Xiao D, Hu X, Xu S, et al. Metformin targets Clusterin to control lipogenesis and inhibit the growth of bladder cancer cells through SREBP-1c/FASN axis. Signal Transduct Target Ther. 2021;6(1).

142. Ryu YK, Park HY, Go J, Choi DH, Kim YH, Hwang JH, et al. Metformin Inhibits the Development of l-DOPA-Induced Dyskinesia in a Murine Model of Parkinson's Disease. Mol Neurobiol . 2018;55(7):5715–26.

143. Zheng J, Xu M, Walker V, Yuan J, Korologou-Linden R, Robinson J, et al. Evaluating the efficacy and mechanism of metformin targets on reducing Alzheimer's disease risk in the general population: a Mendelian randomisation study. Diabetologia. 2022;65(10):1664–75.

144. Simm A. Protein glycation during aging and in cardiovascular disease. J Proteomics. 2013; 92:248–59.

145. Hossain KFB, Akter M, Rahman MM, Sikder MT, Rahaman MS, Yamasaki S, et al. Amelioration of Metal-Induced Cellular Stress by α-Lipoic Acid and Dihydrolipoic Acid through Antioxidative Effects in PC12 Cells and Caco-2 Cells. Int J Environ Res Public Health. 2021;18(4):2126.

146. Rochette L, Ghibu S, Muresan A, Vergely C. Alpha-lipoic acid: molecular mechanisms and therapeutic potential in diabetes. Can J Physiol Pharmacol. 2015;93(12):1021–7.

147. Ikuta N, Okamoto H, Furune T, Uekaji Y, Terao K, Uchida R, et al. Bioavailability of an R-α-lipoic acid/γ-cyclodextrin complex in healthy volunteers. Int J Mol Sci. 2016;17(6).

148. Suzuki YJ, Aggarwal BB, Packer L. α-Lipoic acid is a potent inhibitor of NF-κB activation in human T cells. Biochem Biophys Res Commun. 1992;189(3):1709–15.

149. Gorąca A, Huk-Kolega H, Piechota A, Kleniewska P, Ciejka E, Skibska B. Lipoic acid – biological activity and therapeutic potential. Pharmacological Reports. 2011;63(4):849–58.

150. Jomova K, Vondrakova D, Lawson M, Valko M. Metals, oxidative stress and neurodegenerative disorders. Mol Cell Biochem. 2010;345(1–2):91–104.

151. Rutten BPF, Steinbusch HWM, Korr H, Schmitz C. Antioxidants and Alzheimer's disease: from bench to bedside (and back again). Curr Opin Clin Nutr Metab Care. 2002;5(6):645–51.

152. Feng Y, Wang X. Antioxidant Therapies for Alzheimer's Disease. Oxid Med Cell Longev. 2012; 2012:1–17.

153. Ghasemi M, Turnbull T, Sebastian S, Kempson I. The MTT Assay: Utility, Limitations, Pitfalls, and Interpretation in Bulk and Single-Cell Analysis. Int J Mol Sci. 2021;22(23):12827.

154. Verebey K, Volavka J, Mulé SJ, Resnick RB. Naltrexone: Disposition, metabolism, and effects after acute and chronic dosing. Clin Pharmacol Ther. 1976;20(3):315–28.

155. Taylor-Whiteley TR, Le Maitre CL, Duce JA, Dalton CF, Smith DP. Recapitulating Parkinson's disease pathology in a three-dimensional human neural cell culture model. Dis Model Mech. 2019.

156. Skotak M, Wang F, Chandra N. An in vitro injury model for SH-SY5Y neuroblastoma cells: Effect of strain and strain rate. J Neurosci Methods. 2012;205(1):159–68.

157. Schikora J, Kiwatrowski N, Förster N, Selbach L, Ostendorf F, Pallapies F, et al. A Propagated Skeleton Approach to High Throughput Screening of Neurite Outgrowth for In Vitro Parkinson's Disease Modelling. Cells. 2021;10(4):931.

158. Påhlman S, Ruusala AI, Abrahamsson L, Mattsson MEK, Esscher T. Retinoic acid-induced differentiation of cultured human neuroblastoma cells: a comparison with phorbolester-induced differentiation. Cell Differ. 1984;14(2):135–44.

159. Encinas M, Iglesias M, Liu Y, Wang H, Muhaisen A, Ceña V, et al. Sequential Treatment of SH-SY5Y Cells with Retinoic Acid and Brain-Derived Neurotrophic Factor Gives Rise to Fully Differentiated, Neurotrophic Factor-Dependent, Human Neuron-Like Cells. J Neurochem. 2002;75(3):991–1003.

160. Moore TB, Sidell N, Chow VJT, Medzoyan RH, Huang JI, Yamashiro JM, et al. Differentiating Effects of 1,25-Dihydroxycholecalciferol (D3) on LA-N-5 Human Neuroblastoma Cells and Its Synergy with Retinoic Acid. J Pediatr Hematol Oncol. 1995;17(4):311–7.

161. Sarkanen JR, Nykky J, Siikanen J, Selinummi J, Ylikomi T, Jalonen TO. Cholesterol supports the retinoic acid-induced synaptic vesicle formation in differentiating human SH-SY5Y neuroblastoma cells. J Neurochem. 2007;102(6):1941–52.

162. Yirün A, Çakır DA, Sanajou S, Erdemli Köse SB, Özyurt AB, Zeybek D, et al. Evaluation of the effects of herpes simplex glycoprotein B on complement system and cytokines in in vitro models of Alzheimer's disease. Journal of Applied Toxicology. 2023;43(9):1368–78.

163. Zheng L, Roberg K, Jerhammar F, Marcusson J, Terman A. Autophagy of amyloid beta-protein in differentiated neuroblastoma cells exposed to oxidative stress. Neurosci Lett. 2006;394(3):184–9.

164. Leroy K, Yilmaz Z, Brion JP. Increased level of active GSK-3? in Alzheimer's disease and accumulation in argyrophilic grains and in neurones at different stages of neurofibrillary degeneration. Neuropathol Appl Neurobiol. 2007;33(1).

165. Ryder J, Su Y, Ni B. Akt/GSK3β serine/threonine kinases: evidence for a signalling pathway mediated by familial Alzheimer's disease mutations. Cell Signal. 2004;16(2):187–200.

166. Wang Y, Yang R, Gu J, Yin X, Jin N, Xie S, et al. Cross talk between PI3K-AKT-GSK-3β and PP2A pathways determines tau hyperphosphorylation. Neurobiol Aging. 2015;36(1):188–200.

167. Tolstykh T. Carboxyl methylation regulates phosphoprotein phosphatase 2A by controlling the association of regulatory B subunits. EMBO J. 2000;19(21):5682–91.

168. Harrison-Uy SJ, Pleasure SJ. Wnt Signaling and Forebrain Development. Cold Spring Harb Perspect Biol. 2012;4(7): a008094–a008094.

169. Inestrosa NC, Arenas E. Emerging roles of Wnts in the adult nervous system. Nat Rev Neurosci. 2010;11(2):77–86.

170. Zhang L, Yang X, Yang S, Zhang J. The Wnt /β-catenin signaling pathway in the adult neurogenesis. European Journal of Neuroscience. 2011;33(1):1–8.

171. Kitagawa M, Hatakeyama S, Shirane M, Matsumoto M, Ishida N, Hattori K, et al. An F-box protein, FWD1, mediates ubiquitin-dependent proteolysis of β-catenin. EMBO J. 1999;18(9):2401–10.

172. Scali C, Caraci F, Gianfriddo M, Diodato E, Roncarati R, Pollio G, et al. Inhibition of Wnt signaling, modulation of Tau phosphorylation and induction of neuronal cell death by DKK1. Neurobiol Dis. 2006;24(2):254–65.

173. Zhang L, Li K, Lv Z, Xiao X, Zheng J. The effect on cell growth by Wnt1 RNAi in human neuroblastoma SH-SY5Y cell line. Pediatr Surg Int. 2009;25(12):1065–71.

174. Huang C, Ma J, Li B, Sun Y. Wnt1 silencing enhances neurotoxicity induced by paraquat and maneb in SH-SY5Y cells. Exp Ther Med. 2019.

175. Uemura K, Kitagawa N, Kohno R, Kuzuya A, Kageyama T, Shibasaki H, et al. Presenilin 1 mediates retinoic acid-induced differentiation of SH-SY5Y cells through facilitation of Wnt signaling. J Neurosci Res. 2003;73(2):166–75.

176. Wei L, Sun C, Lei M, Li G, Yi L, Luo F, et al. Activation of Wnt/β-catenin Pathway by Exogenous Wnt1 Protects SH-SY5Y Cells Against 6-Hydroxydopamine Toxicity. Journal of Molecular Neuroscience. 2013;49(1):105–15.

177. Cassidy L, Fernandez F, Johnson JB, Naiker M, Owoola AG, Broszczak DA. Oxidative stress in alzheimer's disease: A review on emergent natural polyphenolic therapeutics. Complement Ther Med. 2020; 49:102294.

178. Montine TJ, Neely MD, Quinn JF, Beal MF, Markesbery WR, Roberts LJ, et al. Lipid peroxidation in aging brain and Alzheimer's disease1,2 1Guest Editors: Mark A. Smith and George Perry 2This article is part of a series of reviews on "Causes and Consequences of Oxidative Stress in Alzheimer's Disease." The full list of papers may b. Free Radic Biol Med. 2002;33(5):620–6.

179. Butterfield DA, Lauderback CM. Lipid peroxidation and protein oxidation in Alzheimer's disease brain: potential causes and consequences involving amyloid β-peptide-associated free radical oxidative stress 1,2 1Guest Editors: Mark A. Smith and George Perry 2This article is part of a ser. Free Radic Biol Med. 2002;32(11):1050–60.

180. A. Ma Z. The Role of Peroxidation of Mitochondrial Membrane Phospholipids in Pancreatic β -Cell Failure. Curr Diabetes Rev. 2012;8(1):69–75.

181. Saharan S, Mandal PK. The Emerging Role of Glutathione in Alzheimer's Disease. Journal of Alzheimer's Disease. 2014;40(3):519–29.

182. Adams JD, Klaidman LK, Odunze IN, Shen HC, Miller CA. Alzheimer's and Parkinson's disease. Mol Chem Neuropathol. 1991;14(3):213–26.

183. Balazs L, Leon M. Evidence of an oxidative challenge in the Alzheimer's brain. Neurochem Res. 1994;19(9):1131–7.

184. Perry TL, Yong VW, Bergeron C, Hansen S, Jones K. Amino acids, glutathione, and glutathione transferase activity in the brains of patients with Alzheimer's disease. Ann Neurol. 1987;21(4):331–6.

185. Kuperstein F, Yavin E. Pro-apoptotic signaling in neuronal cells following iron and amyloid beta peptide neurotoxicity. J Neurochem. 2004;86(1):114–25.

186. Pieńkowska N, Fahnestock M, Mahadeo C, Zaborniak I, Chmielarz P, Bartosz G, et al. Induction of Oxidative Stress in SH-SY5Y Cells by Overexpression of hTau40 and Its Mitigation by Redox-Active Nanoparticles. Int J Mol Sci. 2022;24(1):359.

187. Singh A, Kukreti R, Saso L, Kukreti S. Oxidative stress: A key modulator in neurodegenerative diseases. Molecules. 2019;24(8):1–20.

188. Exley C, House ER. Aluminium in the human brain. Monatsh Chem. 2011;142(4):357–63.

189. Kumar V, Gill KD. Aluminium neurotoxicity: neurobehavioural and oxidative aspects. Arch Toxicol. 2009;83(11):965–78.

190. Harrington CR, Wischik CM, McArthur FK, Taylor GA, Edwardson JA, Candy JM. Alzheimer's-disease-like changes in tau protein processing: association with aluminium accumulation in brains of renal dialysis patients. The Lancet. 1994;343(8904):993–7.

191. Khanna P, Nehru B. Antioxidant Enzymatic System in Neuronal and Glial Cells Enriched Fractions of Rat Brain After Aluminum Exposure. Cell Mol Neurobiol. 2007;27(7):959–69.

192. Kumar V, Gill KD. Aluminium neurotoxicity: neurobehavioural and oxidative aspects. Arch Toxicol. 2009;83(11):965–78.

193. Wu Z, Du Y, Xue H, Wu Y, Zhou B. Aluminum induces neurodegeneration and its toxicity arises from increased iron accumulation and reactive oxygen species (ROS) production. Neurobiol Aging. 2012;33(1):199.e1-199.e12.

194. Campbell A, Prasad KN, Bondy SC. Aluminum-induced oxidative events in cell lines: glioma are more responsive than neuroblastoma. Free Radic Biol Med. 1999;26(9–10):1166–71.

195. Yang MHH, Chen SCC, Lin YFF, Lee YCC, Huang MYY, Chen KCC, et al. Reduction of aluminum ion neurotoxicity through a small peptide application – NAP treatment of Alzheimer's disease. J Food Drug Anal. 2019;27(2):551–64.

196. Draper HH, Hadley M. [43] Malondialdehyde determination as index of lipid Peroxidation. In 1990: 421–31.

197. Rizvi SHM, Parveen A, Ahmad I, Ahmad I, Verma AK, Arshad Md, et al. Aluminum Activates PERK-EIF2α Signaling and Inflammatory Proteins in Human Neuroblastoma SH-SY5Y Cells. Biol Trace Elem Res. 2016;172(1):108–19.

198. Mustafa Rizvi SH, Parveen A, Verma AK, Ahmad I, Arshad M, Mahdi AA. Aluminium Induced Endoplasmic Reticulum Stress Mediated Cell Death in SH-SY5Y Neuroblastoma Cell Line Is Independent of p53. Ahmad S, editor. PLoS One. 2014;9(5): e98409.

199. Kaneko N, Sugioka T, Sakurai H. Aluminum compounds enhance lipid peroxidation in liposomes: Insight into cellular damage caused by oxidative stress. J Inorg Biochem. 2007;101(6):967–75.

200. Golub MS, Han B, Keen CL, Gershwin ME. Effects of dietary aluminum excess and manganese deficiency on neurobehavioral endpoints in adult mice. Toxicol Appl Pharmacol. 1992;112(1):154–60.

201. Orihuela D, Meichtry V, Pregi N, Pizarro M. Short-term oral exposure to aluminium decreases glutathione intestinal levels and changes enzyme activities involved in its metabolism. J Inorg Biochem. 2005;99(9):1871–8.

202. Jozefczak M, Remans T, Vangronsveld J, Cuypers A. Glutathione Is a Key Player in Metal-Induced Oxidative Stress Defenses. Int J Mol Sci. 2012;13(3):3145–75.

203. Lee M, Cho S, Roh K, Chae J, Park JH, Park J, et al. Glutathione alleviated peripheral neuropathy in oxaliplatin-treated mice by removing aluminum from dorsal root ganglia. Am J Transl Res. 2017;9(3):926–39.

204. Atakisi O, Dalginli KY, Gulmez C, Kalacay D, Atakisi E, Zhumabaeva TT, et al. The Role of Reduced Glutathione on the Activity of Adenosine Deaminase, Antioxidative System, and Aluminum and Zinc Levels in Experimental Aluminum Toxicity. Biol Trace Elem Res. 2023;201(9):4429–36.

205. Öztürk ME, Yirün A, Erdemli-Köse SB, Balcı-Özyurt A, Çakır DA, Oral D, et al. Evaluation of the toxic effects of thimerosal and/or aluminum hydroxide in SH-SY5Y cell line. Hum Exp Toxicol. 2022;41.

206. Nehru B, Bhalla P. Reversal of an aluminium induced alteration in redox status in different regions of rat brain by administration of centrophenoxine. Mol Cell Biochem. 2006;290(1–2):185–91.

207. Wang J zhi, Tung YC, Wang Y, Li XT, Iqbal K, Grundke-Iqbal I. Hyperphosphorylation and accumulation of neurofilament proteins in Alzheimer disease brain and in okadaic acid-treated SY5Y cells. FEBS Lett. 2001;507(1):81–7.

208. Justin-Thenmozhi A, Dhivya Bharathi M, Kiruthika R, Manivasagam T, Borah A, Essa MM. Attenuation of Aluminum Chloride-Induced Neuroinflammation and Caspase Activation Through the AKT/GSK-3β Pathway by Hesperidin in Wistar Rats. Neurotox Res. 2018;34(3):463–76.

209. Zhang B, Li Q, Chu X, Sun S, Chen S. Salidroside reduces tau hyperphosphorylation via up-regulating GSK-3β phosphorylation in a tau transgenic Drosophila model of Alzheimer's disease. Transl Neurodegener. 2016;5(1):21.

210. Parekh KD, Dash RP, Pandya AN, Vasu KK, Nivsarkar M. Implication of novel bis-imidazopyridines for management of Alzheimer's disease and establishment of its role on protein phosphatase 2A activity in brain. Journal of Pharmacy and Pharmacology. 2013;65(12):1785–95.

211. Walton JR. An aluminum-based rat model for Alzheimer's disease exhibits oxidative damage, inhibition of PP2A activity, hyperphosphorylated tau, and granulovacuolar degeneration. J Inorg Biochem. 2007;101(9):1275–84.

212. Hernandez F, Lucas JJ, Avila J. GSK3 and Tau: Two Convergence Points in Alzheimer's Disease. Journal of Alzheimer's Disease. 2013 Jan 1;33(s1): S141–4.

213. Lovell MA, Xiong S, Xie C, Davies P, Markesbery WR. Induction of hyperphosphorylated tau in primary rat cortical neuron cultures mediated by oxidative stress and glycogen synthase kinase-3. Journal of Alzheimer's Disease. 2005;6(6):659–71.

214. Guerra-Araiza C, Amorim MAR, Camacho-Arroyo I, Garcia-Segura LM. Effects of progesterone and its reduced metabolites, dihydroprogesterone and tetrahydroprogesterone, on the expression and phosphorylation of glycogen synthase kinase-3 and the microtubule-associated protein Tau in the rat cerebellum. Dev Neurobiol. 2007;67(4):510–20.

215. Hanger DP, Noble W. Functional Implications of Glycogen Synthase Kinase-3-Mediated Tau Phosphorylation. Int J Alzheimers Dis. 2011; 2011:1–11.

216. Inestrosa NC, Varela-Nallar L. Wnt signaling in the nervous system and in Alzheimer's disease. J Mol Cell Biol. 2014;6(1):64–74.

217. Libro R, Bramanti P, Mazzon E. The role of the Wnt canonical signaling in neurodegenerative diseases. Life Sci. 2016;158:78–88.

218. Xian YF, Ip SP, Mao QQ, Lin ZX. Neuroprotective effects of honokiol against beta-amyloid-induced neurotoxicity via GSK-3β and β-catenin signaling pathway in PC12 cells. Neurochem Int. 2016; 97:8–14.

219. Aghaizu ND, Jin H, Whiting PJ. Dysregulated Wnt Signalling in the Alzheimer's Brain. Brain Sci. 2020;10(12):902.

220. Huang W, Wang P, Shen T, Hu C, Han Y, Song M, et al. Aluminum Trichloride Inhibited Osteoblastic Proliferation and Downregulated the Wnt/β-Catenin Pathway. Biol Trace Elem Res. 2017;177(2):323–30.

221. Cao Z, Fu Y, Sun X, Zhang Q, Xu F, Li Y. Aluminum trichloride inhibits osteoblastic differentiation through inactivation of Wnt/β-catenin signaling pathway in rat osteoblasts. Environ Toxicol Pharmacol. 2016; 42:198–204.

222. Sun X, Cao Z, Zhang Q, Liu S, Xu F, Che J, et al. Aluminum trichloride impairs bone and downregulates Wnt/β-catenin signaling pathway in young growing rats. Food and Chemical Toxicology. 2015; 86:154–62.

223. Mohamed EA, Ahmed HI, Zaky HS, Badr AM. Boswellic acids ameliorate neurodegeneration induced by AlCl3: the implication of Wnt/β-catenin pathway. Environmental Science and Pollution Research. 2022;29(50):76135–43.

224. Abu-Elfotuh K, Hussein FH, Abbas AN, Al-Rekabi MD, Barghash SS, Zaghlool SS, et al. Melatonin and zinc supplements with physical and mental activities subside neurodegeneration and hepatorenal injury induced by aluminum chloride in rats: Inclusion of GSK-3β-Wnt/β-catenin signaling pathway. Neurotoxicology. 2022; 91:69–83.

225. Nagu P, Sharma V, Behl T, Pathan AKA, Mehta V. Molecular Insights to the Wnt Signaling During Alzheimer's Disorder: a Potential Target for Therapeutic Interventions. Journal of Molecular Neuroscience. 2022;72(4):679–90.

226. Arredondo SB, Valenzuela-Bezanilla D, Mardones MD, Varela-Nallar L. Role of Wnt Signaling in Adult Hippocampal Neurogenesis in Health and Disease. Front Cell Dev Biol. 2020; 8:860.

227. Hyman BT, Eslinger PJ, Damasio AR. Effect of naltrexone on senile dementia of the Alzheimer type. J Neurol Neurosurg Psychiatry. 1985;48(11):1169–71.

228. Ip K, Song G, Banov D, Bassani AS, Valdez BC. In vitro evaluation of Naltrexone HCl 1% Topical Cream in XemaTop^{TM} for psoriasis. Arch Dermatol Res. 2020;312(2):145–54.

229. Bondy SC. The neurotoxicity of environmental aluminum is still an issue. Neurotoxicology. 2010;31(5):575.

230. Kandimalla R, Vallamkondu J, Corgiat EB, Gill KD, Jayalakshmi Vallamkondu; Corgiat EB, et al. Understanding aspects of aluminum exposure in Alzheimer's disease development. Brain Pathology. 2016;26(2):139–54.

231. Kawahara M, Kato-Negishi M. Link between aluminum and the pathogenesis of Alzheimer's disease: The integration of the aluminum and amyloid cascade hypotheses. Int J Alzheimers Dis. 2011;2011.

232. Plank JR, Glover SC, Moloney BD, Hoeh NR, Sundram F, Sumner RL, et al. A randomized, double-blind, placebo-controlled, hybrid parallel-arm study of low-dose naltrexone as an adjunctive anti-inflammatory treatment for major depressive disorder. Trials. 2022;23(1).

233. Wu CC, Chang CY, Shih KC, Hung CJ, Wang YY, Lin SY, et al. β-Funaltrexamine Displayed Anti-Inflammatory and Neuroprotective Effects in Cells and Rat Model of Stroke. Int J Mol Sci. 2020:3866.

234. Glass CK, Saijo K, Winner B, Marchetto MC, Gage FH. Mechanisms underlying inflammation in neurodegeneration. Cell. 2010;140(6):918–34.

235. Vallée A, Vallée JN, Lecarpentier Y. WNT/β-catenin Pathway: a Possible Link Between Hypertension and Alzheimer's Disease. Curr Hypertens Rep. 2022.

236. Turel AP, Oh KH, Zagon IS, McLaughlin PJ. Low Dose Naltrexone for Treatment of Multiple Sclerosis. J Clin Psychopharmacol . 2015;35(5):609–11.

237. Lie MRKL, van der Giessen J, Fuhler GM, de Lima A, Peppelenbosch MP, van der Ent C, et al. Low dose Naltrexone for induction of remission in inflammatory bowel disease patients. J Transl Med. 2018 Mar 9;16(1).

238. Tawfik DI, Osman AS, Tolba HM, Khattab A, Abdel-Salam LO, Kamel MM. Evaluation of therapeutic effect of low dose naltrexone in experimentally-induced Crohn's disease in rats. Neuropeptides. 2016; 59:39–45.

239. Uddin MS, Stachowiak A, Al Mamun A, Tzvetkov NT, Takeda S, Atanasov AG, et al. Autophagy and Alzheimer's disease: From molecular mechanisms to therapeutic implications. Front Aging Neurosci. 2018;10(JAN):4.

240. Li Q, Liu Y, Sun M. Autophagy and Alzheimer's Disease. Cell Mol Neurobiol. 2017 Apr 1;37(3):377–88.

241. D'Mello SR. When Good Kinases Go Rogue: GSK3, p38 MAPK and CDKs as Therapeutic Targets for Alzheimer's and Huntington's Disease. Int J Mol Sci. 2021;22(11):5911.

242. Chen G, Yee Gan S, Jiang CS, Lu J, Xu X, Gu L, et al. Inhibitory Effects of Macelignan on Tau Phosphorylation and Aβ Aggregation in the Cell Model of Alzheimer's Disease. Frontiers in Nutrition. 2022; 1:892558.

243. Martin L, Latypova X, Wilson CM, Magnaudeix A, Perrin ML, Terro F. Tau protein phosphatases in Alzheimer's disease: The leading role of PP2A. Ageing Res Rev. 2013;12(1):39–49.

244. Ooi L, Patel M, Münch G. The thiol antioxidant lipoic acid and Alzheimer's disease. Systems Biology of Free Radicals and Antioxidants. 2012;2275–88.

245. Maczurek A, Hager K, Kenklies M, Sharman M, Martins R, Engel J, et al. Lipoic acid as an anti-inflammatory and neuroprotective treatment for Alzheimer's disease. Adv Drug Deliv Rev. 2008;60(13–14):1463–70.

246. Al-Otaibi SS, Arafah MM, Sharma B, Alhomida AS, Siddiqi NJ. Synergistic Effect of Quercetin and α -Lipoic Acid on Aluminium Chloride Induced Neurotoxicity in Rats. J Toxicol. 2018; 2018:1–8.

247. Khan H, Singh TG, Dahiya RS, Abdel-Daim MM. α-Lipoic Acid, an Organosulfur Biomolecule a Novel Therapeutic Agent for Neurodegenerative Disorders: An Mechanistic Perspective. Neurochem Res. 2022;47(7):1853–64.

248. Greenamyre JT, Garcia-Osuna M, Greene JG. The endogenous cofactors, thioctic acid and dihydrolipoic acid, are neuroprotective against NMDA and malonic acid lesions of striatum. Neurosci Lett. 1994;171(1–2):17–20.

249. Koenig ML, Meyerhoff JL. In vitro neuroprotection against oxidative stress by pre-treatment with a combination of dihydrolipoic acid and phenyl-butyl nitrones. Neurotox Res. 2003;5(4):265–72.

250. Holmquist L, Stuchbury G, Berbaum K, Muscat S, Young S, Hager K, et al. Lipoic acid as a novel treatment for Alzheimer's disease and related dementias. Pharmacol Ther. 2007;113(1):154–64.

251. Metwaly HH, Fathy SA, Abdel Moneim MM, Emam MA, Soliman AF, El-Naggar ME, et al. Chitosan and solid lipid nanoparticles enhance the efficiency of alpha-lipoic acid against experimental neurotoxicity. 2021;32(4):268–79.

252. Suh JH, Zhu BZ, deSzoeke E, Frei B, Hagen TM. Dihydrolipoic acid lowers the redox activity of transition metal ions but does not remove them from the active site of enzymes. 2013;9(1):57–61.

253. Mora-Diez N, Monreal-Corona R, Biddlecombe J, Ippolito A. Theoretical study of the iron complexes with lipoic and dihydrolipoic acids: Exploring secondary antioxidant activity. Antioxidants. 2020;9(8):1–21.

254. Kawabata T, Yap SC, Packer L. The Short-Chain Homologue of Dihydrolipoic Acid, Tetranordihydrolipoate, Protects against Iron-Induced Lipid Peroxidation in the Aqueous Phase. Biochem Biophys Res Commun. 1994;199(1):361–7.

255. Uddin MS, Kabir MT. Oxidative stress in alzheimer's disease: Molecular hallmarks of underlying vulnerability. Biological, Diagnostic and Therapeutic Advances in Alzheimer's Disease: Non-Pharmacological Therapies for Alzheimer's Disease. 2019;91–115.

256. Ahmadvand H, Jamor P. Effects of alpha lipoic acid on level of NO and MPO activity in diabetic rats. Annals of Research in Antioxidants. 2017;2(2).

257. Wojsiat J, Zoltowska KM, Laskowska-Kaszub K, Wojda U. Oxidant/Antioxidant Imbalance in Alzheimer's Disease: Therapeutic and Diagnostic Prospects. Oxid Med Cell Longev. 2018; 2018:1–16.

258. Dinicola S, Proietti S, Cucina A, Bizzarri M, Fuso A. Alpha-Lipoic Acid Downregulates IL-1β and IL-6 by DNA Hypermethylation in SK-N-BE Neuroblastoma Cells. Antioxidants. 2017;6(4):74.

259. Shin RW. Interaction of Aluminum with Paired Helical Filament Tau Is Involved in Neurofibrillary Pathology of Alzheimer's Disease. Gerontology. 1997;43(Suppl. 1):16–23.

260. Huang W, Cheng P, Yu K, Han Y, Song M, Li Y. Hyperforin attenuates aluminum-induced Aβ production and Tau phosphorylation via regulating Akt/GSK-3β signaling pathway in PC12 cells. Biomedicine and Pharmacotherapy. 2017;96(59):1–6.

261. Pan B, Lu X, Han X, Huan J, Gao D, Cui S, et al. Mechanism by Which Aluminum Regulates the Abnormal Phosphorylation of the Tau Protein in Different Cell Lines. ACS Omega. 2021;6(47):31782–96.

262. Lei P, Ayton S, Finkelstein DI, Spoerri L, Ciccotosto GD, Wright DK, et al. Tau deficiency induces parkinsonism with dementia by impairing APP-mediated iron export. Nature Medicine 2012;18(2):291–5.

263. Liu Z, Li T, Li P, Wei N, Zhao Z, Liang H, et al. The Ambiguous Relationship of Oxidative Stress, Tau Hyperphosphorylation, and Autophagy Dysfunction in Alzheimer's Disease. Oxid Med Cell Longev. 2015;2015.

264. Su B, Wang X, Lee H gon, Tabaton M, Perry G, Smith MA, et al. Chronic oxidative stress causes increased tau phosphorylation in M17 neuroblastoma cells. Neurosci Lett. 2010;468(3):267–71.

265. Petersen Shay K, Hagen TM. Age-associated impairment of Akt phosphorylation in primary rat hepatocytes is remediated by alpha-lipoic acid through PI3 kinase, PTEN, and PP2A. Biogerontology. 2009;10(4):443–56.

266. Xiong WP, Yao WQ, Wang B, Liu K. BMSCs-exosomes containing GDF-15 alleviated SH-SY5Y cell injury model of Alzheimer's disease via AKT/GSK-3β/β-catenin. Brain Res Bull. 2021; 177:92–102.

267. Wang SH, Cui LG, Su XL, Komal S, Ni RC, Zang MX, et al. GSK-3β-mediated activation of NLRP3 inflammasome leads to pyroptosis and apoptosis of rat cardiomyocytes and fibroblasts. Eur J Pharmacol. 2022; 920:174830.

268. Zhu X, Wang S, Yu L, Yang H, Tan R, Yin K, et al. TL-2 attenuates β-amyloid induced neuronal apoptosis through the AKT/GSK-3β/β-catenin pathway. Int J Neuropsychopharmacol. 2014;17(09):1511–9.

269. Alberi L, Sichh S, Durrant CS, Bovolenta P, Palomer E, Buechler J, et al. Wnt Signaling Deregulation in the Aging and Alzheimer's Brain. 2019.

270. Tapia-Rojas C, Inestrosa N. Loss of canonical Wnt signaling is involved in the pathogenesis of Alzheimer's disease. Neural Regen Res. 2018;13(10):1705.

271. Ardura-Fabregat A, Boddeke EWGM, Boza-Serrano A, Brioschi S, Castro-Gomez S, Ceyzériat K, et al. Targeting Neuroinflammation to Treat Alzheimer's Disease. CNS Drugs. 2017;31(12):1057–82.

272. Verdile G, Keane KN, Cruzat VF, Medic S, Sabale M, Rowles J, et al. Inflammation and Oxidative Stress: The Molecular Connectivity between Insulin Resistance, Obesity, and Alzheimer's Disease. Mediators Inflamm. 2015; 2015:105828.

273. Steen E, Terry BM, J. Rivera E, Cannon JL, Neely TR, Tavares R, et al. Impaired insulin and insulin-like growth factor expression and signaling mechanisms in Alzheimer's disease – is this type 3 diabetes? Journal of Alzheimer's Disease. 2005;7(1):63–80.

274. Wei Z, Koya J, Reznik SE. Insulin Resistance Exacerbates Alzheimer Disease via Multiple Mechanisms. Front Neurosci. 2021;15.

275. De Felice FG, Vieira MNN, Bomfim TR, Decker H, Velasco PT, Lambert MP, et al. Protection of synapses against Alzheimer's-linked toxins: Insulin signaling prevents the pathogenic binding of Aβ oligomers. Proceedings of the National Academy of Sciences. 2009;106(6):1971–6.

276. Lee SH, Zabolotny JM, Huang H, Lee H, Kim YB. Insulin in the nervous system and the mind: Functions in metabolism, memory, and mood. Mol Metab. 2016;5(8):589–601.

277. Zhao WQ, Townsend M. Insulin resistance and amyloidogenesis as common molecular foundation for type 2 diabetes and Alzheimer's disease. Biochimica et Biophysica Acta (BBA) - Molecular Basis of Disease. 2009;1792(5):482–96.

278. Bloch-Damti A, Bashan N. Proposed Mechanisms for the Induction of Insulin Resistance by Oxidative Stress. Antioxid Redox Signal. 2005;7(11–12):1553–67.

279. Ciotti S, Iuliano L, Cefalù S, Comelli M, Mavelli I, Di Giorgio E, et al. GSK3β is a key regulator of the ROS-dependent necrotic death induced by the quinone DMNQ. Cell Death Dis. 2020;11(1):2.

280. Lee S, Tong M, Hang S, Deochand C, de la Monte S. CSF and Brain Indices of Insulin Resistance, Oxidative Stress and Neuro-Inflammation in Early versus Late Alzheimer's Disease. J Alzheimers Dis Parkinsonism. 2013;3(04):128.

281. Chen F, Dong RR, Zhong KL, Ghosh A, Tang SS, Long Y, et al. Antidiabetic drugs restore abnormal transport of amyloid-β across the blood–brain barrier and memory impairment in db / db mice. Neuropharmacology. 2016; 101:123–36.

282. Li W, Chaudhari K, Shetty R, Winters A, Gao X, Hu Z, et al. Metformin Alters Locomotor and Cognitive Function and Brain Metabolism in Normoglycemic Mice. Aging Dis. 2019;10(5):949.

283. Song Y, Liu Z, Zhu X, Hao C, Hao W, Wu S, et al. Metformin alleviates the cognitive impairment caused by aluminum by improving energy metabolism disorders in mice. Biochem Pharmacol. 2022; 202:115140.

284. Li L, Liu M, Jiang X, Xia Z, Wang Y, A D, et al. Metformin inhibits Aβ $_{25-35}$ -induced apoptotic cell death in SH-SY5Y cells. Basic Clin Pharmacol Toxicol. 2019;125(5):439–49.

285. Binlateh T, Reudhabibadh R, Prommeenate P, Hutamekalin P. Investigation of mechanisms underlying the inhibitory effects of metformin against proliferation and growth of neuroblastoma SH-SY5Y cells. Toxicology in Vitro. 2022;83(June):105410.

286. Katila N, Bhurtel S, Park PH, Choi DY. Metformin attenuates rotenone-induced oxidative stress and mitochondrial damage via the AKT/Nrf2 pathway. Neurochem Int. 2021;148(April):105120.

287. Gwak H, Kim Y, An H, Dhanasekaran DN, Song YS. Metformin induces degradation of cyclin D1 via AMPK/GSK3β axis in ovarian cancer. Mol Carcinog. 2017;56(2):349–58.

288. Zhou X, Liu S, Lin X, Xu L, Mao X, Liu J, et al. Metformin Inhibit Lung Cancer Cell Growth and Invasion in Vitro as Well as Tumor Formation in Vivo Partially by Activating PP2A. Medical Science Monitor. 2019; 25:836–46.

289. Kickstein E, Krauss S, Thornhill P, Rutschow D, Zeller R, Sharkey J, et al. Biguanide metformin acts on tau phosphorylation via mTOR/protein phosphatase 2A (PP2A) signaling. Proceedings of the National Academy of Sciences. 2010;107(50):21830–5.

290. Du MR, Gao QY, Liu CL, Bai LY, Li T, Wei FL. Exploring the Pharmacological Potential of Metformin for Neurodegenerative Diseases. Front Aging Neurosci. 2022;14.

291. Kang HE, Seo Y, Yun JS, Song SH, Han D, Cho ES, et al. Metformin and niclosamide synergistically suppress wnt and yap in apc-mutated colorectal cancer. Cancers (Basel). 2021;13(14):1–19.

292. Conza D, Mirra P, Fiory F, Insabato L, Nicolò A, Beguinot F, et al. Metformin: A New Inhibitor of the Wnt Signaling Pathway in Cancer. Cells. 2023;12(17):2182.

293. Zhang T, Wang F, Li K, Lv C, Gao K, Lv C. Therapeutic effect of metformin on inflammation and apoptosis after spinal cord injury in rats through the Wnt/β-catenin signaling pathway. Neurosci Lett. 2020;739(September 2019):135440.

294. OWEN MR, DORAN E, HALESTRAP AP. Evidence that metformin exerts its anti-diabetic effects through inhibition of complex 1 of the mitochondrial respiratory chain. Biochemical Journal. 2000;348(3):607–14.

295. Brunmair B, Staniek K, Gras F, Scharf N, Althaym A, Clara R, et al. Thiazolidinediones, Like Metformin, Inhibit Respiratory Complex I. Diabetes. 2004;53(4):1052–9.

296. Carvalho C, Correia S, Santos MS, Seiça R, Oliveira CR, Moreira PI. Metformin promotes isolated rat liver mitochondria impairment. Mol Cell Biochem. 2008;308(1–2):75–83.

297. Vinothkumar KR, Zhu J, Hirst J. Architecture of mammalian respiratory complex I. Nature. 2014;515(7525):80–4.

298. Diniz Vilela D, Gomes Peixoto L, Teixeira RR, Belele Baptista N, Carvalho Caixeta D, Vieira de Souza A, et al. The Role of Metformin in Controlling Oxidative Stress in Muscle of Diabetic Rats. Oxid Med Cell Longev. 2016; 2016:1–9.

299. Chukwunonso Obi B, Chinwuba Okoye T, Okpashi VE, Nonye Igwe C, Olisah Alumanah E. Comparative study of the antioxidant effects of metformin, glibenclamide, and repaglinide in alloxan-induced diabetic rats. J Diabetes Res. 2016; 2016:1–5.

300. Dehkordi AH, Abbaszadeh A, Mir S, Hasanvand A. Metformin and its anti-inflammatory and anti-oxidative effects; new concepts. J Renal Inj Prev. 2018;8(1):54–61.

8. SUPPLEMENTS

Supplement 1: Digital receipt Thesis Originality Report

turnitin

Dijital Makbuz

Bu makbuz ödevinizin Turnitin'e ulaştığını bildirmektedir. Gönderiminize dair bilgiler şöyledir:

Gönderinizin ilk sayfası aşağıda gönderilmektedir.

Gönderen:	Sonia Sanajou
Ödev başlığı:	Quick Submit
Gönderi Başlığı:	Investigation of Possible Protective Effects of Certain Xenobi...
Dosya adı:	tez_draftsonia_sanajou_30.102023.pdf
Dosya boyutu:	3.59M
Sayfa sayısı:	160
Kelime sayısı:	40,462
Karakter sayısı:	224,742
Gönderim Tarihi:	03-Kas-2023 11:21ÖÖ (UTC+0300)
Gönderim Numarası:	2216126259

T.C.
REPUBLIC OF TURKEY
HACETTEPE UNIVERSITY
GRADUATE SCHOOL HEALTH SCIENCES

Investigation of Possible Protective Effects of Certain Xenobiotics on
Aluminum Toxicity in SH-SY5Y Cell Line

Sonia SANAJOU, Pharm D., DVM

Program of Pharmaceutical Toxicology
DOCTOR OF PHILOSOPHY THESIS

ANKARA
2023

Supplement 2: Thesis Originality Report

Investigation of Possible Protective Effects of Certain
Xenobiotics on Aluminum Toxicity in SH-SY5Y Cell Line

ORİJİNALLİK RAPORU

%18	%18	%	%
BENZERLİK ENDEKSİ	İNTERNET KAYNAKLARI	YAYINLAR	ÖĞRENCİ ÖDEVLERİ

BİRİNCİL KAYNAKLAR

1 www.lifesciencesite.com
İnternet Kaynağı — %1

2 portal.webdepozit.sk
İnternet Kaynağı — %1

3 www.ncbi.nlm.nih.gov
İnternet Kaynağı — %1

4 www.agriculturedefensecoalition.org
İnternet Kaynağı — %1

5 ir.niist.res.in:8080
İnternet Kaynağı — %1

6 www.science.gov
İnternet Kaynağı — %1

7 core.ac.uk
İnternet Kaynağı — <%1

8 repository.up.ac.za
İnternet Kaynağı — <%1

9 www.nature.com
İnternet Kaynağı — <%1

9. RESUME